Systematic characterization of extracellular vesicle biogenesis pathways and their role on the RNA and protein repertoire released from cells

Juan Carlos A. Padilla Antúnez

Division of Experimental Medicine, Department of Medicine

Faculty of Medicine and Health Sciences

McGill University

Montréal, Québec, Canada

A thesis submitted to McGill University in partial fulfillment of the requirements of the degree of

Doctor of Philosophy

Table of Contents

Dedication

Alfonso, gracias por todo.

Abstract

Intercellular communication is of vital importance to all organisms, as it facilitates the exchange of bioactive molecules between cells. Recently, a group of nanoparticles known as extracellular vesicles (EVs), have come to the forefront as novel mediators of this exchange. EVs represent a heterogeneous collection of lipid-bound nanostructures of diverse subcellular origin. Upon their release from cells, EVs have the capacity to travel through the extracellular environment, and then fuse with and deliver their contents to recipient cells, altering their behaviour. Of the biomolecules present in the EV-repertoire, RNAs are an important group, but the extent of their involvement in cell-cell communication remains elusive.

In the first chapter of this thesis, I explore some of the accumulated knowledge in the field of EV biology, with a particular focus on EV biogenesis pathways and their RNA and RNA-binding protein (RBP) repertoire. In the second chapter, we present evidence on the important role of sphingolipid metabolism in the EV-mediated release of RNA and RBPs from cells. To investigate the functions that ceramide-dependent EV biogenesis pathways play in the recruitment of cargoes for release, we utilized chemical inhibitors to prevent the metabolism of sphingomyelin, present in membranes, by sphingomyelinases. Sphingomyelinases exist in neutral (NSM) and acid (ASM) varieties, and act at different cellular milieus. NSM acts on the endosomal compartment, leading to the formation of intraluminal vesicles (and therefore exosomes), whereas ASM acts at the plasma membrane, resulting in the generation of microvesicles. RNA sequencing and proteomics analysis of human MCF7 cells and EVs revealed that inhibition of NSM resulted in an overall reduction of EV RBPs, similarly we observed a reduction in RNA within the EV population, but the RNA diversity was not affected. Contrastingly, ASM inhibition resulted in an overall increase in EV RBPs, however a downregulation in RNA diversity was also observed. Furthermore, EVs isolated from ASM-inhibited human MCF7 cells induced increased cell migration and protein translation phenotypes on recipient human MCF10A

cells. These results suggest that sphingomyelinase-driven EV biogenesis pathways are a major route of RBP and RNA trafficking outside of the cell.

Mounting evidence has suggested that RNAs present in EVs may be in fragmented forms, with limited examples describing functional mRNAs. To investigate the full-length transcriptome available within EVs, the RNAs of human K562 EVs were profiled with Oxford Nanopore long-read RNA sequencing. Our findings showed the presence of 443 and 280 RNAs that were respectively enriched or depleted in EVs relative to cells (log_2FC >2 or <-2, Adj*P*<0.01). EV-enriched poly(A) transcripts include a variety of biotypes, consist of mRNAs, long noncoding RNAs, and pseudogenes. Strikingly, 10.58% of all reads present in EVs corresponded to known full-length transcripts, 58.13% of which were mRNAs. We also observed that for many well-represented coding and non-coding genes, diverse full-length transcript isoforms were present in EV specimens, and were reflective- of but often in different ratio to cellular samples. These data provide novel insights into the EV RNA repertoire, revealing that EVs contain numerous full-length transcripts.

The characterization of the RNA and protein repertoire of EVs remains an important nexus in our understanding of EVs and their role in intercellular communication. The results reported in this thesis represent an important contribution to the field, describing the role of lipid metabolism on the content of EVs, and providing transcriptome-level evidence for the specific recruitment of full-length RNAs to sites of EV biogenesis for their release from cells.

Résumé

La communication intercellulaire est importante pour tous les organismes, facilitant l'échange de molécules d'une cellule à l'autre. Récemment, un groupe de nanoparticules nommées vésicules extracellulaires (VE) sont devenus d'importants médiateurs de cet échange. Les VE sont un groupe hétérogène de nanostructures membranaires sécrétées par les cellules. Les VE peuvent voyager à travers l'environnement extracellulaire et fusionner avec d'autres cellules et leur livrer leur contenu, modifiant leur comportement. Parmi les biomolécules présentes dans les VE, les ARN sont un groupe sous-étudié et leur rôle dans la communication cellule-cellule reste nébuleuse.

Dans le premier chapitre de cette thèse, j'explore certaines des connaissances accumulées dans le domaine de la biologie des VE, avec un accent sur leur biogenèse et leur répertoire d'ARN et de protéines de liaison à l'ARN (référées dorénavant par *RNA-binding protein*, RBP). Dans le deuxième chapitre, je présente des évidences du rôle des céramides dans la sécrétion d'ARN et de RBP via les VE. Pour étudier le rôle des céramides dans le recrutement des cargaisons, j'ai utilisé des inhibiteurs chimiques pour bloquer la métabolisation de la sphingomyéline présente dans les membranes par les sphingomyélinases (SMase). Les SMase existent en types neutre (NSM) et acide (ASM), qui sont localisés dans des milieux cellulaires spécifiques. Les NSM agissent au niveau du compartiment endosomal, entraînant la formation de vésicules intraluminales (et donc de futurs exosomes), tandis que l'ASM agit au niveau de la membrane plasmique, entraînant la génération de microvésicules. Le séquençage de l'ARN et l'analyse protéomique des cellules MCF7 et leurs VE montrent que l'inhibition de la NSM entraînait une réduction globale des VE RBP, de même, nous avons observé une réduction de l'ARN, mais la diversité de l'ARN n'a pas été affectée. D'autre part, l'inhibition de l'ASM a entraîné une augmentation globale des VE RBP, mais une régulation négative de la diversité de l'ARN a également été observée. De plus, les VE isolés de cellules MCF7 dont l'ASM a été inhibé induisent une traduction accrue des protéines dans des cellules MCF10A réceptrices et entraînent une augmentation du phénotype de migration

cellulaire. Ces résultats suggèrent que la vésiculation dépendante des céramides représente une voie majeure de trafic de RBP et d'ARN vers les VE.

Beaucoup d'évidences suggèrent que les ARN dans les VE sont fragmentés, avec peu d'exemples décrivants des ARNm fonctionnels. Pour investiguer ceci, j'ai séquencé les ARN des VE dérivé de cellules K562 à l'aide du séquenceur MinION d'Oxford Nanopore. Nos résultats démontrent la présence de 443 ARNs enrichis et 280 ARNs appauvris dans les VE comparativement aux cellules (facteur multiplicatif log2 >2 ou <-2, Paj<0.01). Les transits poly(A) enrichis dans les VE comprennent une variété de biotypes, tels les ARNm, les ARN long non-codants, et des pseudogènes. Étonnamment, 10.58% de toutes les séquences lues correspondent à des transcrits pleine-longueur connus, dont 58.13% sont des ARNm. Nous avons aussi observé que, pour plusieurs gènes codants et non-codants fort représentées, une diversité d'isoformes est présente dans les populations VE et reflètent souvent les populations cellulaires, mais dans des ratios différents. Ces données présentent les premières évidences transcriptomiques du recrutement spécifique d'ARN de pleine longueur dans les VE.

La caractérisation du répertoire d'ARN et de protéines des VE reste un angle important dans l'étude des VE et de leur rôle dans la communication intercellulaire. Les résultats rapportés dans cette thèse représentent une contribution importante dans le domaine, montrant à la fois l'effet du métabolisme lipidique sur le contenu des VE et fournissant des évidences transcriptomiques du recrutement spécifique d'ARN de pleine longueur aux sites de biogenèse des VE pour leur sécrétion par les cellules.

Traduit par Philippe Jolivet. Merci, Phil !

List of Figures

List of Tables

List of Abbreviations

Abbreviation	Expanded Term
× *g*	Relative centrifugal force
3’-UTR	3’-untranslated region
AD	Alzheimer’s disease
ALIX	Programmed cell death 6 interacting protein
ALS	Amyotrophic later sclerosis
ANO6	Anoctamin 6
ANXA2	Annexin A2
ARF	ADP ribosylation factor
ASM	Acid sphingomyelinase
ATP	Adenosine 5′-triphosphate
Ca^{2+}	Calcium ions
CCM	Cell conditioned media
CD63	Lysosomal-associated membrane protein 3
CD81	CD81 antigen (Target of antiproliferative antibody 1)
CD82	Metastasis suppressor kangai-1
CD9	Cell growth-inhibiting gene 2 protein
CDK	Cyclin-dependent kinase
circRNA	Circular ribonucleic acid
CO_2	Carbon dioxide
CRM	Cis-regulatory motif
CSF	Cerebrospinal fluid
dFBS	Extracellular vesicle-depleted foetal bovine serum
DMSO	Dimethyl sulfoxide
DNA	Deoxyribonucleic acid
DTT	Dithiothreitol
eCLIP	Enhanced ultraviolet crosslinking and immunoprecipitation
EdU	5-ethynyl-2'-deoxyuridine
EGFR	Epidermal growth factor receptor
EGFRvIII	Epidermal growth factor receptor variant III
ESCRT	Endosomal sorting complex required for transport
EV(s)	Extracellular vesicles
FBS	Foetal bovine serum

FDR	False-discovery rate
FTY720	2-Amino-2-[2-(4-octyl-phenyl)-ethyl]-propane-1,3-diol hydrochloride, Fingolimod hydrochloride
Gg	Gigabase
GO	Gene ontology
GW4869	N,N′-Bis[4-(4,5-dihydro-1H-imidazol-2-yl)phenyl]-3,3′-p-phenylene-bis-acrylamide dihydrochloride
HCS	High-content screening
HD	Huntington disease
hnRNP	Heterogeneous nuclear ribonucleoprotein
hnRNPA2B1	Heterogeneous nuclear ribonucleoprotein A2/B1
hnRNPC1	Heterogeneous nuclear ribonucleoprotein C1
hnRNPK	Heterogeneous nuclear ribonucleoprotein K
hnRNPQ (SYNCRIP)	Heterogeneous nuclear ribonucleoprotein Q/ Synaptotagmin binding cytoplasmic RNA interacting protein
HuR	Human antigen R
IGF2BP1	Insulin-like growth factor 2 mRNA-binding protein 1
ILV	Intraluminal vesicle
kDa	Kilodalton
LC-MS/MS	Liquid chromatography tandem mass spectrometry
LDELS	LC3-dependent EV loading and secretion
lncRNA	Long non-coding ribonucleic acid
LOD	Logarithm (base 10) of the odds ratio
MAP1LC3B (LC3)	Microtubule associated protein 1 light chain 3 beta
MDS	Multidimensional scaling
MET	Mesenchymal-to-epithelial transition
miRNA	Micro ribonucleic acid
mRNA	Messenger ribonucleic acid
MVB	Multivesicular body
MVE	Multivesicular endosomes
MVP	Major vault protein
NMWL	Nominal molecular weight limit
NSM	Neutral type II sphingomyelinase
nt	Nucleotide
NTA	Nanoparticle tracking analysis
OOPS	Orthogonal organic phase separation

OPP	O-propargyl-puromycin
ORA	Overrepresentation analyses
$P2X_7$	Purinergic receptor P2X 7
*P*adj./Adj*P*	Adjusted *P*-value
PBS	Phosphate buffered saline
PCA	Principal component analysis
PCR	Polymerase chain reaction
PD	Parkinson's disease
pH	Potential of hydrogen (historically)
piRNA	Piwi-interacting ribonucleic acid
Poly(A)	Polyadenylated
pre-mRNA	Precursor messenger ribonucleic acid
PTM	Post-translational modification
qPCR	Quantitative polymerase chain reaction
RBP	Ribonucleic acid-binding protein
RIPA	Radioimmunoprecipitation assay
RNA	Ribonucleic acid
RNP	Ribonucleoprotein
ROCK	Rho-associated protein kinase
rRNA	Ribosomal ribonucleic acid
RWD	Relative wound density
SDS	Sodium dodecyl-sulfate
SDS-PAGE	Sodium dodecyl-sulfate polyacrylamide gel electrophoresis
SEC	Size exclusion chromatography
shRNA	Small hairpin ribonucleic acid
SMase	Sphingomyelinase
SMPD1	Sphingomyelin phosphodiesterase 1 (Acid sphingomyelinase)
SMPD2	Sphingomyelin phosphodiesterase 2 (Neutral sphingomyelinase)
SMPD3	Sphingomyelin phosphodiesterase 3 (Neutral sphingomyelinase II)
snoRNA	Small nucleolar ribonucleic acid
snRNA	Small nuclear ribonucleic acid
snRNP	Spliceosomal small nuclear ribonucleoprotein complex
SRP	Signal recognition particle

SUMO	Small ubiquitin-like modifier
TEM	Transmission electron microscopy
TFF	Tangential flow filtration
TIC	Total ion current
TLR7	Toll-like receptor 7
TME	Tumour microenvironment
tRNA	Transfer ribonucleic acid
TSG101	Tumor susceptibility 101
V-SSC	Violet side scatter
vtRNA	Vault ribonucleic acid
XRNAX	Protein-cross-linked RNA eXtraction
YBX1	Y-box binding protein

Acknowledgements

First, I would like to express my immense gratitude to my supervisor, Dr. Eric Lécuyer, for gifting me with the opportunity to work in his lab. Eric, I leave your lab a better scientist than I ever was. Your constant support, encouragement, and kindness allowed me to grow and flourish over the years. I will always be grateful for the supportive environment that you have fostered in your lab. This has truly been a life-altering experience for the better.

Thank you to my thesis committee members: Dr. Janusz Rak, Dr. Nada Jabado, Dr. Artur Kania, and Dr. Martin Sauvageau. Your guidance and encouragement were invaluable to the completion of this thesis.

Thank you to all the members, both past and present, of the Lécuyer Lab for their support and friendship over the years. It was truly a privilege to work alongside such wonderful and talented scientists. I have learnt so much from all of you, for which I am eternally grateful. Thank you to Xiaofeng (Andy) Wang and Dr. Fabio Lefebvre for their support during the early days. Andy, thank you for teaching me with kindness and patience. Fabio, thank you for your cheerful disposition and for all the encouragement as I transitioned into the world of EVs. Thank you to the amazing Dr. Eunjeong Kwon. EJ, I am forever grateful for your constant kindness and unwavering assistance all these years. Your guidance, advice, and resourcefulness have contributed significantly to my development as a scientist. Thank you to Dr. Seda Barutcu, Dr. Jonathan Boulais, and Dr. Louis Philip Benoit Bouvrette for their enormous contributions in making sense of the transcriptomic and proteomic data over the years.

Thank you to my colleagues, and dear friends, Philippe Jolivet, Dr. Neera Sriskandarajah, Dr. Dhara Patel, Carolina Aguilar, Samantha Bovaird, Yiran (Judy) Chen, Easin Syed, and the many others, who have made this adventure so much better. Thank you for always providing a compassionate ear and going the extra mile whenever I needed your support. I will never forget all the wonderful memories together: outings,

lunches, reunions, hikes, coffee dates, and the list goes on. Your friendship lifted me up from dark places more times than I can count, and for that I am forever indebted.

Thank you to members of Janusz Rak's lab for their guidance over the years. Dr. Dongsic Choi, thank you for your excellent training in the isolation and characterization of EVs. You truly provided the foundation for the beginning of my exploration of EV biology. Thank you also to Laura Montermini, your technical advice was invaluable.

Thank you to my student interns: Pier-Luc Goupil, Katia Hitache, Jonathan Besna, and Ludovic Malet for their invaluable help throughout the various stages of my Ph.D. studies.

Thank you to the *Institut de Recherches Cliniques de Montréal* (IRCM) for providing me with necessarily tools and support to acquire a world-class scientific training. Additionally, I thank the IRCM's Molecular Biology and Functional Genomics; Mass Spectrometry and Proteomics; and Bioinformatics platforms, as well as McGill University's Facility for Electron Microscopy Research. Their scientific expertise and technical knowhow were essential in the furtherance of my scientific endeavours. I further extend my sincere gratitude to McGill University and, in particular, the Division of Experimental Medicine for their steadfast support from the very beginning.

Thank you to the Division of Experimental Medicine of McGill University, the IRCM (*et la Fondation de l'IRCM*), and *Les Fonds de Recherche du Québec - Santé* (FRQS) for their generous support in financing my doctoral education.

Thank you to my family and friends in Belize, Mexico, the United States, Canada, and elsewhere, who have been a constant source of love, inspiration, and reassurance. *Gracias a mi amada madre, Rosalba Antúnez de Medina, por siempre creer en mi en y por todos sus sacrificios en su búsqueda de darnos la mejor oportunidad de crecer en todos los aspectos*. Thank you to my siblings for all the love, for cheering me on, and for always believing. *Gracias a mis suegros en México, Alfonso Vargas e Irma Tena, me siento muy afortunado de tener su apoyo y amor*. Thank you to my amazing *tía*, Dunia

Méndez, you are the best teacher I ever had; your love will always stay with me. *Gracias a mi abuela, Angelita Young, por todo lo que hizo por mí, siempre la llevaré en mi corazón*. *Finalmente, gracias a mi amado esposo, Alfonso Vargas. Poncho: nunca pararé de estar agradecido contigo por haberme acompañado, incondicionalmente, en esta larga aventura de estudios de posgrado, maestría y doctorado, en dos diferentes países. Eres una persona realmente extraordinaria y soy muy afortunado en tenerte*.

Contribution to Original Knowledge

My doctoral thesis makes the following contributions to the field of EV biology:

In **Chapter II** of this thesis, we investigated the contributions of sphingolipid metabolism by neutral and acid sphingomyelinases on the export of RNAs and proteins from cells through extracellular vesicles (EVs). We provide evidence that inhibition of neutral sphingomyelinase reduces the overall RNA content in EVs, while the inhibition of acid sphingomyelinase directly affects the diversity of RNAs detected in EVs. Next, we identified the unique contributions of both metabolic pathways on the proteomic composition of EVs, describe the specific EV cargoes affected by the inhibition of each, and comment on the possible intracellular machineries that associate with each pathway. Furthermore, we show that neutral sphingomyelinase is essential for the EV-mediated export of RBPs from cells, along with their binding partners. Importantly, we demonstrate that protein modules involved in RNA regulation are exported through sphingomyelinase-driven pathways. Finally, we demonstrate that sphingomyelinase inhibition can alter the intercellular communication potential of EVs, resulting in different phenotypic impacts on recipient cells. This research provides the novel findings on the role of lipid metabolism during the biogenesis and sorting of RNA and RBP cargoes into EVs.

In **Chapter III** of this thesis, we investigated the full-length transcriptome of polyadenylated RNAs present in EVs. We identified the diversity of full-length polyadenylated RNAs in EVs, and detected novel full-length transcripts not previously described. Next, we determined the enrichment of all transcripts relative to their parental

cells. Furthermore, we determined the proportion of identified transcripts that display their known full-length sequence. Finally, we identified transcript isoforms can exhibit preferential recruitment in EVs relative to their cells of origin. To the best of our knowledge, this research provides the first report of a long-read sequenced transcriptome of human EVs, revealing that EVs contain numerous full-length transcripts. These finding address an important open question in the field of EV biology.

Contribution of Authors

CHAPTER I: Introduction

Juan Carlos A. Padilla Antúnez performed the literature review and wrote the introduction of this thesis. He designed and generated all figures presented in this chapter. Figures 1.1, 1.2, and 1.4 were generated with BioRender.com. Figure 1.5 is reproduced from a review article he co-first authored with Samantha Bovaird and Dhara Patel (DOI: 10.1002/1873-3468.13228).

CHAPTER II: Impact of Inhibiting Sphingolipid Metabolism on the EV-Mediated Export of RNAs and RNA Binding Proteins From Cells

Juan Carlos A. Padilla Antúnez, Jonathan Boulais, Seda Barutcu, Yiran Chen, Eunjeong Kwon, Eric Lécuyer

Juan Carlos A. Padilla Antúnez designed and performed the experiments described in this chapter. He developed, optimized, and implemented the tissue culture and extracellular vesicle (EV) isolation pipelines, EV-inhibitor treatments, nanoparticle tracking analysis, transmission electron microscopy, single vesicle nanoflow cytometry, EV-labelling approaches, scratch wound assays, protein synthesis assays, cell proliferation assays, high-content screening microscopy, and preparation of samples for RNA-sequencing and liquid chromatography tandem mass spectrometry (LC-MS/MS). Western blots were generated by Eunjeong Kwon. Yiran Chen provided significant assistance in performing EV isolations and characterizations. The IRCM's Molecular

Biology and Functional Genomics platform performed the RNA-sequencing. The IRCM's Mass Spectrometry and Proteomics platform performed the LC-MS/MS. The RNA-sequencing analysis pipeline was developed and implemented by Seda Barutcu. The RNA-sequencing data was analysed by Seda Barutcu with support by Juan Carlos A. Padilla Antúnez. The proteomics analysis pipeline was developed and implemented by Jonathan Boulais. The proteomics data was analysed by Jonathan Boulais with support by Juan Carlos A. Padilla Antúnez. All other data was analysed by Juan Carlos A. Padilla Antúnez. Eunjeong Kwon provided critical feedback in experimental design and interpretation of results. Eric Lécuyer conceived the project and provided critical guidance at all levels of experimental design, implementation, analysis, and interpretation of data. Juan Carlos A. Padilla Antúnez wrote the manuscript and compiled all figures. All authors provided significant feedback and guidance during the analysis of data and writing of the manuscript.

CHAPTER III: Profiling the Full-Length Transcriptome of Extracellular Vesicles With Oxford Nanopore Sequencing

Juan Carlos A. Padilla Antúnez, Seda Barutcu, Ludovic Malet, Virginie Calderon, Eunjeong Kwon, Eric Lécuyer

Juan Carlos A. Padilla Antúnez and Seda Barutcu designed the experiments. Juan Carlos A. Padilla Antúnez optimized, and performed all experiments described in this chapter. He performed the tissue culture and extracellular vesicle (EV) isolation, prepared all samples for nanopore RNA-sequencing, performed quality control steps, generated the nanopore RNA-sequencing libraries, and sequenced all samples. Bioanalyzer profiles

were generated by the IRCM's Molecular Biology and Functional Genomics platform. The RNA-sequencing analysis pipeline was developed and implemented by Seda Barutcu. Additional analysis support was provided by Ludovic Malet and Virginie Calderon of the IRCM's Bioinformatics platform. The RNA-sequencing data was analysed by Seda Barutcu and Gabrielle Deschamps-Francoeur, as well as Ludovic Malet and Virginie Calderon from the IRCM's Bioinformatics platform with support by Juan Carlos A. Padilla Antúnez. Eunjeong Kwon provided critical feedback in experimental design and interpretation of results. Eric Lécuyer conceived the project and provided critical guidance at all levels of experimental design, implementation, analysis, and interpretation of data. Juan Carlos A. Padilla Antúnez wrote the manuscript and compiled all figures. All authors provided significant feedback and guidance during the analysis of data and writing of the manuscript.

CHAPTER IV: General Discussion

Juan Carlos A. Padilla Antúnez performed the literature review and wrote the general discussion chapter.

Additional Contributions Not Included in This Thesis

1. Bovaird, S.*, Patel, D.*, **Padilla, J. C. A.*** & Lécuyer, E. (2018). *Biological functions, regulatory mechanisms, and disease relevance of RNA localization pathways*. **FEBS Letters**, 592(17), 2948-2972. (*Co-first authored)
2. **Padilla, J. C. A.**, Chin, A., Patel, D., Wang, X., Jolivet, P., & Lécuyer, E. (2021). *RNA Interference (RNAi) Screening in Cultured Drosophila Cells*. In **Mapping Genetic Interactions** (pp. 97-112). Humana, New York, NY.

Chapter I:

Introduction

Review of the Literature

1.1. Introduction

Intercellular communication refers to the diverse mechanisms utilized by cells to communicate with one another, a process which is mediated via the transfer of molecular signals from one cell to the next. This exchange of information requires a variety of processes/ mechanisms, which can arise individually or in coordinated response to the physiological state of the cells or in the context of disease [1, 2]. This type of transmission of molecular instructions is utilized as a response to the cell's constantly changing microenvironment, and it results in the maintenance of homeostasis or the progression of pathological states [1-4]. Classically, intercellular communication has been thought to be mediated by two general mechanisms: one driven by soluble biochemical species, such as hormones and cytokines, and a second which is enabled by direct cell to cell contact such as cellular junctions [1, 3]. More recently, however, a group of membrane-bound nanoparticles known as extracellular vesicles (EVs), have come to the forefront as novel mediators of the exchange of biological cargoes between near and distant cells [1, 2, 5]. Most cell types, both eukaryotic and prokaryotic, have so far been shown to release EVs and thus the secretion of these particles is conserved throughout evolution [6, 7].

Elucidating the biological role of EVs is an emerging area of research, with an exponentially growing body of literature pointing to the specialized roles that they play in the intercellular exchange of information [8-14]. EVs represent a collection of cell-secreted lipid-bilayer nanostructures of a spherical shape, which encompass diverse biological origins. The designation 'EV' is therefore an umbrella term for a highly

heterogenous group of vesicles of extracellular nature. Indeed, this inherent heterogeneity has hindered their characterization, and thus their manipulation [15]. Initially thought of as a means for the cell to dispose of unwanted materials, there is an ever-growing body of evidence demonstrating that these nanoparticles are more than just a means of waste disposal mechanism [15-17]. This redefinition to an effector role has been largely attributed to their capacity to act as vehicles, shuttling an array of bioactive molecules: lipids, proteins, metabolites, and nucleic acids from one cell to the next

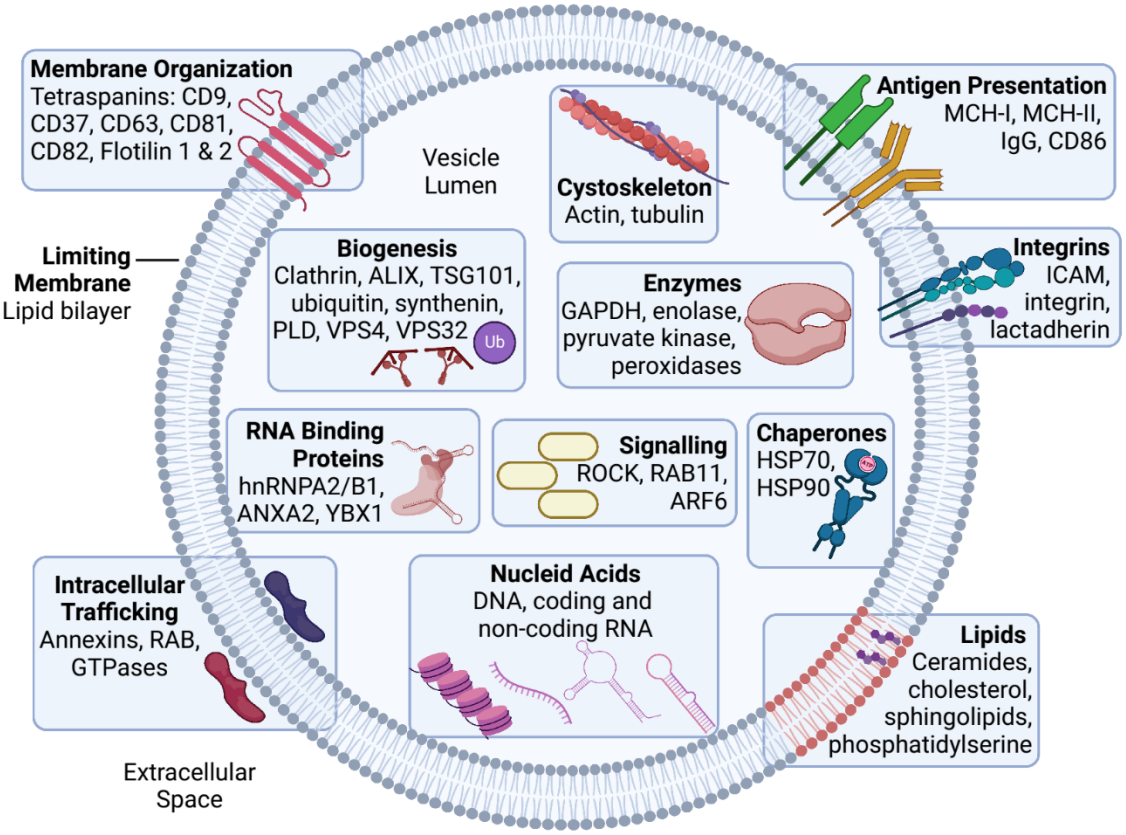

FIGURE 1.1 Diagrammatic representation of the general components and physical characteristics of extracellular vesicles (EVs). EVs are cell secreted lipid bilayer nanoparticles containing a variety of molecular cargoes including lipids, nucleic acids (RNA, DNA), their binding partners (RBPs), signalling molecules, enzymes, and other structural components. Depending on their mode of biogenesis, EVs may present a diversity of different architectural elements and bioactive factors. These features are incorporated through regulated sorting mechanisms, and they directly dictate the fate and function of EVs upon their release from cells to the extracellular space.

(**Figure 1.1**) [18]. Upon release from their cells of origin, EVs have the capability to travel through the extracellular environment over both short and long distances, then fuse with and deliver their contents to recipient cells. These contents are then able to induce phenotypic changes, which alter the behaviour of recipient cells as a response to normal homeostatic processes or because of pathological conditions [15, 18-21]. Reports about their involvement in cancer, for example, have begun to shed light on their participation in the induction of tumour formation via the transfer of oncogenic signals that stimulate cell proliferation, angiogenesis, and metastasis [22-27]. Because of EVs' unique abilities, diverse composition, innate heterogeneity, and diverse cellular origins, one can presume that their role in cell-cell communication may be vast and is only beginning to be unravelled.

1.2. A Short History of Extracellular Vesicles

While the experiments that definitively described EVs as unique structures with biologically relevant properties were first carried out in the 1980s and 1990s, there exist reports which can be retrospectively interpreted as hinting at the existence of these entities dating before the 20th century (reviewed elsewhere by Hargett and Bauer, 2013) [28, 29]. These early studies focused on the investigation of blood coagulation, and over the next centuries would lead to the discovery of what we now call EVs (**Figure 1.2**). The first reports in which EVs were isolated can be attributed to experiments performed by Erwin Chargaff and Randolph West in the 1940s, which demonstrated that high speed sedimentation (31,000 × *g*) of plasma supernatant not only shortened its clotting time, but that this clotting activity could be attributed to a 'particulate fraction' which sedimented at

this speed [30, 31]. These observations can be construed as the beginning of EV biology in the modern sense; however, it would be more than 20 years before another scientist, Peter Wolf, would put a face to this particulate material [32]. Using electron microscopy, Wolf showed that these particles – which he described as 'platelet dust' – had a diameter of 20 to 50 nm, and that they displayed a density of 1.020 to 1.025 g/mL [32]. In a 1971, further images of these particles were published by Neville Crawford. He demonstrated that these particles, which had been isolated from platelet-free plasma, contained lipids and that they carried ATP and proteins as cargoes. He called these particles 'microparticles' [33]. These ground-breaking studies provided the first sets of experimental data pointing to the existence of cell-free nano-entities of possible biological relevance.

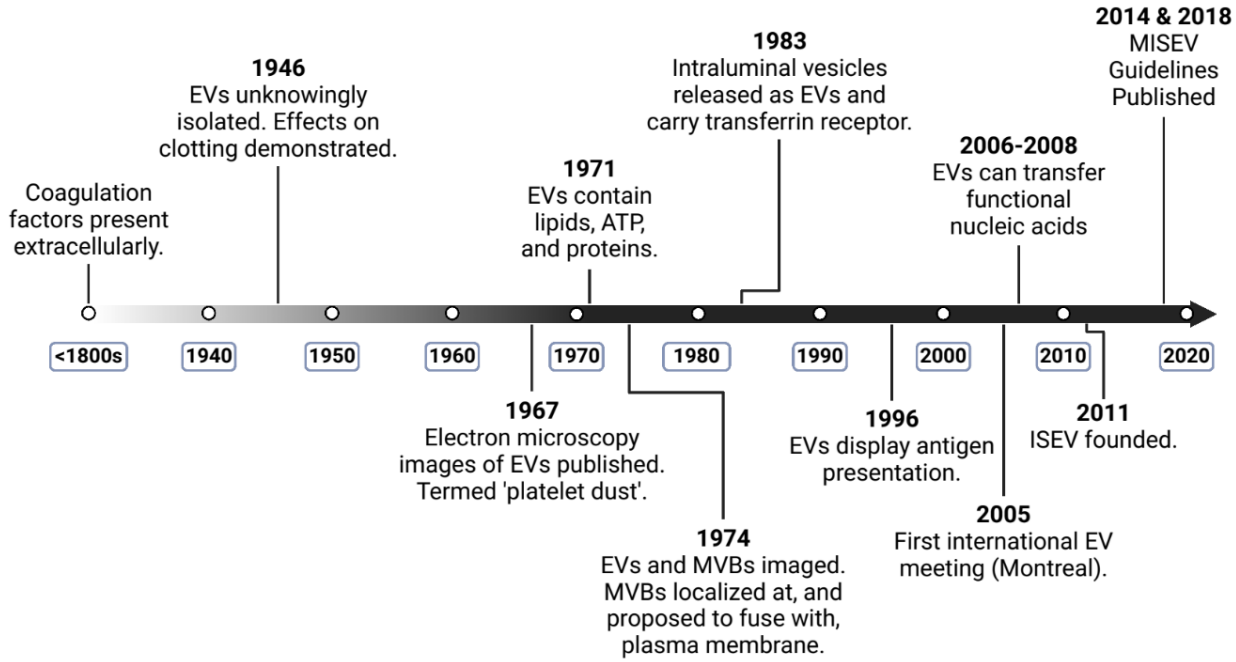

FIGURE 1.2 Timeline of selected landmark achievements in the field of EV biology. From coagulation factors to critical players during intercellular communications, the field of EV biology has a long history. While the field took a more formal shape at the beginning of the 1980s, its major phases of expansion have taken place over the last 15 years.

In the 1960s and 1970s, multiple electron microscopy studies provided further happenstance evidence to the existence of nanostructures consistent with EVs [34-37]. As an interesting development, in 1974 Núñez *et al*. reported on the presence of 'extracellular vesicles' in the thyroid glands of bats during awakening from hibernation and further showed that multivesicular bodies (MVBs) exhibited a localization to the apical plasma membrane [37]. Moreover, they proposed that these MVBs may fuse with the plasma membrane, releasing their vesicles [37]. In 1975, Albert J. Dalton published a paper detailing the presence of 'microvesicles' in foetal bovine serum (FBS), and further, provided evidence that similar structures were present in a suspension culture of human lymphoblastoid cells [38].

From the 1980s to the end of the millennium, various expansions in the field laid the foundation to a more detailed understanding of the biology of EVs. In 1983, two seminal studies were published describing the release of intraluminal vesicles during reticulocyte maturation, resulting in the loss of the Transferrin Receptor [39, 40]. Later, Rose Johnstone would propose the term 'exosomes' to describe these vesicles [41]. In 1991, Johnstone would go on to publish a study that indicated that exosomes may be utilized by cells as a way to rid themselves of transmembrane proteins that they no longer needed [17]. This idea of EVs serving only as a mechanism of waste disposal would propagate globally for the next decade [29]. Nevertheless, many important strides were made in the understanding of the biology of EVs, including: evidence for the diffusion of proteins across vesicle membranes [42], the presence and activity of flippases [43], the discovery of several important structural components (Rab, ARF, tetraspanins) [44, 45],

the presence of active enzymes [46, 47], and the altered number of EVs in the context of disease [48-50]. In the late 1990s, two landmark studies were published which presented the potential of harnessing EVs as anti-tumoral vaccines [51, 52]. These marked a turning point in the field, as they provided evidence that EVs could act as agents able to directly influence recipient cells.

In the first decade of the 21st century, many important contributions were made to the field of EV biology. These included the first descriptions of the EV proteome and lipidome [53-56], the role of EVs in the immune system [57, 58], the EV-mediated transfer of functional nucleic acids [59-61], and the ability of tumour cells to 'share' oncogenic proteins [62]. Moreover, a growing body of evidence has highlighted EVs as potential sources of biomarkers in a variety of pathological ailments, and many recent reviews have been written about the topic [63-68]. The growing body of literature pointing to the significant roles that EVs may play in the biology of cells, their possible use as delivery systems, and their significance as biomarkers has catapulted the field into the mainstream scientific consciousness. As a testament to the overwhelming interest in EVs, the number of articles in PubMed mentioning the term 'extracellular vesicles' (or exosomes, microvesicles, oncosomes) has grown from under 6,000 by 2009 to over 44,600 at the time of this writing. A timeline of selected landmark achievements is show in **Figure 1.2**.

1.3. Biogenesis and Classification of Extracellular Vesicles

The biogenesis of EVs is multifaceted, involving multiple intracellular compartments and different regulatory pathways [15]. As a result, the term 'EV' is quite

generic and only describes an ever-expanding heterogenous population of cell-secreted nanoparticles that are delimited by a membrane composed of a lipid bilayer. This has, of course, made it very difficult to study EVs as a group, and much more so specific subpopulations of them [15, 69]. Adding further complexity, many different names have been used to describe EVs in the literature, particularly in the early years, and in many cases EVs were assigned names based on their cells of origin (e.g. synaptic vesicles, dexosomes, prostasomes) [69]. Nevertheless, significant advances have been made in the field to better define subpopulations of EVs through concerted efforts via the use of biochemical, immunological, electron microscopy, and *omics* approaches to name a few. The categorization of EVs is multifactorial, being broadly defined by their biogenesis process, size, and functions [70]. Currently, EVs can be classified into two main categories: exosomes and microvesicles (shedding bodies). However, the term shedding bodies may also apply to apoptotic bodies formed upon programmed cellular death [7, 70, 71].

The classification of EVs has been largely hindered due to numerous limitations in the current methods used to isolate them, both from tissue culture supernatants and other biofluids, resulting in a heterogenous of EVs population of unknown origin [72, 73]. Furthermore, the overlapping size ranges, similar morphological features, and diversity in content make precise nomenclatures a herculean task [74]. Nevertheless, a number of extensive studies have been performed to identify molecular markers associated to various EV subpopulations [72, 75-77]. The defining feature of the two main categories of EVs relates to their modes of biogenesis, with each group being formed at distinct

intracellular sites (**Figure 1.3**). It must be noted, however, that both modes share common intracellular machineries and membrane-trafficking processes [15].

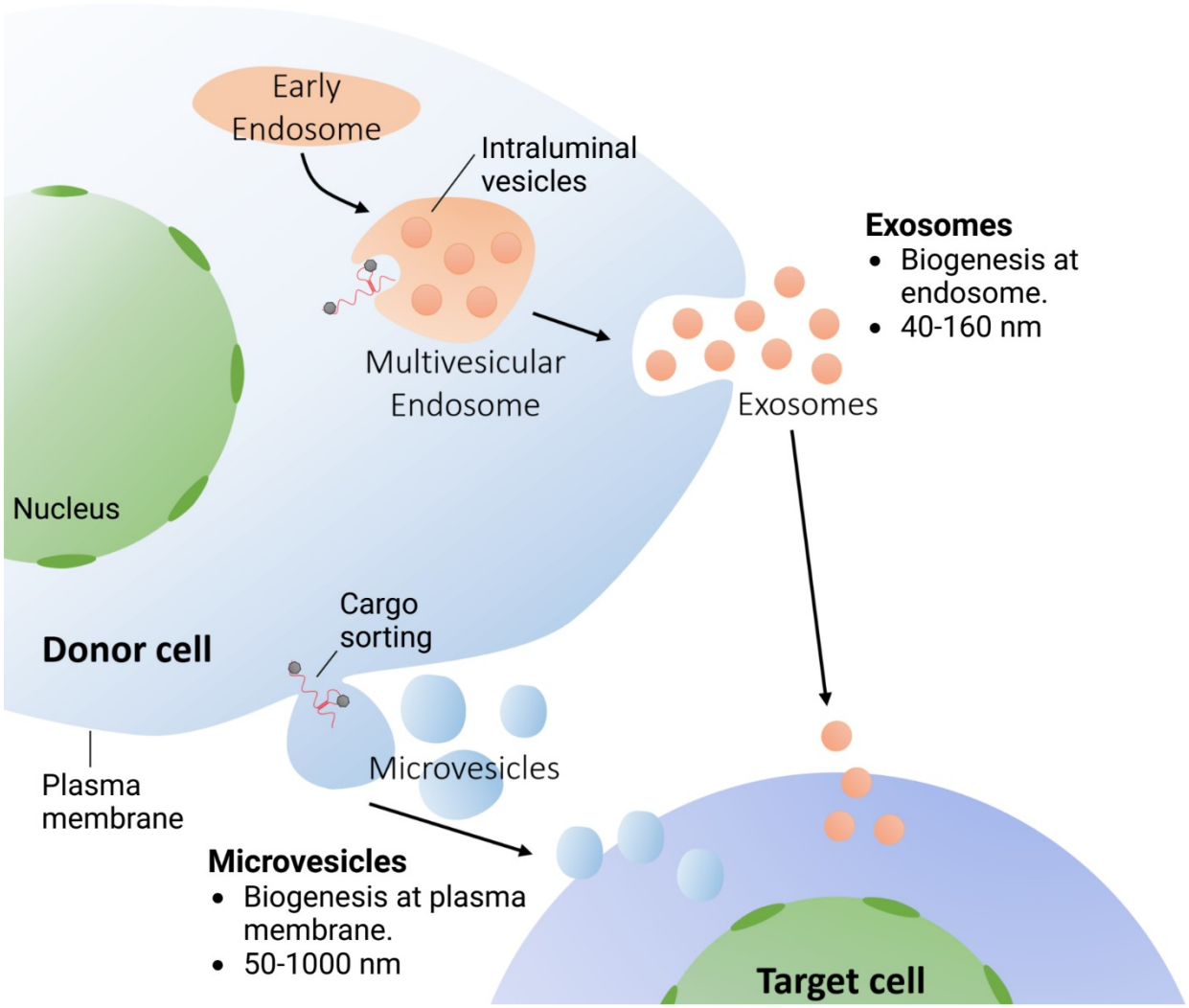

FIGURE 1.3 Biogenesis modes of extracellular vesicles. Extracellular vesicles form at distinct cellular locations, forming two major groups. Depending on their mode of biogenesis they are assigned different names and can be of distinct sizes. Nevertheless, they exhibit an overlap in size range. *Exosomes* arise from invaginations of the endosome limiting membrane, forming the intraluminal vesicle components of the multivesicular endosome (MBE). The MBE then fuses with the plasma membrane, releasing exosomes. Exosomes are typically between 40-160 nm in diameter. *Microvesicles* are generated at the plasma membrane. They arise from the outward budding and fission of the plasma membrane. Microvesicles are typically between 50-1000 nm in diameter.

1.3.1. The Biogenesis of Exosomes

Exosomes are a class of intraluminal vesicles of about 40-160 nm in diameter, which arise from the inward budding of the endosomal compartment, leading to formation of intraluminal vesicles (ILVs) during the maturation process of multivesicular endosomes (MVEs). These MVEs are then able to fuse with the cell membrane via association with actin, microtubules, and related molecular motors, thus leading to a release of their contents (EVs) into the extracellular environment (**Figure 1.3**) [15, 70]. Exosomes are generated by inward invaginations occurring on the limiting membrane of the endosomal compartment, and this process can be driven by different mechanisms and sorting machineries. These machineries are intricately involved in both the sorting of cargoes, as well as the mechanical processes driving the budding and fission of these invaginations into the lumen, thus forming ILVs [70]. The driving processes behind these invaginations involve two main mechanisms, the endosomal sorting complex required for transport (ESCRT)-dependent and the ESCRT-independent pathways. As the name implies, the ESCRT-dependent pathway relies on the activity of ESCRT-associated machineries. The ESCRT-independent pathways, on the other hand, require the enzymatic metabolism of sphingolipids by sphingomyelinases or the activity of transmembrane tetraspanins (**Figure 1.4**) [7, 15, 70].

During ESCRT-dependent EV biogenesis, the ESCRT complex acts in a stepwise fashion, with the various components acting in concert, one after the next. First, ESCRT-0 and ESCRT-I subunits gather ubiquitylated transmembrane proteins found within the

limiting membrane of the endosome, and then associated with ESCRT-II, recruit ESCRT-III which control the budding and fission of the microdomain [15, 78-80]. Other accessory proteins have also been implicated in this pathway including popular EV-markers such as Syntenin and ALIX, which act to bridge cargoes [81]. Additionally, exosomes may be generated through the metabolism of sphingomyelin by Neutral type II sphingomyelinase (NSM) (encoded by *SMPD3*), which converts the sphingolipids present in the limiting membrane of the endosome to ceramide and phosphorylcholine [82]. The accumulation of ceramides leads to the formation of microdomains that in turn impose a negative curvature on the membrane [83]. Additionally, the resulting ceramides may be further metabolized to sphingosine-1-phosphate, which in turn activates the G_i-protein-coupled sphingosine-1-phosphate receptor necessary for the sorting of cargoes to ILVs [84]. Finally, several members of the tetraspanin protein family, including CD63, CD9, CD81, and CD82, have been implicated in ESCRT-independent formation of ILVs. They are thought to act on the formation of ILVs by acting in unison with other tetraspanins and cytosolic proteins to induce the generation of microdomains on the membrane of the endosome [85]. Moreover, these various tetraspanins have been shown to be intimately involved in the sorting of cargoes to EVs in several contexts [86-91].

1.3.2. The Biogenesis of Microvesicles

Microvesicles constitute a group of EVs shed directly from the plasma membrane of cells, and whose formation mechanisms include many components also implicated in the generation of exosomes [92, 93]. Vesicles of this type may range in size from about

50-1000 nm in diameter, in the case of microvesicles (also called microparticles or ectosomes) (**Figure 1.3**), but may up to 10 μm in diameter in the case of large oncosomes, a subtype of EVs released by cancer cells [6, 15, 70, 94]. The biogenesis of these vesicles depends on the reorganization of molecular components within the plasma

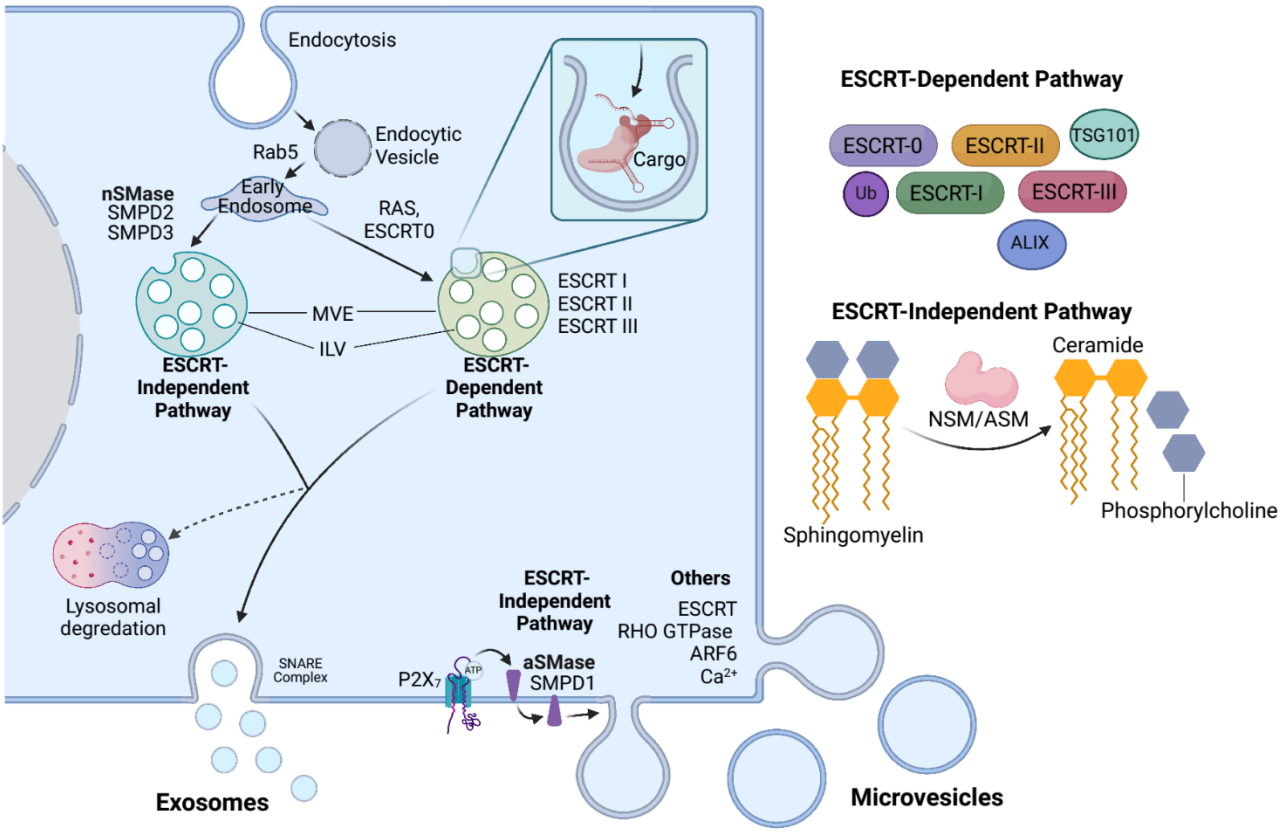

FIGURE 1.4 ESCRT-dependent and ESCRT-independent modes of EV biogenesis. Extracellular vesicles are generated through two main mechanisms. The first mechanism utilizes various machineries of the endosomal sorting complex required for transport (ESCRT). The ESCRT machineries systematically recruit each other along with other accessory factors. Membrane curvature occurs as a result of this process, followed by fission. This mechanism is known as the *ESCRT-dependent pathway*. The second mechanism employs a family of enzymes known as sphingomyelinases (NSM/ASM). Sphingomyelinases metabolize sphingolipids present in membranes to ceramide and phosphorylcholine. The resulting ceramides interact with each other and result in curvature and fission. This mechanism is known as the *ESCRT-independent pathway*.

membrane of cells, resulting in the budding and fission. These components may include changes in the protein and lipid composition, as well as levels of Ca^{2+} [95]. Indeed, several Ca^{2+}-dependent molecular machines (e.g. flippases, scramblases, Calpain) are known to drive membrane reorganization, leading to the exposure of phosphatidylserine at the membrane's outer leaflet, and resulting in a physical curving that favors budding and fission [62, 96]. Mutations in Anoctamin 6 (ANO6), a transmembrane protein associated with lipid scramblases, has been shown to partially abrogate the release of microvesicles, however microvesicles may still be released even when lipid asymmetry is maintained [96, 97]. Regulators of actin dynamics, such as members of the Rho family of small GTPases and the Rho-associated protein kinase (ROCK) have also been shown to regulate microvesicle production in certain cancer cells [98]. Additionally, microvesicle shedding can arise from actin and myosin interactions followed by ATP-dependent contractions in cancer cells [99].

Acid sphingomyelinase (ASM) (encoded by *SMPD1*) has been reported as contributing to the budding of microvesicles from the plasma membrane (**Figure 1.4**) [82, 100]. ASM is an enzyme typically associated with the lysosome, but also commonly found in the plasma membrane as a result of the fusion of the lysosome to membrane [101]. In cells that express $P2X_7$, an ATP receptor, ASM is thought to induce the microvesicle formation upon the receptor's activation. After activation, an Scr-protein tyrosine kinase can interact with $P2X_7$ leading to the rapid phosphorylation of P38 MAP kinase, and as result the translocation of ASM to the outer leaflet of the plasma membrane [56, 102-104].

Once there, ASM is able to convert sphingolipids extracellularly and the resulting ceramides perturb the membrane curvature as previously described with NSM [105].

1.4. Cargo Sorting to Sites of Extracellular Vesicles Biogenesis

The cargoes present in EVs are specific to their cells of origin, the physiological state of the cells, their modes of biogenesis, and the stimuli that drive their production [95]. All of these conditions also reflect on their associated components, and their relative abundance in the extracellular milieu [106]. Their cargoes, as previously noted, are also highly involved in their biogenesis processes and act in an overlapping fashion at different intracellular locations. For instance, the ESCRT machinery plays a critical role in both the membrane rearrangements required for the formation of ILVs, as well as the sorting of ubiquitylated proteins into invagination pockets during EV formation [70, 107].

Despite the varied efforts to understand the sorting of cargoes to EVs, the mechanisms utilized by cells remain an enigma [108, 109]. Studies investigating the nature of the cargoes present in EVs have shown that some proteins require post-translational modifications (PTMs), such as ubiquitylation, in order for sorting to be carried out by ESCRT machineries, tetraspanin microdomains, and associated components [110, 111]. In fact, the ubiquitous detection of PTMs in protein cargoes of EVs is well documented and numerous common types have been identified [111]. Their abundance provides an interesting paradigm as they can act as critical tools required for the rapid regulation of membrane plasticity, and sorting of components in and out of EVs. PTMs identified in EV cargoes include ubiquitylation [112-114], SUMOylation [115-117],

deamination [118], glycosylation [119], and phosphorylation [119, 120] among others. Other, previously not considered, machineries may also be necessary for EV sorting to occur. For instance, a recent study demonstrated that the autophagy-related protein MAP1LC3B (LC3), typically associated with lysosomal degradation, is involved in the packaging of RNA binding proteins (RBPs) and small non-coding RNAs into EVs (termed LC3-Dependent EV Loading and Secretion (LDELS)) [121]. This development highlights the alternative routes that the cell may utilize to sort cargoes for release outside the cell.

1.4.1. RNA Sorting to Sites of Extracellular Vesicle Biogenesis

RNAs represent a fascinating group of cargoes in EVs both for their diversity, and their marked selective recruitment. Although the transcriptomic profiles of EVs broadly reflect the nature of their parental cells, they exhibit their own unique identities and enrichment for specific RNA species and biotypes [94, 122, 123]. Indeed, the RNA repertoire identified in EVs include multiple biotypes such as messenger RNAs (mRNAs), microRNAs (miRNAs), ribosomal RNAs (rRNAs), long non-coding RNAs (lncRNAs), small nuclear RNAs (snRNAs), small nucleolar RNAs (snoRNAs), circular RNAs (circRNAs), transfer RNAs (tRNAs), vault RNAs (vtRNAs), Y-RNAs, and Piwi-interacting RNAs (piRNAs) [60, 124]. This diversity in RNA molecules highlights the extensive pathways they may affect, and their incorporation into EVs may serve as a protective and efficient mechanism for transferring these genetic signals to recipient cells by preventing their degradation [125, 126]. The distinctive transcriptomic identity of EVs relative to their

parental cells, therefore, demonstrate that specific RNA sorting mechanisms underly their recruitment to sites of EV biogenesis.

Cellular asymmetry is an important and pervasive feature in cells, as it permits them to organize their components into discreet compartments [127]. One of the instruments used by cells to organize their genetic products involves the subcellular localization of RNA molecules, a tightly regulated process that modulates the distribution of RNAs from their sites of transcription to specific locations inside the cell and beyond [128]. This subcellular targeting of RNA molecules is a highly conserved layer of gene regulation that is typically mediated by *cis*-regulatory motifs (CRMs) intrinsic of the RNA molecules, which are recognized by *trans*-acting RBPs. These ribonucleoprotein (RNP) complexes then dictate the localization route and local delivery of RNA molecules (**Figure 1.5**) [127-130]. The mechanisms involved in the recruitment of RNAs to sites of EV biogenesis are intricate and require interplay of different molecular machineries, including the formation of RNPs [109, 131]. In recent years, it has become increasingly evident that RBPs play a major role in the enrichment of RNAs into EVs. Furthermore, sequence features of the RNA, such as RNA sequence motifs, have been shown to be important for EV targeting. In fact, several studies have identified unique RNA motifs involved in the association of RNAs to individual RBPs [131], and a recent study identified various sequences in microRNA that determined their release via EVs or their retention in cells [132]. These findings confirm that RNA-RBP interactions can determine the loading of specific RNA species into EVs.

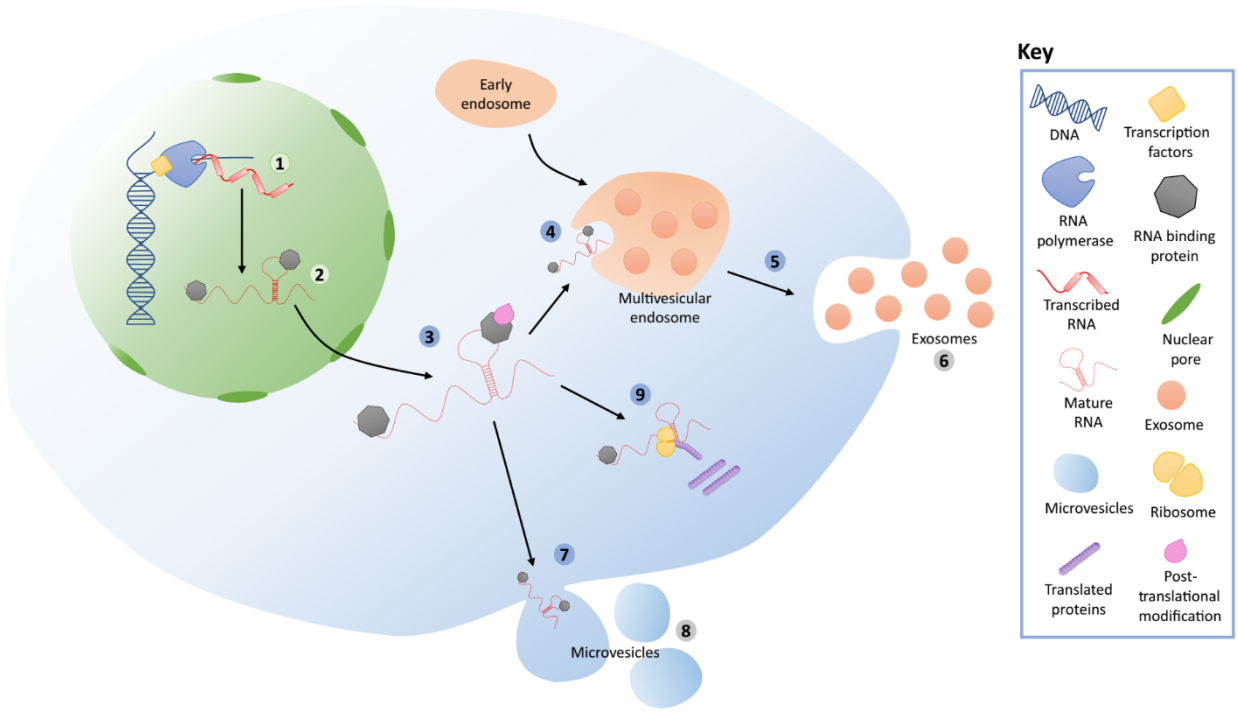

FIGURE 1.5 RNA localization and sorting to sites of extracellular vesicle biogenesis. (1-3) RNA is transcribed from genomic DNA via RNA Polymerase II in association with transcription factors (TFs). Next, RNA-binding proteins interact with nascent RNA transcripts in various maturation processes including splicing, 50-capping, polyadenylation and folding. Following various maturation steps, mature RNA is exported from the nucleus via nuclear pores to the cytoplasmic space, where its life cycle may proceed. (4-6) Subsets of RNA transcripts are selectively recruited to sites of exosome-biogenesis via the use of post-translationally modified RBPs (e.g., SUMOylated hnRNPA2B1). These RNAs are incorporated into endosomal bodies via invagination processes that lead to the formation of intraluminal vesicles (ILVs) sequestered within multivesicular endosomes (MVEs). Next, MVEs fuse with the cell membrane and release exosomes to the extracellular space. (7, 8) Subsets of RNA transcripts are selectively recruited to sites of microvesicle-biogenesis via the use of post-translationally modified RBPs. Microvesicles or shedding bodies arise from the outward blebbing of the cell membrane. Next, a fission process leads to the release of these microvesicles to the extracellular milieu. (9) Alternatively, RNA may not be sorted to these vesicular bodies at all and is rather transported to various subcellular compartments for localized translation of their encoded proteins. Figure reproduced from Bovaird, S., **Padilla, J.C.A**. et al., *Biological functions, regulatory mechanisms, and disease relevance of RNA localization pathways*. FEBS Lett, 2018.

1.4.2. RBPs Implicated in the Sorting of RNAs Into Extracellular Vesicles

Over the years, hundreds of RBPs have been identified in reported EV proteomes. Yet, only a small number of them have conclusively been shown to be required for the EV targeting of specific RNA species [131]. One of the first RBPs described as an essential player in the sorting of RNAs into EVs was the Heterogeneous nuclear ribonucleoprotein (hnRNP) A2/B1 (hnRNPA2B1). This study revealed that a SUMOylated form hnRNPA2B1 was required for this activity to occur, and that this protein directly interacted with a GGAG motif located in the 3'-end of certain EV-enriched miRNAs [133]. Since then, numerous members of the hnRNP family of proteins have been identified as key players in the release of various RNAs via EVs. hnRNPs represent a large family of ubiquitously expressed RBPs associated with various facets of nucleic acid metabolism including: stabilization, maturation, alternative splicing, transcriptional regulation, transport, and translation regulation [134]. Their large portfolio of regulatory activities during the life cycles of RNAs has been widely reported, and their dysregulation has been implicated in a variety of diseases [134]. Perhaps not surprisingly, several members have now been identified as key players in the sorting of RNAs to EVs. These include: hnRNPC1 [135], hnRNPK [121, 136, 137], and SYNCRIP (hnRNPQ) [138]. Of these, hnRNPC1 and SYNCRIP have been linked to the exit of specific miRNAs [135, 138]. Moreover, SYNCRIP was found to recognize an EV-enriched GGCU consensus motif, and its cargoes did not overlap those of hnRNPA2B1 [138]. hnRNPK, on the other hand, has been implicated in the export of the lncRNA 9H1 during colorectal cancer progression

[136]. It has also been shown that this RBP requires LDELS for its secretion through EVs, and that this activity is dependent NSM [121].

Apart from hnRNP members, several other RBPs have been described. The Y-box binding protein (YBX1) is an RBP known to interact with a variety of non-coding RNA biotypes such as lncRNAs, Y-RNAs, miRNAs, and spliceosomal RNAs to name a few [131]. YXB1 activity has been implicated in the release of a variety of small RNA classes through EVs, including tRNAs, Y-RNAs, and vtRNAs [139, 140]. Furthermore, there is evidence that its activity may require recurrent hairpin structures found in the 3'-untranslated region (3'-UTR) of EV mRNAs [141]. Another RBP, the Human antigen R (HuR), has been shown to accelerate the release of release of miRNAs through EVs [142]. The Insulin-like growth factor 2 mRNA-binding protein 1 (IGF2BP1) is a conserved RBP, and its overexpression has linked to poor prognosis in lung adenocarcinoma [143]. IGFBP1 has been linked to the sorting of RNA cargoes to EVs release by metastatic melanoma [144]. Small hairpin RNA (shRNA) knockdown of this RBP resulted in the differential enrichment of pro-metastatic genes in the EV transcriptome. Intriguingly, the enriched motifs (A/C)AGGGG and AUGACGUA were reported as upregulated and down regulated, respectively [144]. Annexin A2 (ANXA2), a calcium-dependent phospholipid binding protein, is a non-conventional RBP known to impact the metabolism and transport of both coding and non-coding RNAs [145]. ANXA2 has been found to play an important role in the sorting of a variety of miRNAs into EVs, and its binding efficiency appears to be modulated by Ca^{2+} [146]. The Major vault protein (MVP) is an RBP component of the vault complex, which binds vtRNAs. This complex has been linked to multi-drug

resistance through as yet poorly understood mechanisms [147, 148]. The associated components form large structures which are known for shuttling small molecules and proteins from the nucleus to cytoplasm [149, 150]. Intriguingly, MVP has been detected in EVs from variety of cell lines and biological fluids [131]. In one study, silencing of this RBP has been found to reduce by ~50% the amounts of EV-derived RNAs from human epithelial cells [137]. However, it must be noted that a recent publication has found that the vault complex may be released to the extracellular space in an EV-independent manner [77].

1.5. EV RNA Molecules and Their Roles in Disease

EVs are active participants in the physiological and pathogenic states of their recipient cells. These effects are mediated by their cargoes, including RNA [18, 69, 124, 151]. Upon their release into recipient cells, the RNA cargoes are actively involved in the induction of in a variety cellular process, including phenotypic changes associated in the proliferation of diseases such as cancer [61, 151]. The idea of extracellular RNA's influence in intercellular communication has been bounced around for decades [152]. Yet, only recently has evidence emerged detailing the regulatory effects that both coding and non-coding RNA may have on recipient cells [25, 60, 109, 153, 154]. Apart from these regulatory effects on recipient cells, EV RNAs also hold great potential as biomarkers for an ever-growing list of diseases [155-159].

1.5.1. EV RNAs in Cancer

The tumour microenvironment (TME) refers to an organ-like structure composed of a dynamic collection of cancerous and non-cancerous cells actively interacting to promote the reorganization and expansion of tumours [160]. The TME is essential in tumour biology, playing key roles in tumorigenesis and response to treatment. EVs are crucial members of the TME, acting bidirectionally in the exchange of molecular signals that enhance the proliferation, migration, and invasion of cancer cells [161, 162]. Moreover, they can induce phenotypic reprogramming of non-malignant cells to enhance tumour growth [163, 164]. Numerous studies have focused on the content and biological activity of EVs in cancer, and it is becoming quite apparent that they are active agents in the progression of associated pathologies [160, 163, 164]. The nucleic acid content of EVs can therefore be used as biomarkers for a growing number of cancers [162, 165-168].

The RNA cargoes of EVs have become increasingly implicated as an important aspect of tumorigenesis. For example, oncogenic RNAs can be transferred from cancer cells to their non-malignant counterparts in the TME, changing their phenotypic behaviour [163]. In one study, mononuclear cells were converted into a leukemia-like phenotype, a process which was mediated by the transfer of *miR-146b-5p* by EVs derived from chronic myelogenous leukemia cells [169]. A rapid cell death phenotype was also recently reported as arising from the EV-based transfer of *RNY5* fragments to recipient primary cells, suggesting that these RNAs may play a role in establishing a favourable cancer

niche [131, 170]. Functional mRNAs of *EGFRvIII*, a highly tumorigenic mutant variant of the Epidermal growth factor receptor (EGFR), has been reported in EVs derived from glioblastoma cells [61]. MicroRNAs such as *miR-200*, a known regulator of the mesenchymal-to-epithelial transition (MET), and thus the promotion of metastasis, has been identified in EVs [23]. Another, *miR-181c*, known for promoting perturbations of the blood-brain barrier, and thereby aiding in brain metastases, has also been reported [171]. Other non-coding RNAs such as the lncRNA *TUC339* has been linked to tumour cell adhesion and growth [172]. Therapy resistance in cancer has also been linked to EVs, for instance cancer-associated fibroblast and adipocytes release *miR-21*-containg EVs that induce paclitaxel resistance in ovarian cancer cells, inhibiting their apoptosis [173].

1.5.2. EV RNAs in Neurodegenerative Disorders

Neurodegenerative disorders are progressive age-associated diseases causing irreversible damage to tissues of the central nervous system [174-176]. Multiple diseases can fall under this term, including amyotrophic later sclerosis (ALS), Parkinson's disease (PD), Huntington disease (HD), and Alzheimer's disease (AD). These diseases are currently augmenting as result of the extended lifespan of the aging population, as well as environmental conditions such as pollution [177]. Characteristic of these diseases is the increased necrosis and dysfunction of neuronal cells, which in turn compromises cognitive and motor functioning. Furthermore, oxidative stress caused by an accumulation of free radicals has been critically linked to the pathogenesis of such disorders [177-179]. EVs are of particular interest in neurological disorders because of

their ability to package misfolded proteins and nucleic acids associated to the progression of these diseases, moreover they have been shown to be able to cross the blood-brain barrier [180, 181]. As these diseases are typically characterized by the spread of these features, the intercellular transport of the same is to be expected.

Let-7 is a highly conserved miRNA implicated in a variety of pathological afflictions including neurodegenerative disorders [182]. This miRNA has been detected in the cerebrospinal fluid (CSF) of PD patient, and it has also been shown to be overexpressed in models of PD [183, 184]. EV-mediated release of *Let-7* in neurons has been implicated in the activation of Toll-like receptor 7 (TLR7), resulting in neurodegeneration [185]. In ALS, the differential expression of miRNAs in CSF, blood serum, and plasma of patients and healthy controls has been noted in multiple studies [186-190]. The cellular sources of these miRNAs are yet to confirmed; however, their pathogenic activity is beginning to be unravelled. In one study, astrocytes derived from ALS patients with *c9orf72* mutation were shown to release EVs containing miRNAs capable of afflicting the maintenance and survival of recipient motor neurons [191]. Abundantly expressed in the brain, *miR-125b-5p* has been shown to be upregulated in the CSF of young onset AD patients [192]. This miRNA has been implicated in a variety of processes associated with the progression of AD including tau hyperphosphorylation, and defects in associative memory [193]. Finally, given the detection of differentially expressed of circulating miRNAs in ALS patient fluids, and the non-invasive nature of these tests, EVs represent a potential source of ALS biomarkers [194, 195].

1.6. Extracellular Vesicles as Drug Delivery Vehicles

The physiological and delivery properties of EVs, as well as their ability to incorporate a diversity of cargoes, make them incredibly appealing as natural vehicles for the transport of therapeutic agents. Additionally, EVs may be isolated from a variety of cell types such as mesenchymal stem cells, which are regenerative and non-inflammatory, or red blood cells which can be easily loaded with cargoes [196-198]. EVs from other cell types, such as dendritic cells, can present antigens that can activate the immune response, making them particularly useful in the development of vaccines [199, 200]. It is no surprise then, that the selective incorporation of a wide array of gene products, including RNAs, is an emerging area of EV biology research.

The loading of RNAs into EVs can be done using two main approaches: endogenously whereby the donor cell is modulated to increase the inclusion of specific RNAs at EV-biogenesis sites, or exogenously whereby the RNAs are incorporated on a previously isolated EV population [151]. During the endogenous loading approach, cells may be altered to overexpress a particular RNA of interest increasing its incidence in the resulting EV population [201]. The RNAs may also be modified to include specific sequences recognized by RBPs known to be enriched in the EV population [202]. A variety of approaches have been tested to incorporate RNAs into EVs exogenously including electroporation [203, 204], sonication [205], the use of transfection reagents [206], and the inclusion of a lipophilic moiety [207]. However, the extent to which additional RNA can be added to purified EVs may be limited, as they are inherently already packed with other cargoes.

Aside from loading with cargoes, other biological aspects also need to be considered. These include the amounts of EVs that can be produced by donor cells, their stability, the targeting of specific cell populations, and increasing the cytosolic release of RNAs in recipient cells. As the isolation of EVs typically requires copious amounts of cells and reagents, it is imperative that cells are stimulated to produce as many EVs as possible. Depending on the context of the cells, several different approaches can be used to induce an increase in released EVs. For example, EV production can be increase by elevating the intracellular levels of Ca^{2+} via the treatment with monesin or serotonin [208, 209]. Low pH, hypoxia, and oxidative stress have also been reported as factors increasing EV release [210-212]. Increasing the targeting of EVs to specific cell population also poses a significant challenge, as previous reports have noted that EVs delivered *in vivo* are rapidly cleared by cells in the lungs, liver, spleen, and kidneys [213-215]. As such, EVs need to be re-engineered to include specific ligands such as proteins, lipid moieties, antibodies, or RNA aptamers that would improve cellular uptake in the clinically relevant cell population [216]. The cytosolic delivery of RNAs inside recipient cells poses another problem in the use of EVs as transport vehicles. This is because EVs can be accepted by cells through the endosomal pathway and, thus, may be degraded by the lysosome before their cargoes can be released [217, 218]. It has been suggested that this effect can be ameliorated by the inclusion of pH-sensitive fusion proteins in the membranes of EVs, thereby enhancing membrane fusion to the endosome luminal membrane [151]. This effect can also be bypassed by direct fusion of EVs to the plasma membrane of

recipient cells, a process which has been shown to increase with the presence of certain cargoes such as Syncytin 1 and Syncytin 2 [219].

Notwithstanding the many inherent difficulties of using EVs as drug delivery vehicles, they present a plethora of advantages over other mediums. This can include being able to be isolated from an assortment of sources, acting as protective vehicles for nucleic acids or other bioactive agents, displaying surface antigens in their membranes, and when isolated from individual patients can be immune neutral. It is no wonder then that there is an enthusiastic response to the use of EVs for the delivery of therapeutic RNAs and proteins for various clinical ailments. In fact, numerous studies have been conducted (or are on-going) both at the pre-clinical, as well as the clinical level [151]. Diseases being target with EV-mediated delivery mechanisms include Huntington disease [220], osteoporosis [221], Parkinson disease-associated neurodegeneration [202], the treatment of bone tissue defects (ClinicalTrials.gov ID NCT05520125), and COVID-19 moderate-to-severe acute respiratory distress syndrome (ARDS) (NCT05125562), among others.

1.7. Rational and Objectives

Extracellular vesicles are critical players in the exchange of information between cells. However, their heterogenous nature has made it difficult to ascertain the contributions of individual EV populations during this essential phenomenon. Although progress has been made to better define EV populations based on their modes of biogenesis, much work remains to be done in order to elucidate the key features and cargoes conferred by each.

This thesis aims to provide novel insights into the role of EV biogenesis pathways on the loading of RNA and protein cargoes for export from cells. Furthermore, it reports on the full-length transcriptome present in the heterogenous EV population.

The first objective of this thesis was to determine the role of sphingolipid metabolism on the recruitment of RNA and protein cargoes for export in EVs. As EVs can be generated through various intracellular mechanisms, we sought to explicitly investigate the role of sphingomyelinases at sites of EV biogenesis, thereby infering their roles in cargo loading. Sphingomyelin metabolism is derived from a family of enzymes including neutral and acid sphingomyelinase variants, all of which metabolize lipids to ceramide – a critical factor in the membrane remodelling mechanisms used by cells for EV generation. Interestingly, the activity of these enzyme variants can occur at the endosome or the plasma membrane. Both of these locations are contributors to two different EV populations: exosomes and microvesicles, respectively. By inhibiting these enzyme variants individually, we were able to see unique cargo features attributed to each mode of biogenesis, and in so doing provide insights into the heterogenous EV populations released by human MCF7 epithelial adenocarcinoma cells.

The second objective of this thesis was to define the full-length transcriptome of EVs. Although EV-mediated transfer of full-length functional RNAs to recipient cells has been described in various contexts, there are currently no reports on the available full-length RNAs carried by EVs. Furthermore, it has been assumed that many RNAs present within EVs may present in fragmented form. Using Oxford nanopore RNA sequencing,

we investigated the polyadenylated population of RNAs present in EVs in human K562 chronic myelogenous leukemia cells. Nanopore sequencing provides a unique platform, as it allows us to study the transcriptome of EVs in their native lengths. This allowed us to identify EV-enriched full-length RNAs, to discover novel transcripts, and to determine the population of RNAs mapping to their known full-length sequencing. This preliminary study provides a first transcriptome-level report of full-length polyadenylated RNAs, as determined by long-read RNA sequencing, present in human EVs.

Chapter II:

Manuscript I

Impact of Inhibiting Sphingolipid Metabolism on the EV-Mediated Export of RNAs and RNA Binding Proteins From Cells

Juan Carlos A. Padilla Antúnez[1,2], Jonathan Boulais[1], Seda Barutcu[1], Yiran Chen[1,3], Eunjeong Kwon[1], Eric Lécuyer[1,2,3]

1. Institut de Recherches Cliniques de Montréal, Montréal, QC H2W 1R7, Canada
2. Division of Experimental Medicine, McGill University, Montréal, QC H4A 3J1, Canada
3. Département de Biochimie et de Médecine Moléculaire, Université de Montréal, Montréal, QC H3T 1J4, Canada

2.1. Abstract

An important process in intercellular communication involves the release of membrane-bound extracellular vesicles (EVs), which can fuse with and influence other cells. These properties are conferred by the preloading of EVs with bioactive cargoes, but the means of this selective packaging remain unclear. The biogenesis of EVs is a regulated process, driven by mechanisms at specific subcellular milieus. Sphingomyelinases (SMases), which metabolize sphingomyelin in membranes, play a role in EV biogenesis. Their metabolic product, ceramide, induces invaginations at the endosome or blebbing from the plasma membrane, both important in EV-generation. Here, we sought to evaluate the impact of sphingomyelinase inhibition on EV protein and RNA cargoes. Human MCF7 cells were treated with the neutral sphingomyelinase inhibitor GW4869 or the acid sphingomyelinase inhibitor FTY720. EVs were then purified from conditioned media of control or inhibitor-treated cells and characterized by a variety of approaches including LC-MS/MS and RNA-sequencing. Ceramide inhibition result in morphological and phenotypic changes of the heterogenous EV-population. Strikingly, GW4869 resulted in a depletion of nanoparticles, as well as a reduction in EV RNA and protein content, with marked reduction in endosomal, spliceosomal and translation related proteins. Proteomics analyses revealed a reduction of the overall RNA-biding proteins (RBPs) in GW4869 treated EVs. By contrast, FTY720 treatment, which appears to reduce plasma membrane derived vesicles, elicited the opposite response, leading to a marked accumulation of RBP-associated machineries within the EV population. RNA sequencing revealed higher differential expression of RNA biotypes in FTY720 EVs. Furthermore,

FTY720 EVs induced increased cell migration and protein translation on recipient MCF10A cells. These results suggest that ceramide-dependent vesiculation represents a major route of RBP and RNA trafficking outside of the cell, via endosomal pathways.

2.2. Introduction

Most cells have the capacity to emanate signals that alter their surrounding environment. Extracellular vesicles (EVs), a heterogenous group of membranous nanoparticles, have come to the forefront as novel mediators of the exchange of biological information between near and distant cells [5, 7]. Upon release from cells, EVs can act as molecular shuttles travelling through the extracellular environment and then fusing-with and delivering molecules capable of altering the behaviour of recipient cells [19, 20].

The activity of EVs is conferred by the preloading of EVs with bioactive molecular cargoes derived from their cells of origin, of which coding and non-coding RNAs are a select regulatory class [25, 60, 109, 153, 154]. The incorporation of these RNA molecules into EVs may can serve as a protective and efficient means of transferring these genetic signals to local and distant microenvironments by preventing their degradation [125, 126]. The RNA profiles observed in EVs are indicative of, but not identical to, their parental cells, and evidence has emerged of distinct RNA profiles in subpopulations of these nanostructures [94, 122]. The mechanisms of this selective packaging are important for both the biomarker and effector functions of EVs, but they remain to be fully characterized.

The biogenesis of EVs is driven by diverse and highly orchestrated mechanisms, locally occurring within endosomal compartments and at the plasma membrane of cells. Depending on their mode of biogenesis, EVs may take on specific nomenclatures. Exosomes describe EVs arising from the inward budding of the endosomal compartment during the maturation process of multivesicular bodies (MVBs), which then fuse with the

cell membrane and release exosomes into the extracellular environment [15]. Another group of EVs, microvesicles, arise from the outward blebbing of the plasma membrane as a result of actin and myosin interactions followed by ATP-dependent contractions [99]. This process results in the fission and release of microvesicles into the extracellular space. Overlapping both of these EV subpopulations is a metabolic pathway involving sphingomyelinases, a family of enzymes able to convert sphingomyelin, a sphingolipid present in membranes, to ceramide and phosphorylcholine [82, 100, 222]. The resulting ceramides induce the formation of large microdomains which result in membrane budding and/or invaginations, and thereby, the formation of intraluminal vesicles (at the endosome) or microvesicles (at the plasma membrane).

Sphingomyelinases have been reported as important enzymes capable of metabolizing sphingolipids to ceramide and phosphorylcholine [82, 100, 222]. The role played by these enzymes in the release of EVs seems distinct, with different sphingomyelinases likely functioning at separate intracellular milieus. Neutral sphingomyelinases (NSM) have been described as acting on the exosome population birthed from endosomal networks, playing a key role in the invagination processes required for the biogenesis of intraluminal vesicles (ILV) [82]. Conversely, acid sphingomyelinase (ASM) has been reported as contributing to the budding of microvesicles from the plasma membrane [82, 100]. Several pharmacological inhibitors of sphingomyelinases have been reported in the literature, showing varying degrees of success in the abrogation of EV release [223]. GW4869, a well-known cell permeable non-competitive inhibitor of NSM, has been shown to reduce ILV formation and decrease

EV release [82, 121]. Another compound, FTY720 (Fingolimod/Gilenya®) has been reported as an inhibitor of microvesicle formation at the plasma membrane. This effect is thought to result by making ASM separate from lipid membrane, driving its proteolytic degradation [100, 222].

Due to the differing action of SMases, we sought to evaluate the impact of sphingomyelinase inhibition on EV molecular cargoes. To investigate the role of sphingomyelinase-dependent vesiculation on the EV proteome and transcriptome, we treated the human epithelial adenocarcinoma cell line, MCF7, with either GW4869 or FTY720 at doses that do not impair cell viability. EVs were then harvested from the cell-conditioned media and analysed with a variety of biochemical, phenotypic, *omics* and functional assays.

2.3. Methodology

2.3.1. Cell Culture

Human MCF7 epithelial adenocarcinoma cells were cultured in Minimum Essential Medium MEM 1x (Corning, MT10010CV) supplemented with 10% fetal bovine serum (FBS), 0.1 mM non-essential amino acids (Thermo Fisher, MT25025CI), 1 mM sodium pyruvate (Wisent, 600-110-EL), 100 U mL^{-1} penicillin and 100 µg mL^{-1} streptomycin (Wisent, 450-202-EL). The cells were grown under incubation conditions of 37 °C and humidified 5% CO_2 atmosphere.

Human MCF10A non-malignant breast epithelial cells in a 1:1 mixture of Dulbecco's Modified Eagle Medium (DMEM) (Wisent, 319-016-CL) and Ham's F12 Medium (Wisent, 318-010-CL). The media mixture is supplemented with 5% horse serum (HS), 20 ng mL^{-1} human epidermal growth factor (hEGF) (Wisent, 511-110-UM), 500 µg mL^{-1} hydrocortisone (Sigma-Aldrich, H0888-1G), 10 µg mL^{-1} insulin (Gibco, 12585014), 100 ng mL^{-1} cholera toxin from *Vibrio cholerae* (Sigma-Aldrich, C8052-.5MG), 100 U ml^{-1} penicillin and 100 µg ml^{-1} streptomycin (Wisent, 450-202-EL). The cells were grown under incubation conditions of 37 °C and humidified 5% CO_2 atmosphere.

2.3.2. Cell Culture for EV-Isolation

MCF7 epithelial adenocarcinoma cells were cultured in Minimum Essential Media MEM 1x (Thermo Fisher, MT10010CV) supplemented with 0.1 mM non-essential amino acids (Thermo Fisher, MT25025CI), 1 mM sodium pyruvate (Wisent, 600-110-EL), 100 U

ml^{-1} penicillin and 100 µg ml^{-1} streptomycin (Wisent, 450-202-EL), and 10% EV-depleted FBS (dFBS). dFBS was prepared via tangential flow filtration (TFF) using the Labscale TFF System (Millipore-Sigma) equipped with a Pellicon XL50 ultrafiltration module with a 300 kDa Ultracell membrane (Millipore-Sigma, PXC300C50).

2.3.3. Treatment of Cells With EV-Inhibitor Drugs for Purification of EVs

EV-isolation media was supplemented with either EV-inhibitor drugs or vehicle: 0.2% DMSO (Sigma-Aldrich, D8418-100ML), or 10 µM GW4869 (Sigma-Aldrich, D1692-5MG), or 5 µM FTY720 (Sigma-Aldrich, SML0700-5MG). MCF7 cells were plated overnight starting at 1.2×10^7 cells/ T-175 flask in a total of 5 flasks per condition in complete media. The following day, the media was removed, and the cells were rinsed twice with sterile PBS 1x (Wisent, 311-011-CL). The appropriate EV-isolation media was then added to each flask series and the cells were incubated for 1 h at 37°C in humidified 5% CO_2 atmosphere. Following this first incubation, the media was removed, and the cells were rinsed once more with sterile PBS 1x. The appropriate EV-isolation media was then added to each flask series and the cells were incubated for 36 h at 37 °C in humidified 5% CO_2 atmosphere. After 36 h, the cell-conditioned media was collected, along with a sample of cells. The cells were assessed for ≥90% cell viability by Trypan blue exclusion assay. The cell-conditioned media was then used for purification of EVs. All experiments were carried out in triplicates.

2.3.4. Extracellular Vesicle Isolation via Iodixanol Gradient Fractionation

EVs were purified from cell conditioned media using established methodologies [224] with a few modifications. Briefly, the collected cell-conditioned media was cleared of cells and large debris by centrifugation at 500 × *g* for 10 min, and 2000 × *g* 20 min respectively. The supernatant was collected and then concentrated by centrifugation at 2000 × *g* with a 100,000 NMWL molecular cutoff Amicon Ultra-15 Centrifugal Filter Unit (Millipore-Sigma, UFC910024) to a volume of 1.8 mL. Next, OptiPrep (iodixanol) Density Gradient Medium (Sigma-Aldrich, D1556-250ML) was used to generate a non-continuous density gradient consisting of 5% (2.5 mL), 20% (3 mL), and 30% (4.5 mL, sample) iodixanol. The density gradient was then ultracentrifuged for 2.5 h at 200,000 × *g* to separate EVs from other extracellular materials. After centrifugation, 1 mL fractions were carefully collected (10 fractions total) and then diluted in PBS 1x, followed by a second round of ultracentrifugation at 150,000 × *g* for 1.5 h to pellet EVs and other materials. All steps were performed at 4 °C. Fractions 3 to 6 were defined as EV-containing fractions, based on nanoparticle quantifications and immunolabelling with CD81 and pooled together.

2.3.5. EV Samples Preparation for Western Blotting

EVs were isolated by an immune isolation technique using the EasySep Human Pan-Extracellular Vesicle Positive Selection Kit (STEMCELL Technologies, 17891), which utilizes CD9, CD81 and CD63 antibodies. Briefly, cell-conditioned media was cleared of cells and large debris by centrifugation at 500 × *g* for 10 min, and 2000 × *g* 20

min respectively. The supernatant was collected and then concentrated by centrifugation at 2000 × *g* with a 100,000 NMWL molecular cutoff Amicon Ultra-15 Centrifugal Filter Unit (Millipore-Sigma, UFC910024) to a volume of 0.5 mL. EVs were then captured using conjugated beads with the three tetraspanin antibodies in the kit. The EV captured beads were washed and dissolved in RIPA buffer. Cell lysates were also prepared with RIPA buffer. SDS-PAGE was conducted using 10% polyacrylamide gel. For western blotting, following primary antibodies were used: anti-LaminB2 (abcam, ab151735), anti-Tsg101 (GeneTex, GTX118736), anti-CD81 (GeneTex, GTX101766). Goat anti-rabbit IgG-HRP (Jackson lab, 31460) secondary antibody was used at 1:5,000 dilution.

2.3.6. Nanoparticle Tracking Analysis (NTA)

MCF7 cells were plated in 6-well plates at an initial concentration of 600,000 cells per well and incubated for overnight at 37 °C in humidified 5% CO_2 atmosphere. The plating media was then removed and replaced with EV-isolation media containing vehicle or EV-inhibitor drugs using the approach described previously. The cells were then incubated for an additional 36 h. After the incubation period, the cell-conditioned media was recovered and it was cleared of cells and large debris by centrifugation at 500 × *g* for 10 min, and 2000 × *g* for 20 min respectively. The supernatant was collected and used for Nanoparticle Tracking Analysis (NTA) via the NanoSight NS500 (Malvern Panalytical) system. NTA was performed with the 532 nm laser by way of three 30 s recordings at 37 °C. Data processing and analysis was done using the NanoSight NTA software v3.0 (Malvern Panalytical). All experiments were carried out in triplicates.

2.3.7. Transmission Electron Microscopy (TEM)

Purified EVs were imaged by Transmission Electron Microscopy (TEM) through a uranyl acetate negative stain approach. Gradient purified EV samples from were resuspended in PBS 1x and then combined 1:1 with a 5% glutaraldehyde solution (2.5% final concentration) for fixation. 5 µL of the fixed EV samples were then loaded to previously discharged formvar-coated copper grids and allowed to adhere for 3 min. The sample containing grids were then 3 times with water and then placed in droplets of 2% uranyl acetate and incubated for 1 min. The grids were then wash 3 more times with water, blotted to remove excess water, and air dried for 30 mins. The samples were then imaged on the FEI Tecnai T12 120kV (Field Electron and Ion Company) transmission electron microscope.

2.3.8. EV Isolation via Size Exclusion Chromatography

Purification of labelled EVs was carried out using size exclusion chromatography (SEC). MCF7 cells were plated in 6-well plates at an initial concentration of 600,000 cells per well and incubated for overnight. The plating media was then removed and replaced with growth media containing dFBS and the cells were incubated for an additional 36 h. After the incubation period, the cell-conditioned media was recovered and it was cleared of cells and large debris by centrifugation at 500 × *g* for 10 min, and 2000 × *g* for 20 min respectively. The supernatant was collected and then concentrated to 100 µL via a 100,000 NMWL molecular cutoff Amicon Ultra-0.5 Centrifugal Filter Unit (Millipore-Sigma, UFC510096). The concentrated media was recovered and utilized for EV-labelling

experiments (section 2.3.9) followed by purification of EVs using SEC using qEVsingle columns (Izon Science, SP2-USD) according to the manufacturer's recommendations. Briefly, 100 µL of stained nanoparticles are loaded on the column and allowed to elute. Next, 900 µL of 0.1 µm-filtered PBS 1x is loaded and allowed to elute, for a combined 1 mL void volume. Finally, 600 µL of 0.1 µm-filtered PBS 1x are loaded and recovered as the nanoparticle-enriched fraction.

2.3.9. EV-RNA Labeling

50 µL of concentrated media was incubated with 50 µL 0.1 µm-filtered PBS containing 100 µM Syto RNASelect (Thermo Fisher, S32703) (final concentration 50 µM) at room temperature for 2 h in the dark. Next, EVs were recovered via SEC which also removed the unbound dye.

2.3.10. Nanoflow Cytometry of EVs

Nanoflow cytometry of EVs was carried out using a CytoFLEX flow cytometer (Beckman-Coulter) equipped with violet (405 nm), blue (488 nm) and red (640 nm) wavelength lasers. Acquisition and analysis of data was carried out using the CytExpert 2.4 software (Beckman-Coulter) using the parameters detailed on Table 1. The violet side scatter (V-SSC) was utilized using the 405 nm laser along with a gain of 100 on V-SSC and a threshold of 950 on the violet channel. The samples were loaded to 10 µL using a slow sample flow rate of 10 µL/min. Background signal was calculated by acquiring 0.1

μm-filtered PBS (EV suspension buffer) at the same rate. All experiments were carried out in triplicates.

Table 2.1 Parameters utilized for nanoflow cytometry using CytoFLEX

Volume to Record	10 μL	
Sample Flow Rate	10 μL/min	
Acquisition Setting	Gain	
	FSC	22
	SSC	254
	Violet SSC	100
	FITC	3000
	APC	3000
	Threshold	
	Channel	Violet
	Manual, 950>0 (Height)	

2.3.11. Sample Preparation and Protein Precipitation for LC-MS/MS

EVs were purified from MCF7 cells under the vehicle (0.2% DMSO) or drug conditions (10 μM GW4869 or 5 μM FTY20) using the gradient fractionation approach previous described. Pelleted EVs and their cells of origin were resuspended in TRIzol reagent (Thermo Fisher, 15596018) to allow for simultaneous isolation of proteins and RNA from the same samples as per the manufacturer's recommendations. Briefly, the cellular and EV samples were homogenized in 500 μL of TRIzol reagent, followed by the addition 100 μL of chloroform (VWR, BDH1109-4LG) and centrifuged at 12,000 × *g* for 15 min. Following the centrifugation step, the aqueous phase is saved for RNA isolation and the interphase and organic phase is processed for protein precipitation as described

by the manufacturer. For the extracellular vesicle samples (EV), protein extracts were re-solubilized in 20 µL of 8 M urea with vortexing on a Mixmate (Eppendorf) at 1200 RPM for 10 minutes and sonication in a water bath for 10 minutes. For the whole cell protein extracts (WC), 100 µL of 8 M urea, 50 µL of 0.1% SDS and 50 µL of acetonitrile were added to each sample. The same procedure as the EV samples was used to re-solubilize WC samples. Proteins were reduced by adding 5.0 µL (EV) or 50 µL (WC) of the reduction buffer (45 mM DTT, 100 mM ammonium bicarbonate) for 30 min at 37°C, and then alkylated by adding 5.0 µL (EV) or 50 µL (WC) of the alkylation buffer (100 mM iodoacetamide, 100 mM ammonium bicarbonate) for 20 min at 24°C in the dark. Prior to trypsin digestion, 75 µL of 50 mM ammonium bicarbonate was added to EV samples to reduce the urea concentration under 2 M for the digestion step. For the WC samples, 175 µL of 50 mM ammonium bicarbonate was added to reduce the urea concentration under 2 M but also to reduce the concentration of SDS (0.01%) and acetonitrile (10%). 20 µL and 25 of the trypsin solution (100 ng/µL of trypsin sequencing grade from Promega) was added to EV and WC samples, respectively. Protein digestion was performed at 37°C for 18 h. Protein digests were dried down in vacuum centrifuge and stored at -20 °C until LC-MS/MS analysis.

2.3.12. LC-MS/MS

Prior to LC-MS/MS, two different sample cleaning methods were used. EV protein digests were re-solubilized under agitation for 15 min in 10 µL of 0.2% formic acid. Desalting/cleanup of the digests was performed using C18 ZipTip pipette tips (Millipore,

Billerica, MA). Eluates were dried down in vacuum centrifuge and stored at -20 °C until LC-MS/MS analysis. WC protein digests were acidified with trifluoroacetic acid for desalting and removal of residual detergents by MCX (Waters Oasis MCX 96-well Elution Plate) following the manufacturer's instructions. After elution in 10% ammonium hydroxide /90% methanol (v/v), samples were dried down with in vacuum centrifuge and stored at -20 °C until LC-MS/MS analysis. EV and WC samples were reconstituted under agitation for 15 min in 15 µL and 120 uL of 2%ANC-1%FA, respectively, and between 2 and 6 uL was loaded into a 75 µm i.d. × 150 mm Self-Pack C18 column installed in the Easy-nLC II system (Proxeon Biosystems). The buffers used for chromatography were 0.2% formic acid (buffer A) and 100% acetonitrile/0.2% formic acid (buffer B). Peptides were eluted with a two slope gradient at a flowrate of 250 nL/min. Solvent B first increased from 2 to 35% in 124 min and then from 35 to 85% B in 12 min. The HPLC system was coupled to Orbitrap Fusion mass spectrometer (Thermo Scientific) through a Nanospray Flex Ion Source. Nanospray and S-lens voltages were set to 1.3-1.8 kV and 60 V, respectively. Capillary temperature was set to 250 °C. Full scan MS survey spectra (m/z 360-1560) in profile mode were acquired in the Orbitrap with a resolution of 120,000 with a target value at 3e5. The 25 most intense peptide ions were fragmented in the HCD collision cell and analysed in the linear ion trap with a target value at 2e4 and a normalized collision energy at 29. Target ions selected for fragmentation were dynamically excluded for 30 sec after two MS/MS events.

2.3.13. Proteomics Bioinformatics Analyses

LC-MS/MS raw data were analysed with the MaxQuant software (version 1.6.17.0). MS/MS spectra were searched against the human proteome of the Uniprot database (July 10, 2020 release) supplemented with MaxQuant's contaminants option. ITMS match tolerance was set at 0.5 Da, ITMS de novo tolerance was set at 0.25 Da while deisotoping tolerance was set at 0.15 Da. A maximum number of 2 missed cleavages by trypsin was allowed with a maximum of 5 modifications per peptide. Carbamidomethylation of cysteine residues was set as a fixed modification, whereas methionine oxidation was set as variable modifications. False-discovery rate (FDR) for peptides and proteins was set at 1% with a minimum peptide length at 7 and a minimum of 1 unique peptide was required. Match between runs was enabled with a match time window of 2.5 minutes and an alignment time window of 20 minutes. Whole cell and isolated extracellular vesicles raw data were analysed separately. MaxQuant results were next analysed in R (www.r-project.org) with the MSstats package [225]. Once imported to the MSstats format, the data was processed by MSstats with "highQuality" featureSubset, min_feature_count set at 2, while remaining parameters were set as default. Statistical contrasts were also performed by MSstats with the groupComparison function. Statistically significant proteins (adjusted p-value ≤ 0.05 and Log_2 fold change ≤ -1 or ≥ 1) from extracellular vesicles contrasts were selected, and each protein was Z-scored separately among EV and WC samples using mean proteins intensities. Unidentified proteins among triplicate conditions were considered as biologically missing and accordingly assigned a mean intensity value of 0. With the ComplexHeatmap R package [226], a heatmap was

generated by performing a first round of clustering with the “complete” agglomeration method on EV samples with Euclidean distances. After extracting 6 EV clusters, each cluster of proteins was individually re-clustered using the “complete” agglomeration method on EV and WC samples on Euclidean distances. Pearson correlations were calculated with mean proteins intensities in R with the stats package and plotted with the corrplot package, whereas MDS (Multidimensional scaling) analyses were performed with the limma package [227]. Overrepresentation analyses (ORA) of GO-BP (biological processes) were executed on the g:Profiler website (biit.cs.ut.ee/gprofiler/gost) on statistically significant EV_FTY720 or EV_GW4869 proteins (adjusted p-value ≤ 0.05 and Log_2 fold change ≤ -1 or ≥ 1) while applying the Benjamini-Hochberg FDR correction method. A network-based visualization and simplification of statistically significant GO-BP (adj. p-value ≤ 0.05) was next performed. GO-BP with term sizes of less than 500 genes were loaded in Cytoscape’s EnrichmentMap application [228] where similar GO-BP were organized in clusters. Each Clusters was next simplified by assigning a resuming GO-BP in Adobe Illustrator (Adobe Inc.). GraphPad Prism (GraphPad Software Inc.) was used to generate volcano plots of differentially expressed proteins in cells, as well as sub-heatmaps of peptide intensities (relative Z-score) of FTY720 EV downregulated proteins associated to cell junction assembly or the ESCRT complex.

2.3.14. Sample Preparation and RNA Isolation for RNA Sequencing

EVs were purified from MCF7 cells under the vehicle (0.2% DMSO) or drug conditions (10 µM GW4869 or 5 µM FTY20) using the gradient fractionation approach

previous described. Pelleted EVs and their cells of origin were resuspended in TRIzol reagent (Thermo Fisher, 15596018) to allow for simultaneous isolation of proteins and RNA from the same samples as per the manufacturer's recommendations. Briefly, the cellular and EV samples were homogenized in 500 µL of TRIzol reagent, followed by the addition 100 µL of chloroform (VWR, BDH1109-4LG) and centrifuged at 12,000 × *g* for 15 min. Following the centrifugation step, the aqueous phase is processed for RNA purification using the RNA Clean & Concentrator-5 system (Zymo Research, R1013) and in-column DNaseI treatment. All steps were performed according to the manufacturers' protocols. The RNA was eluted in nuclease-free water and quantified by Nanodrop and Bioanalyser. After the extraction of RNAs, the samples were ribodepleted followed by library preparation with the KAPA RNA HyperPrep Kit with RiboErase (HMR) (Roche, 8098140702). Next, starting with 1 µg of total RNA for cellular samples or 2-6ng of total RNA recovered from EV samples from drug-induced conditions, the libraries were amplified for 7 and 16 PCR cycles respectively. The libraries were quantified by qPCR and were loaded at equimolar concentrations for the sequencing on the Novaseq platform with the kit NovaseqS4 at a coverage of 35M paired-end reads per sample.

2.3.15. Transcriptomics Bioinformatics Analyses

FASTQ sequencing files were assessed for quality control with FastQC (The Babraham Institute: https://www.bioinformatics.babraham.ac.uk/projects/fastqc/). The generated RNA sequencing libraries were mapped to the human reference genome (GRCh38), with GENCODE v34 gene annotation, using the STAR alignment tool [229].

The mapped reads per gene were counted using featureCounts [230]. Genes differentially enriched in EV and cell lysate samples were determined by pairwise comparison using DESeq2 [231, 232]. To do this, count tables from featureCounts were used after removing genes with <10 reads in any of the samples. We used a threshold of *P*.adj ≤0.05 and log-fold-change (LFC) ≥2 to determine significant hits. The significant hits were further assessed for gene ontology (GO) enrichment analysis using the FuncAssociate software v3.0 [233].

2.3.16. Protein Synthesis Assay

MCF10A cells were plated at 20,000 cell/well of a 96-well plate and were incubated until confluent at 37 °C in humidified 5% CO_2 atmosphere. Once confluent, and directly before addition of MCF7 EVs, the MCF10A cells were wounded with the Incucyte 96-well WoundMaker Tool (Essen Bioscience, 4563) as per the manufacturer's recommended protocol. EVs were purified from MCF7 cells under the vehicle (0.2% DMSO) or drug conditions (10 μM GW4869 or 5 μM FTY20). Briefly, 1.2×10^7 MCF7 cells were plated overnight starting in a T-175 flask for each condition. On the following day, the plating media was removed and replaced with EV-isolation media containing vehicle or EV-inhibitor drugs using the approach previously described, and the cells were incubated for 36 h at 37 °C in humidified 5% CO_2 atmosphere. The cell-conditioned media was recovered and processed for the isolation of EVs using SEC as described previously. Purified EVs were resuspended in equal volumes of PBS and volumetric equivalents were added to MCF10A cells. An equal volume of blank PBS with was also added as second

control. MCF10A cells were then incubated up to 3, 6, 18, and 24 hours, after which time the media was replaced with fresh EV media containing 20 μM O-propargyl-puromycin (OPP), a component in the Click-iT™ Plus OPP Protein Synthesis Assay Kit (Molecular Probes, C10456) and incubated for an additional 30 minutes. The cells were then fixed with a solution of freshly prepared 3.7% formaldehyde (Fisher Chemical, Cat. No. F79-1) in PBS and labelled via click chemistry for imaging with the Click-iT™ Plus OPP Protein Synthesis Assay Kit (Molecular Probes, C10456) as per the manufacturer's recommended protocol. Image acquisition of fluorescently-labeled cells was carried out with the ImageXpress Micro High-Content Screening (HCS) Microscopy system (Molecular Devices, LLC) and image analysis was done using the MetaXpress 3.1 software (Molecular Devices). GraphPad Prism (GraphPad Software Inc.) was used for statistical analysis.

2.3.17. Cell Proliferation Assay

MCF10A cells were plated at 20,000 cell/well of a 96-well plate and were incubated until confluent at 37 °C in humidified 5% CO_2 atmosphere. Once confluent, and directly before addition of MCF7 EVs, the MCF10A cells were wounded with the Incucyte 96-well WoundMaker Tool (Essen Bioscience, 4563) as per the manufacturer's recommended protocol. EVs were purified from MCF7 cells under the vehicle (0.2% DMSO) or drug conditions (10 μM GW4869 or 5 μM FTY20). Briefly, 1.2×10^7 MCF7 cells were plated overnight starting in a T-175 flask for each condition. On the following day, the plating media was removed and replaced with EV-isolation media containing vehicle or EV-

inhibitor drugs using the approach previously described, and the cells were incubated for 36 h at 37 °C in humidified 5% CO_2 atmosphere. The cell-conditioned media was recovered and processed for the isolation of EVs using SEC as described previously. Purified EVs were resuspended in equal volumes of PBS and were mixed with 5-ethynyl-2'-deoxyuridine (EdU) component of the Click-iT™ EdU Cell Proliferation Kit for Imaging (Invitrogen, C10337), to a final concentration of 10 μM. Volumetric equivalents of the drug induced EVs with EdU were added to MCF10A cells. An equal volume of blank PBS with EdU was also added as second control. MCF10A cells were then fixed at 3, 6, 18, 24 and 40 hours with a solution of freshly prepared 3.7% formaldehyde (Fisher Chemical, Cat. No. F79-1) in PBS and labelled via click chemistry for imaging with the Click-iT™ EdU Cell Proliferation Kit (Invitrogen, C10337) as per the manufacturer's recommended protocol. Image acquisition of fluorescently-labeled cells was carried out with the ImageXpress Micro High-Content Screening (HCS) Microscopy system (Molecular Devices, LLC) and image analysis was done using the MetaXpress 3.1 software (Molecular Devices). GraphPad Prism (GraphPad Software Inc.) was used for statistical analysis.

2.3.18. Scratch-Wound Cell Migration Assay

MCF10A cells were plated at 20,000 cell/well of a 96-well plate and were incubated until confluent at 37 °C in humidified 5% CO_2 atmosphere. Once confluent, and directly before addition of MCF7 EVs, the MCF10A cells were wounded with the Incucyte 96-well WoundMaker Tool (Essen Bioscience, 4563) as per the manufacturer's recommended

protocol. EVs were purified from MCF7 cells under the vehicle (0.2% DMSO) or drug conditions (10 μM GW4869 or 5 μM FTY20). Briefly, 1.2×10^7 MCF7 cells were plated overnight starting in a T-175 flask for each condition. On the following day, the plating media was removed and replaced with EV-isolation media containing vehicle or EV-inhibitor drugs using the approach previously described, and the cells were incubated for 36 h at 37 °C in humidified 5% CO_2 atmosphere. The cell-conditioned media was recovered and processed for the isolation of EVs using SEC as described previously. Purified EVs were resuspended in the same volume of PBS and volumetric equivalents were added to wounded MCF10A cells. An equal volume of PBS was also added as second control. The cells were then live imaged hourly over 24 hours with an Incucyte Microscope (Sartorius) to evaluate for the effects the divergent bioactive cargoes in EVs as induced by the differing drug induced conditions. The Incucyte software Scratch Wound Analysis Software Module (Sartorius) was used for the calculation of percentage of Relative Wound Density (%RWD), while GraphPad Prism (GraphPad Software Inc.) was used for statistical analysis.

2.4. Results

2.4.1. Sphingolipid Metabolism Is required for the Release of RNA from Cells Through EVs

To assess the physical and phenotypic effects of SMase inhibitors on EVs, we first evaluated the impact of these compounds on the viability and proliferation of the human epithelial adenocarcinoma cell line MCF7. To reduce the risk of contamination of the EV populations by apoptotic bodies, titrations were carried out with each compound to assess their most appropriate usage concentrations on MCF7 cells. We chose 5 μM for FTY720 and 10 μM for GW4869, which resulted in ≥ 95% cell viability in both cases after 36 h (**Figure 2.1 B**, **Figure S2.1 A**), the time at which EVs are recovered from cell-conditioned media. The drug vehicle, DMSO, was used as the control condition in a volumetric equivalent percentage to cell culture media. Moreover, the relative number of cells at the time of EV-harvesting was not impacted by either drug treatment (**Figure S2.1 B**). Western blots of EVs and their cells of origin demarcated the samples' purity by the presence the of known EV markers TSG101 and CD81 in EVs, while the negative marker LaminB2 was absent from EV samples (**Figure 2.1 C**). These results suggested that the usage of inhibitor compounds does not completely prevent the release of EVs, a conclusion further supported by Nanoparticle Tracking Analysis (NTA) of cell-conditioned media. NTA quantifications showed drug-defined profiles of nanoparticle sizes (**Figure 2.1 D**), with the control samples having a median size range of 135 ± 3.3 nm while treatment samples had a mean size 162.6 ± 5.0 nm and 161.6 ± 2.6 nm for GW4869 and

FTY720, respectively. Transmission electron micrographs (TEM) of iodixanol gradient-purified EVs displayed nanoparticles exhibiting morphological characteristics of EVs and a diversity in sizes (**Figure 2.1 E**). TEMs were further quantified using the software tool TEM ExosomeAnalyser [234]. The results revealed EVs of diverse sizes under all conditions, with a statistically significant trends both for a larger particle diameter in samples arising from GW4869 treated cells and a reduced mean particle area in EVs samples resulting from FTY720 treatments (**Figure S2.1 C-D**). Furthermore, the particle population statistics denoted a size range of 32.90 - 566.3 nm for the control, 49.12 - 579.4 nm for GW4869-, and 44.75 - 337.7 nm for FTY720-samples. The morphological effects observed on EV populations prompted us to investigate both their relative numbers, as well as their RNA cargoes. Nanoflow cytometry was utilized to investigate number of nanoparticles (events) recorded in 10 µL of samples stained for RNA with SYTO RNASelect and recovered using size exclusion chromatography (SEC). The nanoflow cytometry profiles demarcated specific effects of the inhibitors on the EV population, with an increase in total particles detected per milliliter in FTY720 samples (**Figure 2.1 F**), as well as decreases in in the number of RNA-positive particles (per million events) under both GW4869 and FTY720 conditions, with GW4869 treatments resulting in the most pronounced reduction (**Figure 2.1 G**). We conclude that the treatments with inhibitors of neutral (GW4869) and acid (FTY720) sphingomyelinases lead to distinctive alterations in EV biogenesis.

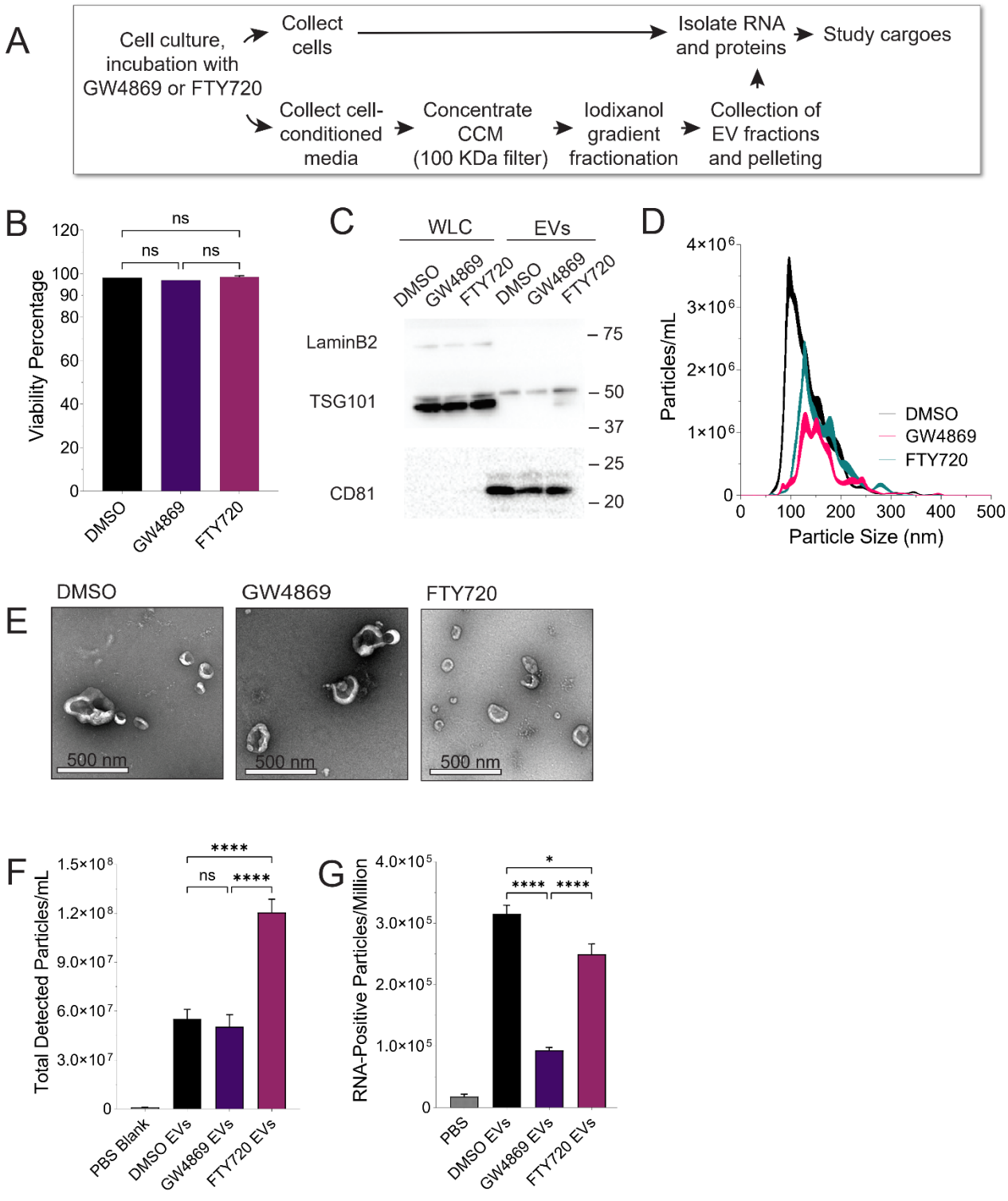
A
Cell culture, incubation with GW4869 or FTY720
Collect cells
Isolate RNA and proteins
Study cargoes
Collect cell-conditioned media
Concentrate CCM (100 KDa filter)
Iodixanol gradient fractionation
Collection of EV fractions and pelleting
B
Viability Percentage
ns
DMSO
GW4869
FTY720
C
WLC
EVs
LaminB2
TSG101
CD81
D
Particles/mL
Particle Size (nm)
DMSO
GW4869
FTY720
E
DMSO
GW4869
FTY720
500 nm
F
Total Detected Particles/mL
PBS Blank
DMSO EVs
GW4869 EVs
FTY720 EVs
G
RNA-Positive Particles/Million
PBS
DMSO EVs
GW4869 EVs
FTY720 EVs

FIGURE 2.1 Ceramide is required for the recruitment of RNAs to EVs. **A.** Outline of the EV-isolation protocol used unless otherwise stated. **B.** Cellular viability of MCF7 cells after treatment with sphingomyelinase inhibitor drugs over 36 h. Control (DMSO vehicle) and treated cells had a cell viability >95%, with no statistical significance as calculated by ordinary one-way ANOVA on GraphPad Prism. **C.** Representative Western blot of cell and EV samples isolated from control and drug treatments. The samples were probed for EV markers TSG101 and CD81 and the negative control marker LaminB2. **D.** Nanoparticle Tracking Analysis (NTA) of cleared cell-conditioned media. Border thickness defines the standard error. **E.** Transmission electron micrographs of iodixanol gradient-purified EVs. EVs were negatively stained with 2% uranyl acetate and imaged on the FEI Tecnai T12 120kV transmission electron microscope. **F.** Nanoflow cytometry quantifications of total detected nanoparticles isolated via size exclusion chromatography and recorded using the CytoFLEX platform. **G.** Nanoflow cytometry quantifications of RNA-positive nanoparticles isolated via size exclusion chromatography and recorded using the CytoFLEX platform. The RNA in the nanoparticles was labelled using SYTO RNASelect, cell-permeable stain of nucleic acids that is selective for RNA. For all bar graphs, unless otherwise stated, the error bars represent the standard error of the mean (SEM) and the statistics were calculated by ordinary one-way ANOVA (where ns=$P>0.05$, *=$P\leq0.05$, **=$P\leq0.01$, ***=$P\leq0.001$, and ****= $P\leq0.0001$) on GraphPad Prism.

2.4.2. Inhibition of ASM Downregulates the RNA Diversity of EVs

The distinguishing features of EVs released by SMase inhibitor-treated cells, and in particular their RNA contents, lead us to characterize their RNA and protein content comprehensively. A non-continuous iodixanol gradient purification approach was used to isolate EVs from cell-conditioned media of MCF7 cells exposed to vehicle (DMSO), GW4869 or FTY720 over 36 h. Purified EV samples were recovered from the iodixanol gradient by ultracentrifugation and washed with PBS. Cellular specimens were also collected to evaluate possible effects that the drugs may provoke. Cell and EV samples were lysed with TRIzol which facilitated the recovery of total protein and RNA contents from the same samples, thereby reducing the need for additional materials, and improving reproducibility. Quantifications from isolated EV specimens denoted a statistically significant increase in the isolated total RNA from FTY720 EV samples (**Figure S2.2 B**), while no significant differences in the isolated total RNA between cellular specimens were observed (**Figure S2.2 A**).

To assess the impact of SMase inhibitors on EV transcriptomes, we next performed total RNA sequencing (rRNA depleted) on biological triplicates of RNA samples from cells or EVs via the Nova-seq platform, with a coverage of ~35M paired-end reads per samples. Principal component analysis (PCA) of sequencing libraries for both cells and EVs revealed class specific distributions, with the cells sequestering to a single group, while EVs segregated into two groups consisting of DMSO/GW4869 or FTY720 samples, respectively (**Figure 2.2 A**). Further analyses of cellular and EV

transcriptomes revealed minor differences in expression correlations of cellular specimens, while marked differences were observed for FTY720 EV specimens relative to GW4869 or DMSO (**Figure S2.2 A**). Differential expression analysis revealed an overall consistency in RNA expression levels across cell specimens, with EVs displaying their own transcriptomic identity relative to parental cells (**Figure 2.2 B**), as noted by an enrichment for specific RNA species and unique, drug-specific, expression profiles (**Figure S2.2 D-H**). Again, FTY720 EVs displayed the most distinctive expression features relative to the DMSO or GW486 EV samples.

Next, each EV transcriptome was compared to their respective cellular transcriptomes and enriched genes were identified (Log_2 fold change ≥2, Adj*P*≤0.01) according to their biotype (**Figure 2.2 C**). This analysis revealed mRNAs as a major cargo across EV samples, which were found in higher proportion in FTY720 EVs, while these specimens also showed a reduced relative abundance of both long non-coding RNA (lncRNA) and processed pseudogenes. To further investigate the unique features resulting from individual drug conditions, their cellular or EV transcriptomes were compared to DMSO controls using volcano plots. The cellular transcriptomes displayed only few instances of downregulated (Log_2 fold change ≤-2, Adj*P*≤0.01) genes resulting from either treatment, while more substantial number of genes were upregulated (Log_2 fold change ≥2, Adj*P*≤0.01) in each condition, with FTY720 treatments impacting a larger number of genes (n=198) (**Figure 2.2 D**). Gene Ontology (GO) enrichment analysis of down- or upregulated cellular mRNAs, as measured by FuncAssociate 3.0 [233], revealed that upregulated genes were enriched for *2'-5'-Oligoadenylate Synthetase Activity*

(logarithm (base 10) of the odds ratio (LOD): 3.04, *P*adj. 0.022). Comparison of EV transcriptomes using these same parameters revealed the GW4869 EVs had few differences to the DMSO control, while the FTY720 EVs were marked by the upregulation (Log_2 fold change ≥2, Adj*P*≤0.01) of a subset of RNAs (n=111) and a major downregulation (Log_2 fold change ≤-2, Adj*P*≤0.01) of RNAs (n=937) relative to control treatments (**Figure 2.2 E**). GO enrichment of downregulated and upregulated FTY720 EV mRNAs revealed an upregulation for transcripts associated with *Cholesterol Biosynthetic Process* (LOD: 1.49, *P*adj. 0.004) and a downregulation of transcripts associated with *Negative Regulation of Translation* (LOD: 1.14, *P*adj. 0.011) and *RNA Binding* (LOD: 0.59, *P*adj. <0.001). Because of the possible effects of the drugs on the cellular expression profiles, the asymmetrical distribution of EV transcripts was compared to the cellular transcriptome. Firstly, the transcriptomes of GW4869 or FTY720 treated cells was compared to the transcriptome of the DMSO control cells to identify aberrantly expressed transcripts. Next, the EV transcriptomes of GW4869 or FTY720 samples was compared to the normalized cell expression data (**Figure 2.2 F**). This allowed for the identification of three groups of EV-detected RNAs: those upregulated in both cells and EVs, those upregulated in EVs but not altered in cells, and those upregulated in EVs but downregulated in cells. This revealed that FTY720 EV-enriched RNAs (Log_2 fold change ≥2, Adj*P*≤0.01) showed GO enrichment for cell cycle regulatory processes, while there was no specific GO enrichment for GW4869 EV-enriched RNAs. Furthermore, cellular transcripts upregulated in either drug condition did not display specific GO enrichment.

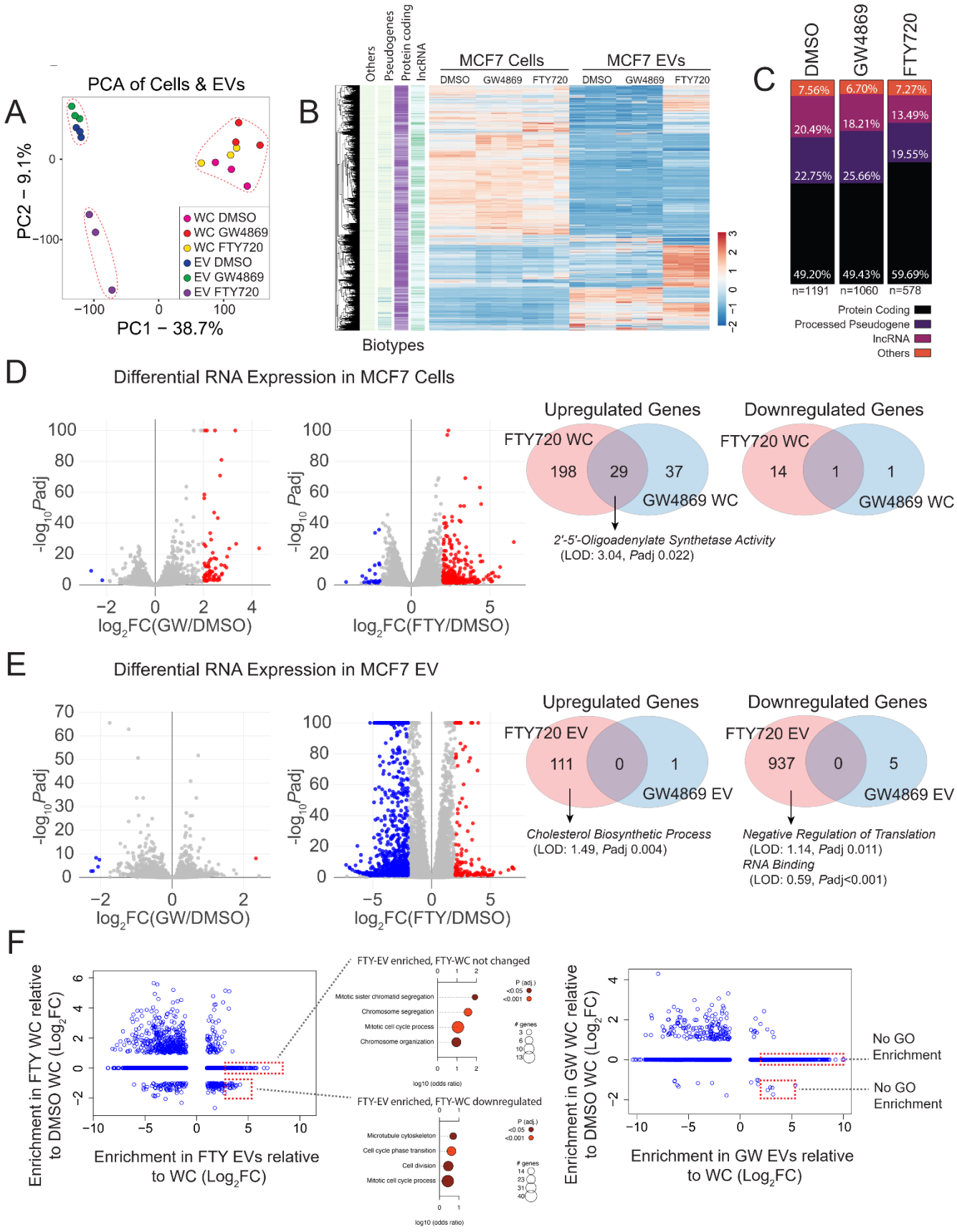
A
PCA of Cells & EVs
PC2 – 9.1%
PC1 – 38.7%
WC DMSO
WC GW4869
WC FTY720
EV DMSO
EV GW4869
EV FTY720
B
Others
Pseudogenes
Protein coding
lncRNA
MCF7 Cells
MCF7 EVs
DMSO
GW4869
FTY720
Biotypes
C
DMSO
GW4869
FTY720
7.56%
20.49%
22.75%
49.20%
6.70%
18.21%
25.66%
49.43%
7.27%
13.49%
19.55%
59.69%
n=1191
n=1060
n=578
Protein Coding
Processed Pseudogene
lncRNA
Others
D
Differential RNA Expression in MCF7 Cells
-log10Padj
log2FC(GW/DMSO)
log2FC(FTY/DMSO)
Upregulated Genes
FTY720 WC
198
29
37
GW4869 WC
2'-5'-Oligoadenylate Synthetase Activity
(LOD: 3.04, Padj 0.022)
Downregulated Genes
FTY720 WC
14
1
1
GW4869 WC
E
Differential RNA Expression in MCF7 EV
-log10Padj
log2FC(GW/DMSO)
log2FC(FTY/DMSO)
Upregulated Genes
FTY720 EV
111
0
1
GW4869 EV
Cholesterol Biosynthetic Process
(LOD: 1.49, Padj 0.004)
Downregulated Genes
FTY720 EV
937
0
5
GW4869 EV
Negative Regulation of Translation
(LOD: 1.14, Padj 0.011)
RNA Binding
(LOD: 0.59, Padj<0.001)
F
Enrichment in FTY WC relative to DMSO WC (Log2FC)
Enrichment in FTY EVs relative to WC (Log2FC)
FTY-EV enriched, FTY-WC not changed
Mitotic sister chromatid segregation
Chromosome segregation
Mitotic cell cycle process
Chromosome organization
P (adj.)
genes
log10 (odds ratio)
FTY-EV enriched, FTY-WC downregulated
Microtubule cytoskeleton
Cell cycle phase transition
Cell division
Mitotic cell cycle process
Enrichment in GW WC relative to DMSO WC (Log2FC)
Enrichment in GW EVs relative to WC (Log2FC)
No GO Enrichment
No GO Enrichment

FIGURE 2.2 Inhibition of ASM downregulates the RNA diversity of EVs. **A.** Principal Component Analysis (PCA) of RNA-sequencing data derived from MCF7 cellular and EV RNA libraries. **B.** Global heatmap of cellular and EV transcriptomes, with the RNAs' biotype identity listed to the left (color denotes presence). **C.** RNA biotype distributions of EV transcriptomes across the different conditions studied. 'Others' includes a varied group of minor transcripts including, but not limited to, miscRNA, snRNA, snoRNA, etc. **D.** Volcano plots of cellular transcriptomes signifying the shift in expression levels in GW4869 or FTY720 treated specimens relative to the DMSO control group. Blue dots represent statistically significant downregulated transcripts (Log_2 fold change ≤-2, Adj*P*≤0.01). Red dots represent statistically significant upregulated transcripts (Log_2 fold change ≥2, Adj*P*≤0.01). Venn diagrams display the total number of genes upregulated or downregulated in each condition and their overlap. Gene groups which displayed specific Gene Ontology (GO) enrichment (FuncAssociate 3.0) are labelled, with respective logarithm (base 10) of the odds (LOD) ratio and *P*adj. listed. **E.** Volcano plots of EV transcriptomes signifying the shift in expression levels in GW4869 or FTY720 treated specimens relative to the DMSO control group. Blue dots represent statistically significant downregulated transcripts (Log_2 fold change≤-2, Adj*P*≤0.01). Red dots represent statistically significant upregulated transcripts (Log_2 fold change ≥2, Adj*P*≤0.01). Venn diagrams display the total number of genes upregulated or downregulated in each condition and their overlap. Gene groups which displayed specific Gene Ontology (GO) enrichment (FuncAssociate 3.0) are labelled, with respective logarithm (base 10) of the odds (LOD) ratio and *P*adj. listed. **F.** Dot plots of transcripts asymmetrically distributed between FTY720 or GW4869 EVs relative to their respective parental cells' transcriptomes normalized to DMSO control cellular transcriptome. Upper red boxes represent statistically significant upregulated transcripts (Log_2 fold change ≥2, Adj*P*≤0.01). Gene groups which displayed specific Gene Ontology (GO) enrichment (FuncAssociate 3.0) are labelled, with their respective logarithm (base 10) of the odds (LOD) ratio and *P*adj. listed.

2.4.3. Neutral and Acid Sphingomyelinases Affect Opposing EV biogenesis Pathways

To improve our understanding of the role that sphingomyelinases play on the diversity of the EV proteome, and in particular its RNA-binding protein (RBP)-repertoire, we performed LC-MS/MS on MCF7 EVs and their cells of origin. After the recovery of RNA, proteins were precipitated from the TRIzol organic phase. To estimate the available protein material between samples, cells or EV specimens were initially loaded in equivalent volumes and their Total Ion Current (TIC) chromatograph area was recorded, which represents the sum of the intensities of all spectral peaks within the same scan. Sample injection volumes were then adjusted for the loading of equal sample amounts (cells or EVs). TIC chromatograph data revealed little differences in total isolated protein samples between the different cellular specimens (**Figure S2.3 A**). At the EV level, the GW4869 samples showed a reduction in total isolated protein levels, while FTY720 samples showed a marked increase (**Figure S2.3 B**). These results mirrored the quantified total EV nanoparticles and RNA contents described above (**Figure 2.1 F-G**, **Figure S2.2 B**). Multidimensional scaling (MDS) and Pearson correlations of cellular proteomes revealed high degrees of similarity (all ≥94%) suggesting that the drug treatments had little effects on proteome composition (**Figure 2.3 A**, **Figure S2.3 C**). By contrast, EV specimens displayed lower correlations between treatment groups but formed discreet, drug defined, clusters by MDS (**Figure 2.3 A**, **Figure S2.3 C**). To highlight proteomic differences between all cellular specimen groups, analyses were performed with the aid of volcano plots. The cellular proteomes revealed an upregulation

of a few autophagy associated proteins (Log_2 fold change ≥1, Adj*P*≤0.05) by both sphingomyelinase inhibitor treatments relative to the DMSO controls (**Figure 2.3 B**). These results suggest that the identified EV-specific effects are not related to aberrant protein expression induced by the drugs in their cells of origin. To globally assess the characteristics of the proteomic data of the different EV groups, a clustering analysis of statistically significant proteins was performed. Inclusion in the analysis required that the identified protein accounted for a statistically significant change in expression (Log_2 fold change ≥1 or ≤-1, *P*adj. ≤0.05) in at least one of the comparison groups (DMSO vs GW4869/ DMSO vs FTY720). The heatmaps, displaying peptide intensities (relative Z-score), of clustered EV proteins demonstrate discrete movements in the expression of proteins in EVs depending on the inhibitor used relative to the DMSO control (**Figure 2.3 C**). Several of the clustered protein groups demonstrated opposite expression changes in GW4869 vs FTY720 treated samples, suggesting specialized functions of neutral vs acid sphingomyelinases. To further investigate the associated cellular machineries affected as a response to sphingomyelinase inhibition, GW4869 and FTY720 EV proteins were analysed with the ClueGO plugin [235] on Cytoscape [236]. Using a similar approach, only significant EV proteins were included, but the proteins were further separated into up- and downregulated classes. This allowed us to generate a network of associated protein clusters based on GO terms related to biological function, which revealed the unique classes of proteins affected by either treatment (**Figure 2.3 D**). For instance, proteins associated with cell junction assembly, plasma membrane dynamics, and cell division regulation (**Figure 2.3 E**, green nodes) were uniquely downregulated in

the FTY720 EV proteome. Interestingly, several members of the endosomal sorting complex required for transport (ESCRT) were also depleted (**Figure 2.3 E**), pointing to a potential role for ASM in this endosomal EV biogenesis pathway. Strikingly, FTY720 EVs showed an enrichment for proteins associated with autophagy, RNA binding proteins, RNA nuclear export and translation regulation (**Figure 2.3 E**, red nodes). By contrast, the GW4869 EV proteome was depleted for proteins associated with autophagy, lipid metabolism, RNA regulatory processes, translation, and protein folding at the ER (**Figure 2.3 F**). Indeed, focused analyses of RBP expression signatures revealed that most these factors were downregulated in response to GW4869 (**Figure S2.3 D**).

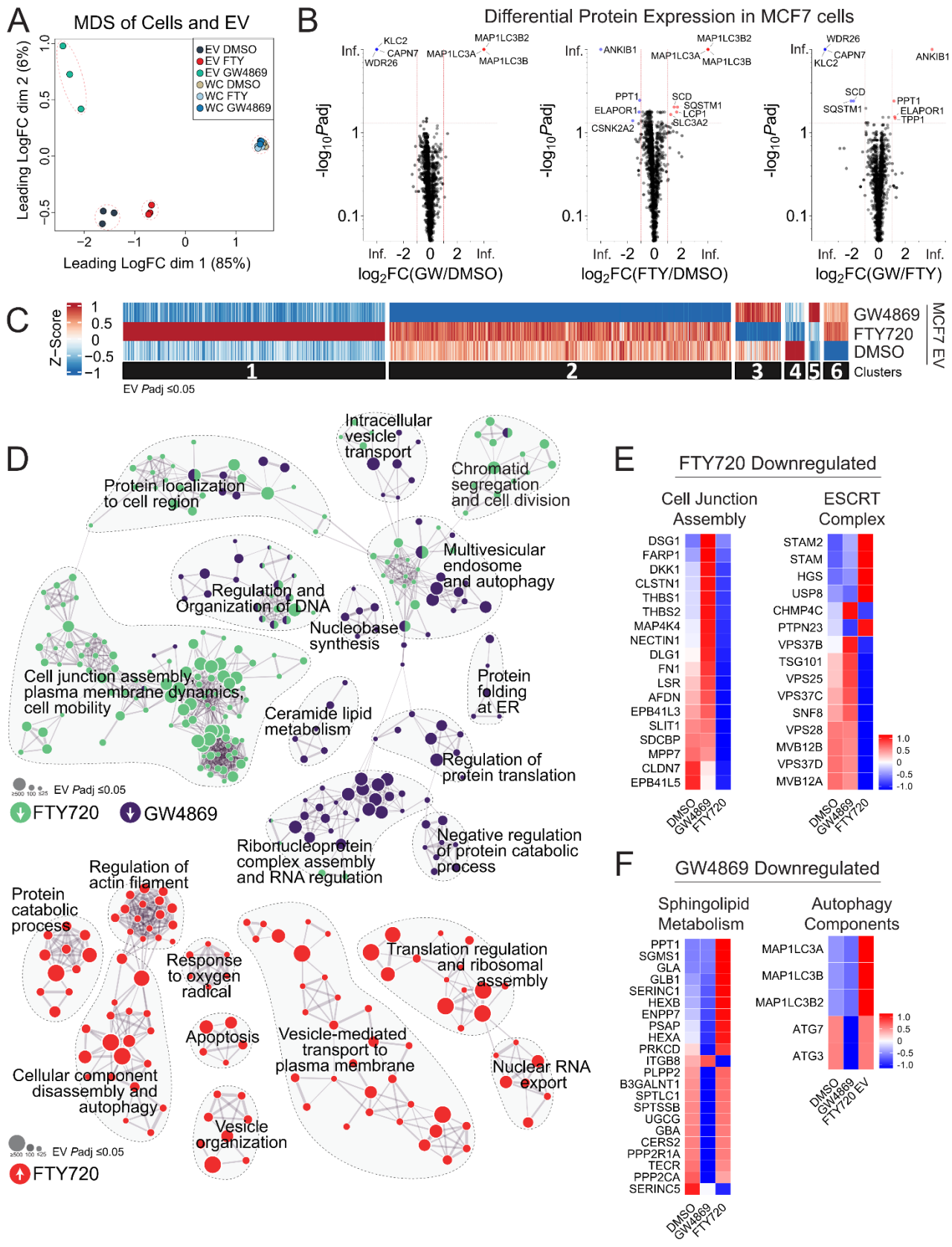
A
MDS of Cells and EV
EV DMSO
EV FTY
EV GW4869
WC DMSO
WC FTY
WC GW4869
Leading LogFC dim 2 (6%)
Leading LogFC dim 1 (85%)
B
Differential Protein Expression in MCF7 cells
-log10Padj
log2FC(GW/DMSO)
log2FC(FTY/DMSO)
log2FC(GW/FTY)
C
Z-Score
EV Padj ≤0.05
GW4869
FTY720
DMSO
MCF7 EV
Clusters
D
Intracellular vesicle transport
Protein localization to cell region
Chromatid segregation and cell division
Multivesicular endosome and autophagy
Regulation and Organization of DNA
Nucleobase synthesis
Cell junction assembly, plasma membrane dynamics, cell mobility
Ceramide lipid metabolism
Protein folding at ER
Regulation of protein translation
Ribonucleoprotein complex assembly and RNA regulation
Negative regulation of protein catabolic process
Regulation of actin filament
Protein catabolic process
Response to oxygen radical
Translation regulation and ribosomal assembly
Apoptosis
Vesicle-mediated transport to plasma membrane
Nuclear RNA export
Cellular component disassembly and autophagy
Vesicle organization
EV Padj ≤0.05
FTY720
GW4869
E
FTY720 Downregulated
Cell Junction Assembly
ESCRT Complex
F
GW4869 Downregulated
Sphingolipid Metabolism
Autophagy Components

FIGURE 2.3 Neutral and acid sphingomyelinases affect different EV biogenesis pathways. **A.** Multidimensional scaling (MDS) of LC-MS/MS proteomics data derived from MCF7 cellular and EV purified proteins. **B.** Volcano plots of cellular proteomes signifying the shift in expression levels in GW4869 or FTY720 treated specimens relative to the DMSO control group or relative to each other. Blue dots represent statistically significant downregulated transcripts (Log_2 fold change ≤-1, Adj*P*≤0.05). Red dots represent statistically significant upregulated transcripts (Log_2 fold change ≥1, Adj*P*≤0.05). **C.** Clustered heatmap analysis of peptide intensities (relative Z-score) of EV proteomes. Blue lines denote lower association, while red lines denote higher association of each protein relative to the other two groups. **D.** Cytoscape ClueGO analysis of statistically significant downregulated (green/purple) or upregulated (red) EV proteomic data displaying a GO (biological process) network of associated protein clusters. **E.** Heatmap of peptide intensities (relative Z-score) of FTY720 EV downregulated proteins associated to cell junction assembly or the ESCRT complex. Blue denotes lower association, while red denotes higher association of each protein relative to the other two groups. **F.** Heatmap of peptide intensities (relative Z-score) of GW4869 EV downregulated proteins associated to sphingolipid metabolism or autophagy. Blue denotes lower association, while red denotes higher association of each protein relative to the other two groups.

2.4.4. RBPs as Major Differentially Regulated EV Cargoes in Response to NSM or ASM Inhibition

As a group, RBPs are crucial cellular regulators involved in all facets of RNA metabolism. Strikingly, we observed opposite effects of SMase inhibitors on RBP levels within EVs. Indeed, inhibition of NSM with GW4869 results in a pronounced downregulation of identified RBPs relative to both DMSO (n=153) and FTY720 (n=274) EV specimens (**Figure 2.4 A-B**). By contrast, a sizeable fraction of RBPs were preferentially exported within EVs as response to FTY720 treatment (n=94) (**Figure 2.4 C**). As the proteomic data pointed to the opposing effects of SMase inhibitors on the EV proteome, and in particular the striking downregulation of RBPs from the GW4869 EVs, we sought to explored whether individual components of bipartite ribonucleoproteins (RNPs) modules are impacted similarly by SMase inhibition and whether this was consistent with the behaviour or RNA biotypes normally bound by these RNP machineries.

Although the impact of NSM inhibition on the EV RNA repertoire was limited, some specific examples do appear. For instance, the secretion of various 7SL RNA family members (e.g. *RN7SL1*, *RN7SL3* and varied 7SL pseudogenes), the RNA components of the Signal Recognition Particle (SRP) involved in targeting translation of mRNAs encoding signal peptides to the ER, exhibit a significantly decreased expression in GW4869 EVs, while they were strongly increased in FTY720 EVs (**Figure S2.2 H**). By contrast, these expressions alterations were observed at the cellular transcriptomic level

(**Figure S2.4 A**). 7SL RNAs play an important scaffolding role for the SRP and, quite interestingly, all SRP proteins respond similarly to their RNA counterparts at the proteomic level (**Figure 2.4 D**), with SRP proteins showing robust depletion in GW4869 EVs and marked over-representation in FTY720 EVs.

Intriguingly, several mRNAs associated with the negative regulation of translation such as *SAMD4A*, *AGO1*, and *NCL* are downregulated in the transcriptomes of FTY720 EVs, but not affected in GW4869 EVs (**Figure 2.4 E**). Again, expression of these transcripts was generally similar across cellular specimens (**Figure S2.4 B**). Another interesting example is that of small nuclear ribonucleoproteins (snRNPs) associated with spliceosomal activity. The EV proteomic reveals that secretion of several spliceosomal RBPs is downregulated in response to GW4869, while the opposite is true for FTY720 samples (**Figure 2.4 F**). This dichotomy is also observed at the transcriptomic level, with spliceosomal snRNAs decreasing in GW4869 EVs. However, apart from a few examples such as *RNVU1-31* and *RNVU1-29*, there is no increase for these RNAs in FTY720 EVs. As with the previous examples, these expression variations were generally not observed in the cellular transcriptome samples (**Figure S2.4 C**).

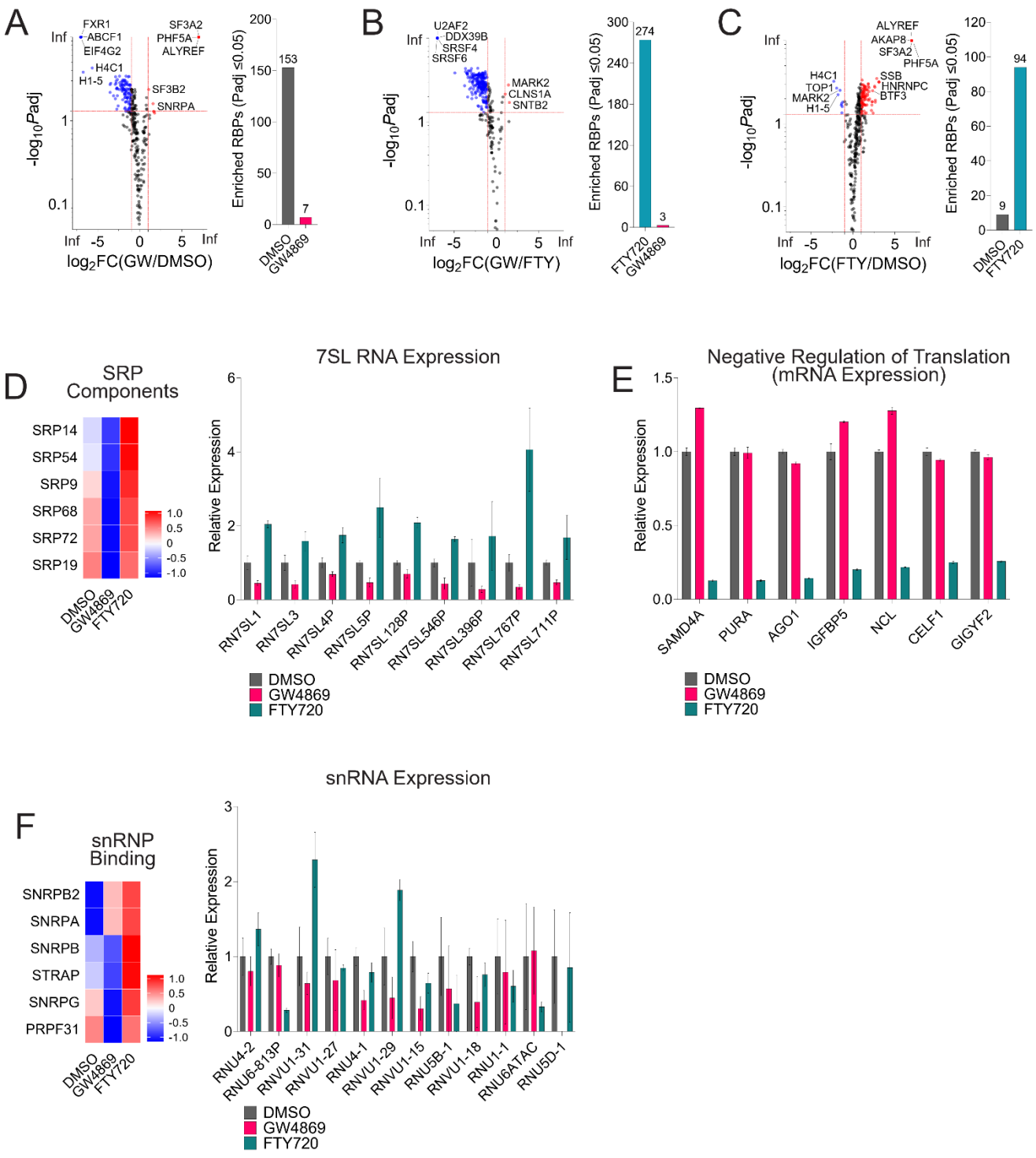
A
FXR1
ABCF1
EIF4G2
H4C1
H1-5
SF3A2
PHF5A
ALYREF
SF3B2
SNRPA
-log10Padj
log2FC(GW/DMSO)
Enriched RBPs (Padj ≤0.05)
153
7
DMSO
GW4869
B
U2AF2
DDX39B
SRSF4
SRSF6
MARK2
CLNS1A
SNTB2
log2FC(GW/FTY)
274
3
FTY720
GW4869
C
ALYREF
AKAP8
SF3A2
PHF5A
SSB
HNRNPC
BTF3
H4C1
TOP1
MARK2
H1-5
log2FC(FTY/DMSO)
9
94
DMSO
FTY720
D
SRP Components
SRP14
SRP54
SRP9
SRP68
SRP72
SRP19
7SL RNA Expression
Relative Expression
RN7SL1
RN7SL3
RN7SL4P
RN7SL5P
RN7SL128P
RN7SL546P
RN7SL396P
RN7SL767P
RN7SL711P
DMSO
GW4869
FTY720
E
Negative Regulation of Translation (mRNA Expression)
SAMD4A
PURA
AGO1
IGFBP5
NCL
CELF1
GIGYF2
F
snRNP Binding
SNRPB2
SNRPA
SNRPB
STRAP
SNRPG
PRPF31
snRNA Expression
RNU4-2
RNU6-813P
RNVU1-31
RNVU1-27
RNU4-1
RNVU1-29
RNVU1-15
RNU5B-1
RNVU1-18
RNU1-1
RNU6ATAC
RNU5D-1

FIGURE 2.4 NSM is essential for the export of RBPs and their binding partners. **A.-B.** Volcano plots of EV proteomes signifying the shift in RBP expression levels in GW4869 or FTY720 treated specimens relative to the DMSO control group or relative to each other. Blue dots represent statistically significant downregulated transcripts (Log_2 fold change ≤-1, Adj*P*≤0.05). Red dots represent statistically significant upregulated transcripts (Log_2 fold change ≥1, Adj*P*≤0.05). **C.** Volcano plots of EV proteomes signifying the shift in RBP expression levels between GW4869 and FTY720. Blue dots represent statistically significant downregulated transcripts (Log_2 fold change ≤-1, Adj*P*≤0.05). Red dots represent statistically significant upregulated transcripts (Log_2 fold change ≥1, Adj*P*≤0.05). **D.** (Left) Heatmap of peptide intensities (relative Z-score) of SRP protein in EVs. Blue denotes lower association, while red denotes higher association of each protein relative to the other two groups. (Right) Expression (TPM) of 7SL RNAs in GW4869 and FTY720 EVs relative to the DMSO control. **E.** Expression (TPM) of RNAs associated to the negative regulation of translation in GW4869 and FTY720 EVs relative to the DMSO control. **F.** Heatmap of peptide intensities (relative Z-score) of snRNP-binding proteins in EVs. Blue denotes lower association, while red denotes higher association of each protein relative to the other two groups. (Right) Expression (TPM) of snRNAs in GW4869 and FTY720 EVs relative to the DMSO control.

2.4.5. FTY720 EVs Enhances Protein Translation in Recipient Cells

The EV-mediated intercellular transfer of RNA molecules and RNP machineries can present key determinants of the biological impact of EVs on recipient cells [2, 151, 161, 237, 238]. In light of the differential impact of SMase inhibitors on EV protein and RNA cargo, this led us to test whether these treatments altered the effects these EVs may have when transferred onto recipient cells. For this, we developed a co-culture system allowing us to quantify the phenotypic response of the recipient cell line, human MCF10A, to EVs isolated from control or inhibitor-treated MCF7 cells. Starting with equal number of cells, volumetrically equivalent samples of SEC-purified EVs in PBS were obtained from MCF7 treated with vehicle (DMSO), GW4869 or FTY720. The quantity of proteins present within the samples was assessed by Qubit protein assays prior to loading on recipient MCF10A cells (**Figure 2.5 A**). These showed minimal differences in the total protein available. Additionally, a volumetric equivalent of PBS was used as a negative control. Guided by the noted depletion or increase of the SRP components induced by drug treatments, we first tested for possible impacts of EVs on translational responses in recipient cells. Using high content screening microscopy as an output, we quantified the intensity of O-propargyl-puromycin (OPP)-labelled foci in MCF10A cells co-cultured with EV specimens. Our quantifications revealed that MCF10A cells co-cultured with FTY720 EVs showed an increased foci intensity signal starting at 6 hours (**Figure S2.5 A**), an effect that was sustained up to 24 hours (**Figure 2.5 B**). By contrast, no effects on MCF10A cell translational activity were observed with EVs from DMSO or GW4869 treated cells. The increased export of cell division associated RNAs in FTY720 EVs

prompted us to investigate the possible effects in cell division. Using a similar approach, we utilized 5-ethynyl-2'-deoxyuridine (EdU) to label nascent DNA in recipient cells and thereby quantify cell proliferation. Quantification of percentage of new cells across the different conditions revealed only slight increase in the percentage of new MCF10A cells after co-cultured with FTY720 EVs over time (**Figure S2.5 B**), but this only becomes statistically significant at 40 hours (**Figure 2.5 C**). We also sought to quantify the migratory response of MCF10A cells upon co-culture with MCF7-derived EVs by performing scratch-wound assays using the Incucyte live cell imaging system (**Figure S2.5 C**). Analysis of the relative wound density (RWD) showed a statistically significant increase in percentage of RWD (%RWD) in MCF10A cells co-cultured with FTY720 EVs (**Figure 2.5 D**), while no discernible effects were observed across the other conditions. These results indicate that the alterations in molecular cargoes elicited by SMase inhibition can significantly alter the biological impact of EVs on recipient cells.

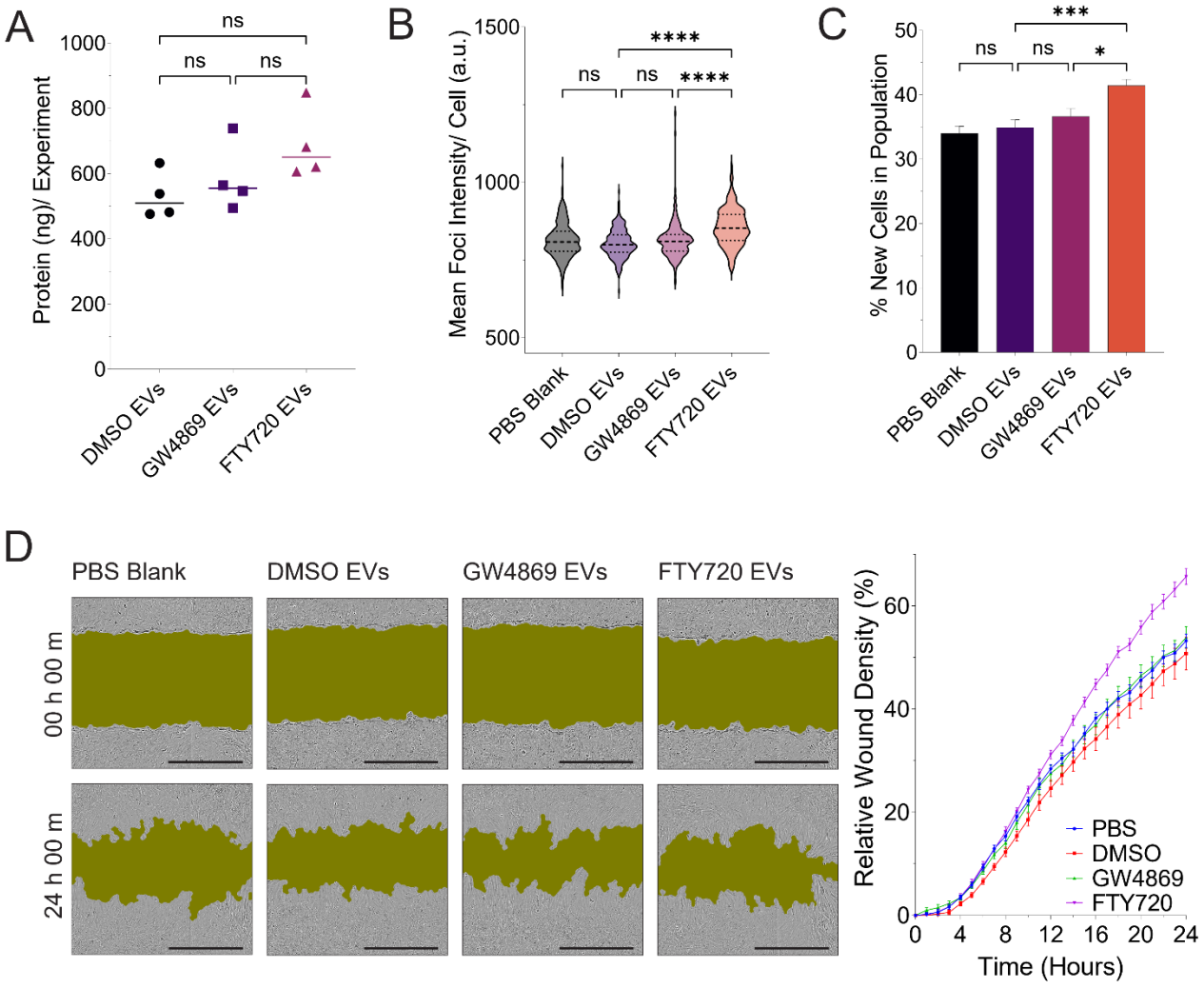

FIGURE 2.5 FTY720 EVs increased protein translation and induce faster migration phenotype in recipient cells. **A.** Qubit protein quantification of SEC purified EVs under different drug treatment conditions or DMSO control. **B.** Violin plots of the distribution of intensities (a.u.) at 24 h of OPP-labelled foci in MCF10A cells upon co-culture with EVs isolated from MCF7 cells treated with SMase inhibitors. **C.** Percentage of new cells at 40 h as labelled by EdU in MCF10A cells upon co-culture with EVs isolated from MCF7 cells treated with SMase inhibitors. **D.** Scratch wound cell migration assay. The %RWD is calculated based on an image taken every hour over 24 h. For all graphs, unless otherwise stated, the error bars represent the standard error of the mean (SEM) and the

statistics were calculated by ordinary one-way ANOVA (where ns=$P>0.05$, *=$P\leq0.05$, **=$P\leq0.01$, ***=$P\leq0.001$, and ****= $P\leq0.0001$) on GraphPad Prism.

2.5. Discussion

Over the last two decades, EVs have gained prominence as key regulators of intercellular communication [1, 2, 5]. Although progress has been made in all aspects of EV biology, their heterogeneity has made it difficult to ascertain the role that specific subpopulations may play in this exchange of information [15]. In fact, EVs may be generated at different subcellular compartments using a diversity of molecular machineries [15, 109, 239]. As such, there is an imperative need to understand the individual sorting mechanisms used by cells to load cargoes to EVs. Two main mechanisms of EV biogenesis have been described, one involving the endosomal sorting complex required for transport (ESCRT) (ESCRT-dependent mechanism), and a second driven by the metabolism of lipids by a family of enzymes called sphingomyelinases (ESCRT-independent mechanism) [7, 15, 70]. Of these two mechanisms, sphingolipid metabolism by sphingomyelinases remains an under studied aspect of EV biogenesis, and the role of these enzymes in the release of bioactive cargoes remains to be clarified.

Sphingomyelinases present themselves in two different varieties: neutral (NSM) and acid (ASM) variants, both of which metabolize membrane-bound sphingomyelin to ceramide and phosphorylcholine [102, 105, 240]. Interestingly, various reports have implicated these variants with the release of two distinct EV subpopulations, exosomes and microvesicles, suggesting that they play specialized roles during EV biogenesis [82, 100, 222]. While the biological activity of both NSM and ASM contribute to distinct EV subpopulations, they do so by using similar mechanisms. This makes them interesting

subjects of study, particularly as it relates to cargo sorting, since exosomes and microvesicles may typically carry different types of cargoes [75, 77]. To investigate the role of these EV biogenesis pathways on the loading of RNA and protein cargoes for extracellular export, we inhibited the two variant enzyme classes implicated in this process.

Various chemical inhibitors of sphingomyelinases have been reported in the literature [223, 241-246]. These resources provide an interesting avenue for functional dissection, as they allow for rapid investigation over genetic knockdowns which are more labor intensive [247]. Our approach at selecting sphingomyelinase inhibitors was focused on evidence that they targeted the activities of either NSM or ASM, impeding the biogenesis of EVs at the endosomal compartment or the plasma membrane [82, 100, 121, 222]. Namely, NSM activity was inhibited with GW4869, and ASM was inhibited with FTY720. As these enzymes have been observed to affect the biogenesis of exosomes or microvesicles, their inhibition allows us to see their individual contributions to the heterogenous EV population. This permitted us to reveal the molecular signatures attributed to each EV subpopulation, as well the potential roles of NSM or ASM in EV cargo loading.

Although both neutral and acid sphingomyelinase variants metabolize sphingolipids within membranes, our results highlight their unique contributions to assortment of cargoes within EV subpopulations. Of note, neither drug treatment resulted in a complete abrogation of EV release, highlighting that cells utilize multiple avenues for

the biogenesis of EVs (**Figure 2.1 C-E**). This phenomenon has been widely reported when inhibiting EVs using a variety of chemical or genetic knockdown approaches, including the drugs here reported [248-256]. Nevertheless, they each had quantifiable effects on the quantity, size distribution, and contents of EVs released (**Figure S2.1 C-D**, **Figure 2.1 D-G**). Nanoflow cytometry of single EVs provided interesting insights into the number of particles released, as well as the cargoes they carried (**Figure S2.1 E**). In general, the relative number particles detected by NSM inhibition was not significant altered relative to the control conditions, however ASM-inhibited cells released more EVs (**Figure 2.1 F**). FTY720 (Fingolimod), the ASM inhibitor used in this study, is currently prescribed as an immunomodulatory drug (Gilenya®) for the treatment of multiple sclerosis [257-259]. Plasma-derived EVs from patients treated with a first dose of this drug showed an increased concentration and a shift in the expression of small non-coding RNAs they carried [255]. However, various studies have shown that FTY720 can reduce the production of membrane-derived microvesicles [248, 260, 261]. In the latter study, endothelial and B-cell-derived microvesicles from multiple sclerosis patients were reduced to the levels of healthy patients after treatment with Fingolimod [261]. Nanoflow cytometry profiles further showed that NSM inhibition with GW4869 resulted in an over all reduction in the relative number of RNA positive events (particles per million) in contrast to the other conditions (**Figure 2.1 G**). Interestingly, while EV release is enhanced by the inhibition of ASM, the relative number of RNA positive events indicate an overall reduction in the RNA-containing population (**Figure 2.1 G**). These results suggest that sphingolipid metabolism is an important component of the machineries used

by cells to release RNA via EVs. They also highlight that cells may utilize alternative routes for the generation of EVs when a particular pathway is perturbed.

At the transcriptome level, our results show that the inhibition of sphingolipid metabolism affects the release of RNA in unexpected ways. While ASM inhibition seems to increase the available extracellular RNA, this merely because of increased EV release (**Figure S2.2 B**), and their incidence in the overall population is decreased (**Figure 2.1 G**). Indeed, there is a general downregulation of RNA species affected when impeding the effects of this enzyme (**Figure 2.2 E**). These results have been partially alluded to previously, where EVs derived from multiple sclerosis patients treated with Fingolimod exhibited differential patterns of RNA expression [255, 262]. Gene ontology (GO) enrichment analysis of these downregulated RNAs revealed that many of these transcripts are associated with the negative regulation of translation and RNA binding. Moreover, the RNA biotypes detected in EVs have a more dramatic shift with ASM inhibition, with protein coding transcripts increasing and lncRNAs and pseudogenes exhibiting a reduction (**Figure 2.2 C**). In opposing effect, the quantified amounts of EV RNAs released after NSM inhibition is less than control EVs (**Figure S2.2 B**), yet there are negligible levels of differential expression (**Figure 2.2 E**). This poses various doubts as to the recruitment specificity of RNA species during sphingomyelinase-drive EV biogenesis. For instance, one would expect that a general decrease in RNA content in EVs by NSM inhibition would result in the downregulation of released transcripts. However, the cell may utilize alternative pathways to continually release transcripts via EVs, such as through ESCRT-dependent machineries [263] or increasing microvesicle

production [264]. Indeed, one study showed that treatments of human and mouse cells with GW4869 decreased the secretion of exosomes while simultaneously increasing the secretion of microvesicles from the plasma membrane [264]. It should be noted, however, that our EV quantifications show that there is an overall reduction of EVs released by cells treated with GW4869, but we make no distinction between subpopulations. On the other hand, one can speculate that the downregulation of RNAs resulting from ASM inhibition may be attributed to major shifts in the ceramide-driven activities of the cell membrane [265-267], whose normal function is essential for the release of all types of EVs [15, 109]. However, whether sphingolipid metabolism at the plasma membrane in relevant to the release of the non-microvesicle EV population is yet to be discerned. Another point of contention is the effects that the drugs may have on the cellular transcriptome, as changes in the baseline transcriptome may affect the levels of the secreted RNA population [268, 269]. While the amounts of RNAs present in cells (**Figure S2.2 A**) and global transcriptomes of cells (**Figure 2.2 A-B, D**, **Figure S2.2 C**) remains relative consistent in all conditions, there is a minor upregulation of RNAs as a result of either treatment (**Figure 2.2 D**). When normalizing to control cells, however, upregulated cellular transcripts do not display any GO enrichment suggesting stochastic effects (**Figure 2.2 F**). This indicates that effects at the cellular level do not appreciably contribute to the differentially expressed RNAs in EVs.

We further demonstrate that the proteomic composition of EVs is greatly impacted by sphingolipid metabolism. While cellular levels of protein expression remain consistent (**Figure S2.3 A**, **Figure 2.3 A-B**), EV proteomic composition is affected in opposing

directions as a result of drug treatments (**Figure 2.3 C-F**). In fact, discrete groups of proteins are down- or upregulated as a result of NSM or ASM inhibition (**Figure 2.3 C**), with the effects generally occurring in the opposite direction relative to the control group. This data suggests that sphingomyelin metabolism by ASM and NSM is specialized, with specific groups of proteins affected by their inhibition. These findings are supported by previous studies considering the possible role of NSM during the biogenesis of microvesicles, which ultimately showed that NSM activity is not required for the formation of microvesicles at the cell membrane [102, 264]. Rather, the ATP-induced translocation of ASM to the outer leaflet of the plasma membrane is require for the microvesicle population to form [102, 104]. Additionally, it highlights that inhibition of one pathway may induce the increased activity of other proteins for EV biogenesis to continue to occur. Focusing on the statistically significant changes to protein expression of the EV proteome, in both directions, we used ClueGO network analysis to investigate the associated cellular machineries affected (**Figure 2.3 D**). Our results highlight the specificity of the effects by either treatment, with ASM inhibition resulting in a downregulation of proteins associated with plasma membrane dynamics, while NSM inhibition downregulated proteins associated to endosomal and autophagic activity. It must be underscored that these changes are seen only at the EV level, with the expression levels of said proteins not changed at the cellular level. This indicates that sphingolipid metabolism is relevant for the incorporation of proteins associated to various subcellular machineries during EV biogenesis, with many of these likely participating during EV biogenesis to some degree. The effects of the inhibitor drugs on the EV proteome also make sense in the context of

the associated cellular machineries which are involved in the biogenesis of exosomes or microvesicles. For instance, exosomes are formed by ceramide-driven invaginations of the endosomal limiting membrane [82-84], with various other cellular complexes involved in their proper trafficking to the plasma membrane for their release [270]. In addition, components of various other mechanisms, such as the autophagy, have been implicated in the biogenesis of EVs [121]. We observe a downregulation of various of these components reflected by our data (**Figure 2.3 F**), implying an interruption in the normal biological processes associated with EV biogenesis at the endosome. Nevertheless, ESCRT-associated proteins are not impacted by this inhibition (**Figure 2.3 E**), indicating ESCRT-dependent EV biogenesis remains stable. This has been previously indicated with EV inhibition by GW4869 [121]. Quite interestingly, ASM inhibition also downregulated proteins associated with the multivesicular endosome (**Figure 2.3 D**). This could be partially explained by the intricate roles of ASM in the lysosome and, in turn, secretory autophagy, although this remains to be better defined [271-273]. Perhaps not surprisingly, ASM inhibition resulted in an upregulation of various machineries associated to exosome release (**Figure 2.3 D**). The included proteins involved in the release of intracellular vesicles, such as those involved in the trafficking of vesicles to the plasma membrane, further highlighting that ASM inhibition can trigger the increased release of non-membrane derived EVs. Strikingly, NSM inhibition resulted in an EV population which displayed a downregulation for a large number of RNA binding proteins (**Figure 2.3 D**, **Figure S2.3 D**), in contrast to ASM inhibition which increased their release (**Figure 2.3 D**, **Figure S2.3 D**). These results imply that extracellular trafficking of RBPs through EVs

is modulated by the endosomal compartment, with plasma membrane-derived EVs contributing minimally.

RNA-binding proteins play essential roles in the subcellular distribution of RNAs in cells [128-131]. Their role in the loading of RNAs to sites of EV biogenesis has been investigated, but only a small number of them have been conclusively implicated in the loading of various RNA molecules [131]. By isolating proteins from the same EVs used for transcriptomic profiling, we sought to determine whether co-incidence of RBPs correlated to the RNA cargoes in EVs formed during the inhibition of SMase-driven lipid metabolism. Our results showed that the release of RBPs via EVs is highly dependent on sphingolipid metabolism, with NSM inhibition resulting in a major downregulation of RBPs within EV specimens relative to both control and ASM-inhibited samples (**Figure 2.4 A-B**). By contrast, ASM inhibition increased the amounts of RBPs present within the EV population relative to control EV specimens (**Figure 2.4 C**). To further characterize the possible co-tracking of RBPs with their cargoes, we sought to investigate whether their RNA counterparts exhibited similar behaviours. At the transcriptomic level, NSM inhibition resulted in only minor changes to the overall expression of RNA cargoes in EVs, with ASM-inhibited samples showing larger changes to the overall expression of RNAs (**Figure 2.2 E**). This is counterintuitive, as one would expect that RBPs and RNAs would be trafficked in EVs as ribonucleoprotein (RNP) complexes, and as such RNAs in EVs would be downregulated in similar fashion as a response to NSM inhibition. Nevertheless, our data shows that the RNA content of EVs is decreased as a response to this treatment (**Figure 2.1 G**, **Figure S2.2 B**). Notwithstanding, some examples of this RBP-RNA co-

trafficking can be observed in our data. For example, the RBP and RNA components of the Signal Recognition Particle (SRP), and of those involved in the formation of spliceosomal small nuclear ribonucleoprotein complexes (snRNPs), displayed similar trends in downregulation in EVs as a response to treatments with GW4869 (**Figure 2.4 D**, **Figure 2.4 F**). These results indicate that certain RNP complexes may be exported in EVs and that, importantly, this trafficking is associated with sphingolipid metabolism at the endosomal compartment.

The bioactive cargoes of EVs play key roles in the transfer of molecular signals from one cell to the next, altering the physiological state of recipient cells [274]. For instance, unshielded 7SL RNA can be exported through EVs and results in the activation of the viral RNA pattern cognition receptor, Retinoic acid-inducible gene I (RIG-I), in recipient cells [275]. As a result, recipient cells are modified in the tumor microenvironment to allow for more aggressive features of cancer to occur [275, 276]. As our data clearly showed that EV cargoes are impacted by changes to the normal activity of sphingomyelinases in cells, we sought to investigate whether these changes could affect the EVs' ability to transmit information. Using various co-culture experiments, where drug-induced MCF7 EVs were incubated with a recipient cell line (MCF10A), we show that these differences can indeed affect the way that recipient cells respond to the co-culture. First, MCF7 EVs from control or SMase-inhibited cells were isolated using size exclusion chromatography (SEC) in a volumetrically equivalent fashion. These EVs were then used for co-culture with MCF10A cells, a normal human epithelial cell line which has been used previously in similar EV co-culture setups [277-279]. Driven by noted examples

in our transcriptomic and proteomic data sets, namely changes in the export of components of the Signal Recognition Particle (SRP) (**Figure S2.2 H**, **Figure 2.4 D**), which targets nascent proteins containing signal peptides to the endoplasmic reticulum (ER) [280], we evaluated if the translational response of MCF10A to MCF7 EVs could be affected by the inhibition of SMases. O-propargyl-puromycin (OOP)-labelling of nascent peptides in MCF10A cells was quantified by the mean foci intensities observed as a response to their incubation with control or drug-induced MCF7 EVs. Our results showed that MCF10A cells incubated with EVs derived from ASM inhibitor treatments displayed increase foci intensities in comparison to the other conditions tested, which showed no effects in translation activities (**Figure 2.5 B**, **Figure S2.5 A**). This indicates that EVs derived from FTY720 treatments, may play a role in cellular translation phenotypes.

Cell division associated mRNAs were a select class of transcripts upregulated in EVs derived from ASM inhibitor treatments (**Figure 2.2 F**), furthermore, our proteomics data indicated that cell division associated proteins were simultaneously downregulated by this treatment (**Figure 2.3 D**). To investigate whether changes in these cargoes could affect the baseline cell cycle activities of recipient cells, MCF10A cells were incubated with control or drug-induced MCF7 EVs. 5-ethynyl-2'-deoxyuridine (EdU), which incorporates into newly synthesized DNA, was added to MCF10A cells exposed to MCF7 EVs to quantify the number of new cells in the population over time. Our results indicate that MCF10A cells incubated with EVs derived from ASM inhibition had a higher number of new cells in comparison to other conditions, although this effect was only observed at 40 h (**Figure 2.5 C**, **Figure S2.5 B**). While more moderate than the translational response

we also observed, EVs derived from ASM inhibitor treatments may also differentially impact the cell proliferation dynamics of MCF10A cells.

With the observed changes to physiological properties of MCF10A cells co-cultured with control or drug-induced EVs, we next sought to characterize whether these changes could impact cell migration. We developed a scratch wound healing assay to quantify the relative wound density (%RWD), over time, of wounded confluent monolayers of MCF10A co-cultured with EVs from control or SMase-inhibited MCF7 cells (**Figure S2.5 C**). Using the Incucyte live cell imaging platform, we captured images of wounded cellular cultures every hour over 24 h, and then quantified the relative wound density of each condition over time. An equivalent volume of PBS to PBS-EV suspension was used as a negative control. Using this approach, we show that MCF10A cells exposed to MCF7 EVs derived from treatments with ASM inhibitor, FTY720, displayed higher %RWD over time versus the other conditions investigated (**Figure 2.5 D**). These data indicate that FTY720 EVs can enhance the migratory response of MCF10A cells, an effect which can possibly be attributed to the changes in molecular cargoes of EVs resulting from ASM inhibition.

Here, we report an in-depth characterization of the role of sphingolipid metabolism in the incorporation of cargoes within the heterogenous EV population. Together, the results here described provide compelling evidence of the importance of sphingomyelinase-drive lipid metabolism for the loading of cargoes during EV biogenesis. We show that EV biogenesis resulting from sphingolipid metabolism is enzyme variant

dependent (NSM versus ASM), and that the cell will use alternate routes for the generation of EVs when one pathway is inhibited. Our data reveals that NSM and ASM contribute differentially to the cargoes sorted to EVs, with NSM inhibition downregulating the export of RNP modules, while ASM inhibition differentially impacts the export of RNAs. Moreover, NSM generated EVs present as major hubs for the export of molecular cargoes from cells. We also provide evidence that changes to the EV population, as a result of the inhibition sphingomyelin metabolism pathways, can affect their communicatory potential. This indicates that specific subpopulations of EVs may have a higher relevance to intercellular communication.

2.6. Chapter II References

1. Fafián-Labora, J.A. and A. O'Loghlen, *Classical and Nonclassical Intercellular Communication in Senescence and Ageing.* Trends in Cell Biology, 2020. **30**(8): p. 628-639.

2. Berumen Sánchez, G., et al., *Extracellular vesicles: mediators of intercellular communication in tissue injury and disease.* Cell Communication and Signaling, 2021. **19**(1): p. 104.

5. Andaloussi, S.E., et al., *Extracellular vesicles: biology and emerging therapeutic opportunities.* Nat Rev Drug Discov, 2013. **12**(5): p. 347-57.

7. Kalluri, R. and V.S. LeBleu, *The biology, function, and biomedical applications of exosomes.* Science, 2020. **367**(6478): p. eaau6977.

15. van Niel, G., G. D'Angelo, and G. Raposo, *Shedding light on the cell biology of extracellular vesicles.* Nat Rev Mol Cell Biol, 2018. **19**(4): p. 213-228.

19. Yoon, Y.J., O.Y. Kim, and Y.S. Gho, *Extracellular vesicles as emerging intercellular communicasomes.* BMB Rep, 2014. **47**(10): p. 531-9.

20. Robbins, P.D. and A.E. Morelli, *Regulation of immune responses by extracellular vesicles.* Nature Reviews Immunology, 2014. **14**(3): p. 195-208.

25. Vader, P., X.O. Breakefield, and M.J.A. Wood, *Extracellular vesicles: emerging targets for cancer therapy.* Trends in Molecular Medicine, 2014. **20**(7): p. 385-393.

60. Valadi, H., et al., *Exosome-mediated transfer of mRNAs and microRNAs is a novel mechanism of genetic exchange between cells.* Nature Cell Biology, 2007. **9**(6): p. 654-659.

70. Gurunathan, S., et al., *Biogenesis, Membrane Trafficking, Functions, and Next Generation Nanotherapeutics Medicine of Extracellular Vesicles.* Int J Nanomedicine, 2021. **16**: p. 3357-3383.

75. Kowal, J., et al., *Proteomic comparison defines novel markers to characterize heterogeneous populations of extracellular vesicle subtypes.* Proc Natl Acad Sci U S A, 2016. **113**(8): p. E968-77.

77. Jeppesen, D.K., et al., *Reassessment of Exosome Composition.* Cell, 2019. **177**(2): p. 428-445.e18.

82. Trajkovic, K., et al., *Ceramide Triggers Budding of Exosome Vesicles into Multivesicular Endosomes.* Science, 2008. **319**(5867): p. 1244-1247.

83. Goñi, F.M. and A. Alonso, *Effects of ceramide and other simple sphingolipids on membrane lateral structure.* Biochim Biophys Acta, 2009. **1788**(1): p. 169-77.

84. Kajimoto, T., et al., *Ongoing activation of sphingosine 1-phosphate receptors mediates maturation of exosomal multivesicular endosomes.* Nat Commun, 2013. **4**: p. 2712.

94. Lefebvre, F.A., et al., *Comparative transcriptomic analysis of human and Drosophila extracellular vesicles.* Sci Rep, 2016. **6**: p. 27680.

99. Muralidharan-Chari, V., et al., *ARF6-regulated shedding of tumor cell-derived plasma membrane microvesicles.* Curr Biol, 2009. **19**(22): p. 1875-85.

100. Dawson, G. and J. Qin, *Gilenya (FTY720) inhibits acid sphingomyelinase by a mechanism similar to tricyclic antidepressants.* Biochem Biophys Res Commun, 2011. **404**(1): p. 321-3.

102. Bianco, F., et al., *Acid sphingomyelinase activity triggers microparticle release from glial cells.* The EMBO Journal, 2009. **28**(8): p. 1043-1054.

104. Wang, J., U.R. Pendurthi, and L.V.M. Rao, *Sphingomyelin encrypts tissue factor: ATP-induced activation of A-SMase leads to tissue factor decryption and microvesicle shedding.* Blood Adv, 2017. **1**(13): p. 849-862.

105. Verderio, C., M. Gabrielli, and P. Giussani, *Role of sphingolipids in the biogenesis and biological activity of extracellular vesicles.* J Lipid Res, 2018. **59**(8): p. 1325-1340.

109. Abels, E.R. and X.O. Breakefield, *Introduction to Extracellular Vesicles: Biogenesis, RNA Cargo Selection, Content, Release, and Uptake.* Cellular and Molecular Neurobiology, 2016. **36**(3): p. 301-312.

121. Leidal, A.M., et al., *The LC3-conjugation machinery specifies the loading of RNA-binding proteins into extracellular vesicles.* Nature Cell Biology, 2020. **22**(2): p. 187-199.

122. Crescitelli, R., et al., *Distinct RNA profiles in subpopulations of extracellular vesicles: apoptotic bodies, microvesicles and exosomes.* J Extracell Vesicles, 2013. **2**.

125. van der Meel, R., et al., *Extracellular vesicles as drug delivery systems: Lessons from the liposome field.* Journal of Controlled Release, 2014. **195**: p. 72-85.

126. Tetta, C., et al., *Extracellular vesicles as an emerging mechanism of cell-to-cell communication.* Endocrine, 2013. **44**(1): p. 11-19.

128. Chin, A. and E. Lecuyer, *RNA localization: Making its way to the center stage.* Biochim Biophys Acta, 2017. **1861**(11 Pt B): p. 2956-2970.

129. Lecuyer, E., H. Yoshida, and H.M. Krause, *Global implications of mRNA localization pathways in cellular organization.* Curr Opin Cell Biol, 2009. **21**(3): p. 409-15.

130. Bergalet, J. and E. Lecuyer, *The functions and regulatory principles of mRNA intracellular trafficking.* Adv Exp Med Biol, 2014. **825**: p. 57-96.

131. Fabbiano, F., et al., *RNA packaging into extracellular vesicles: An orchestra of RNA-binding proteins?* Journal of Extracellular Vesicles, 2020. **10**(2): p. e12043.

151. O'Brien, K., et al., *RNA delivery by extracellular vesicles in mammalian cells and its applications.* Nat Rev Mol Cell Biol, 2020. **21**(10): p. 585-606.

153. Quesenberry, P.J., et al., *Role of extracellular RNA-carrying vesicles in cell differentiation and reprogramming.* Stem Cell Research & Therapy, 2015. **6**(1): p. 153.

154. Dinger, M.E., T.R. Mercer, and J.S. Mattick, *RNAs as extracellular signaling molecules.* J Mol Endocrinol, 2008. **40**(4): p. 151-9.

161. Maacha, S., et al., *Extracellular vesicles-mediated intercellular communication: roles in the tumor microenvironment and anti-cancer drug resistance.* Molecular Cancer, 2019. **18**(1): p. 55.

222. Trkov, S., et al., *Fingolimod--a sphingosine-like molecule inhibits vesicle mobility and secretion in astrocytes.* Glia, 2012. **60**(9): p. 1406-16.

223. Catalano, M. and L. O'Driscoll, *Inhibiting extracellular vesicles formation and release: a review of EV inhibitors.* Journal of Extracellular Vesicles, 2020. **9**(1): p. 1703244.

224. Choi, D.-S. and Y.S. Gho, *Isolation of Extracellular Vesicles for Proteomic Profiling*, in *Proteomic Profiling: Methods and Protocols*, A. Posch, Editor. 2015, Springer New York: New York, NY. p. 167-177.

225. Choi, M., et al., *MSstats: an R package for statistical analysis of quantitative mass spectrometry-based proteomic experiments.* Bioinformatics, 2014. **30**(17): p. 2524-6.

226. Gu, Z., R. Eils, and M. Schlesner, *Complex heatmaps reveal patterns and correlations in multidimensional genomic data.* Bioinformatics, 2016. **32**(18): p. 2847-9.

227. Ritchie, M.E., et al., *limma powers differential expression analyses for RNA-sequencing and microarray studies.* Nucleic Acids Res, 2015. **43**(7): p. e47.

228. Merico, D., et al., *Enrichment map: a network-based method for gene-set enrichment visualization and interpretation.* PLoS One, 2010. **5**(11): p. e13984.

229. Dobin, A., et al., *STAR: ultrafast universal RNA-seq aligner.* Bioinformatics, 2012. **29**(1): p. 15-21.

230. Liao, Y., G.K. Smyth, and W. Shi, *featureCounts: an efficient general purpose program for assigning sequence reads to genomic features.* Bioinformatics, 2013. **30**(7): p. 923-930.

231. Love, M.I., W. Huber, and S. Anders, *Moderated estimation of fold change and dispersion for RNA-seq data with DESeq2.* Genome Biology, 2014. **15**(12): p. 550.

232. Kucukural, A., et al., *DEBrowser: interactive differential expression analysis and visualization tool for count data.* BMC Genomics, 2019. **20**(1): p. 6.

233. Berriz, G.F., et al., *Characterizing gene sets with FuncAssociate.* Bioinformatics, 2003. **19**(18): p. 2502-2504.

234. Kotrbová, A., et al., *TEM ExosomeAnalyzer: a computer-assisted software tool for quantitative evaluation of extracellular vesicles in transmission electron microscopy images.* Journal of Extracellular Vesicles, 2019. **8**(1): p. 1560808.

235. Bindea, G., et al., *ClueGO: a Cytoscape plug-in to decipher functionally grouped gene ontology and pathway annotation networks.* Bioinformatics, 2009. **25**(8): p. 1091-3.

236. Shannon, P., et al., *Cytoscape: a software environment for integrated models of biomolecular interaction networks.* Genome Res, 2003. **13**(11): p. 2498-504.

237. Bonner, S.E. and E. Willms, *Intercellular communication through extracellular vesicles in cancer and evolutionary biology.* Progress in Biophysics and Molecular Biology, 2021. **165**: p. 80-87.

238. Lizarraga-Valderrama, L.R. and G.K. Sheridan, *Extracellular vesicles and intercellular communication in the central nervous system.* FEBS Letters, 2021. **595**(10): p. 1391-1410.

239. Colombo, M., G. Raposo, and C. Théry, *Biogenesis, Secretion, and Intercellular Interactions of Exosomes and Other Extracellular Vesicles.* Annual Review of Cell and Developmental Biology, 2014. **30**(1): p. 255-289.

240. Xiang, H., et al., *Physiological functions and therapeutic applications of neutral sphingomyelinase and acid sphingomyelinase.* Biomed Pharmacother, 2021. **139**: p. 111610.

241. Arenz, C., *Small molecule inhibitors of acid sphingomyelinase.* Cell Physiol Biochem, 2010. **26**(1): p. 1-8.

242. Lee, D.H., et al., *Identification and evaluation of neutral sphingomyelinase 2 inhibitors.* Arch Pharm Res, 2011. **34**(2): p. 229-36.

243. Kornhuber, J., et al., *Functional inhibitors of acid sphingomyelinase (FIASMAs).* Handb Exp Pharmacol, 2013(215): p. 169-86.

244. Šála, M., et al., *Novel Human Neutral Sphingomyelinase 2 Inhibitors as Potential Therapeutics for Alzheimer's Disease.* J Med Chem, 2020. **63**(11): p. 6028-6056.

245. Kumar, A. and S. Kumar, *Inhibition of extracellular vesicle pathway using neutral sphingomyelinase inhibitors as a neuroprotective treatment for brain injury.* Neural Regen Res, 2021. **16**(12): p. 2349-2352.

246. Carpinteiro, A., et al., *Inhibition of acid sphingomyelinase by ambroxol prevents SARS-CoV-2 entry into epithelial cells.* J Biol Chem, 2021. **296**: p. 100701.

247. MacBeath, G., *Chemical genomics: what will it take and who gets to play?* Genome Biol, 2001. **2**(6): p. Comment2005.

248. Amoruso, A., et al., *Effect of fingolimod action on the release of monocyte-derived microvesicles in multiple sclerosis patients.* J Neuroimmunol, 2018. **323**: p. 43-48.

249. Barman, B., et al., *VAP-A and its binding partner CERT drive biogenesis of RNA-containing extracellular vesicles at ER membrane contact sites.* Developmental Cell, 2022. **57**(8): p. 974-994.e8.

250. Colombo, M., et al., *Analysis of ESCRT functions in exosome biogenesis, composition and secretion highlights the heterogeneity of extracellular vesicles.* J Cell Sci, 2013. **126**(Pt 24): p. 5553-65.

251. Kholia, S., et al., *A novel role for peptidylarginine deiminases in microvesicle release reveals therapeutic potential of PAD inhibition in sensitizing prostate cancer cells to chemotherapy.* J Extracell Vesicles, 2015. **4**: p. 26192.

252. Kosgodage, U.S., et al., *Chloramidine/Bisindolylmaleimide-I-Mediated Inhibition of Exosome and Microvesicle Release and Enhanced Efficacy of Cancer Chemotherapy.* Int J Mol Sci, 2017. **18**(5).

253. Li, X.Q., et al., *Exosomes derived from gefitinib-treated EGFR-mutant lung cancer cells alter cisplatin sensitivity via up-regulating autophagy.* Oncotarget, 2016. **7**(17): p. 24585-95.

254. Matsumoto, A., et al., *Accelerated growth of B16BL6 tumor in mice through efficient uptake of their own exosomes by B16BL6 cells.* Cancer Sci, 2017. **108**(9): p. 1803-1810.

255. Sáenz-Cuesta, M., et al., *The First Dose of Fingolimod Affects Circulating Extracellular Vesicles in Multiple Sclerosis Patients.* Int J Mol Sci, 2018. **19**(8).

256. Zhou, X., et al., *Exosome production and its regulation of EGFR during wound healing in renal tubular cells.* Am J Physiol Renal Physiol, 2017. **312**(6): p. F963-f970.

257. Huwiler, A. and U. Zangemeister-Wittke, *The sphingosine 1-phosphate receptor modulator fingolimod as a therapeutic agent: Recent findings and new perspectives.* Pharmacol Ther, 2018. **185**: p. 34-49.

258. Zaffaroni, M., *Fingolimod in pediatric-onset multiple sclerosis.* Neurol Sci, 2021. **42**(Suppl 1): p. 1-4.

259. Chun, J., et al., *Fingolimod: Lessons Learned and New Opportunities for Treating Multiple Sclerosis and Other Disorders.* Annu Rev Pharmacol Toxicol, 2019. **59**: p. 149-170.

260. Liu, X., et al., *Inhibition of P2X7 receptors improves outcomes after traumatic brain injury in rats.* Purinergic Signalling, 2017. **13**(4): p. 529-544.

261. Zinger, A., et al., *Plasma levels of endothelial and B-cell-derived microparticles are restored by fingolimod treatment in multiple sclerosis patients.* Mult Scler, 2016. **22**(14): p. 1883-1887.

262. Ebrahimkhani, S., et al., *Serum Exosome MicroRNAs Predict Multiple Sclerosis Disease Activity after Fingolimod Treatment.* Mol Neurobiol, 2020. **57**(2): p. 1245-1258.

263. Juan, T. and M. Fürthauer, *Biogenesis and function of ESCRT-dependent extracellular vesicles.* Semin Cell Dev Biol, 2018. **74**: p. 66-77.

264. Menck, K., et al., *Neutral sphingomyelinases control extracellular vesicles budding from the plasma membrane.* J Extracell Vesicles, 2017. **6**(1): p. 1378056.

265. Bollinger, C.R., V. Teichgräber, and E. Gulbins, *Ceramide-enriched membrane domains.* Biochim Biophys Acta, 2005. **1746**(3): p. 284-94.

266. Castro, B.M., M. Prieto, and L.C. Silva, *Ceramide: a simple sphingolipid with unique biophysical properties.* Prog Lipid Res, 2014. **54**: p. 53-67.

267. Okada, T., et al., *Sphingosine kinase/sphingosine 1-phosphate signalling in central nervous system.* Cell Signal, 2009. **21**(1): p. 7-13.

268. de Jong, O.G., et al., *Cellular stress conditions are reflected in the protein and RNA content of endothelial cell-derived exosomes.* J Extracell Vesicles, 2012. **1**.

269. Squadrito, M.L., et al., *Endogenous RNAs modulate microRNA sorting to exosomes and transfer to acceptor cells.* Cell Rep, 2014. **8**(5): p. 1432-46.

270. Liu, J., et al., *The biology, function, and applications of exosomes in cancer.* Acta Pharm Sin B, 2021. **11**(9): p. 2783-2797.

271. Perrotta, C., et al., *The emerging role of acid sphingomyelinase in autophagy.* Apoptosis, 2015. **20**(5): p. 635-44.

272. Justice, M.J., et al., *Inhibition of acid sphingomyelinase disrupts LYNUS signaling and triggers autophagy.* J Lipid Res, 2018. **59**(4): p. 596-606.

273. Buratta, S., et al., *Lysosomal Exocytosis, Exosome Release and Secretory Autophagy: The Autophagic- and Endo-Lysosomal Systems Go Extracellular.* Int J Mol Sci, 2020. **21**(7).

274. van Niel, G., et al., *Challenges and directions in studying cell-cell communication by extracellular vesicles.* Nat Rev Mol Cell Biol, 2022. **23**(5): p. 369-382.

275. Nabet, B.Y., et al., *Exosome RNA Unshielding Couples Stromal Activation to Pattern Recognition Receptor Signaling in Cancer.* Cell, 2017. **170**(2): p. 352-366 e13.

276. Johnson, L.R., et al., *The immunostimulatory RNA RN7SL1 enables CAR-T cells to enhance autonomous and endogenous immune function.* Cell, 2021. **184**(19): p. 4981-4995.e14.

277. Galindo-Hernandez, O., et al., *Extracellular vesicles from women with breast cancer promote an epithelial-mesenchymal transition-like process in mammary epithelial cells MCF10A.* Tumour Biol, 2015. **36**(12): p. 9649-59.

278. Leal-Orta, E., et al., *Role of PI3K/Akt on migration and invasion of MCF10A cells treated with extracellular vesicles from MDA-MB-231 cells stimulated with linoleic acid.* J Cell Commun Signal, 2019. **13**(2): p. 235-244.

279. Ozawa, P.M.M., et al., *Extracellular vesicles from triple-negative breast cancer cells promote proliferation and drug resistance in non-tumorigenic breast cells.* Breast Cancer Res Treat, 2018. **172**(3): p. 713-723.

280. Kellogg, M.K., et al., *SRPassing Co-translational Targeting: The Role of the Signal Recognition Particle in Protein Targeting and mRNA Protection.* Int J Mol Sci, 2021. **22**(12).

2.7. Supplementary Figures

FIGURE S2.1

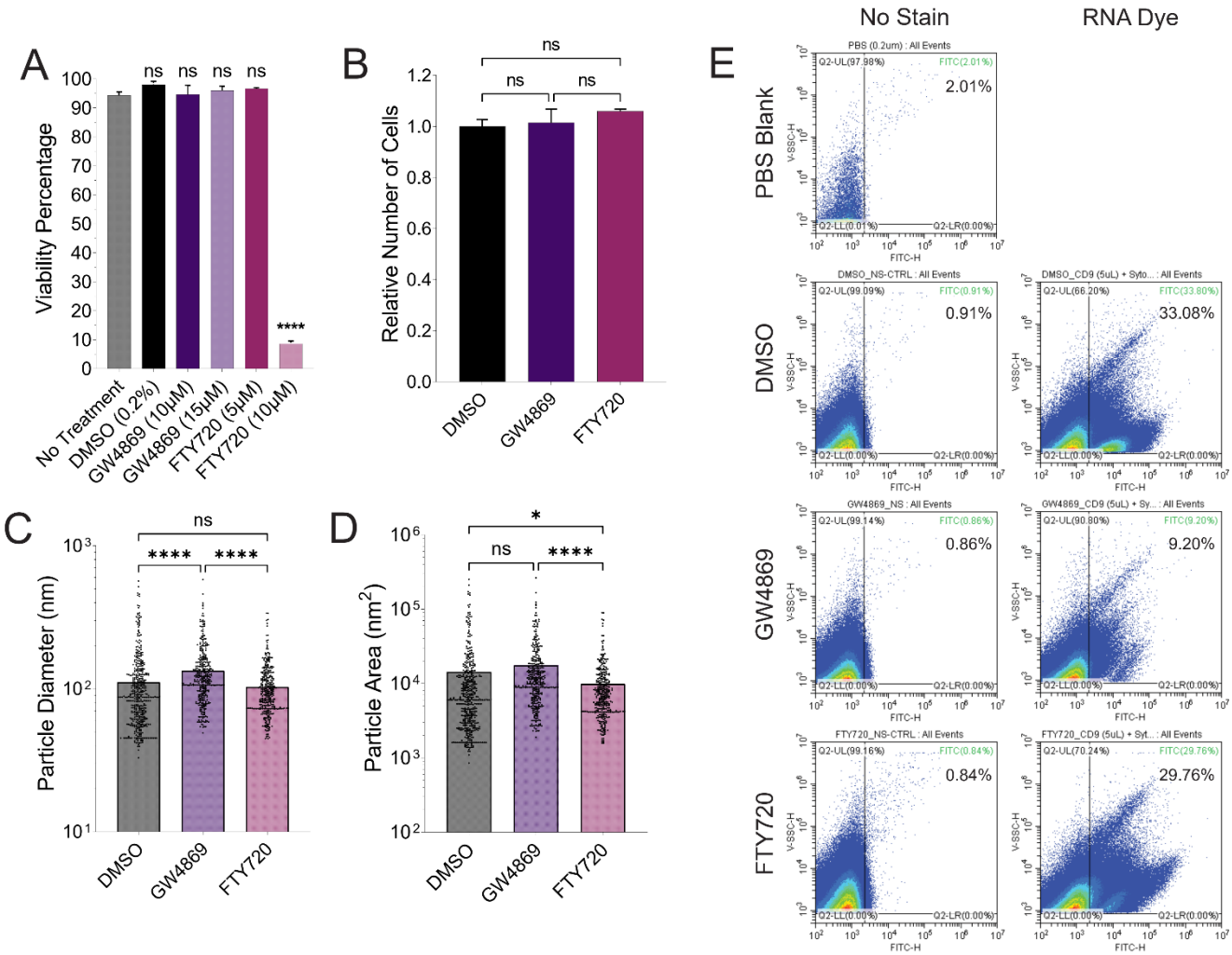

FIGURE S2.1 Ceramide is required for the recruitment of RNAs to EVs. **A.** Cellular viability of MCF7 cells after treatment with different molar concentrations of sphingomyelinase inhibitor drugs over 36 h. DMSO is the drug vehicle and represent the control group. Statistical significance was calculated by ordinary one-way ANOVA on GraphPad Prism. **B.** Relative number of cells under different conditions at the time of EV harvesting. Statistical significance was calculated by ordinary one-way ANOVA on GraphPad Prism. **C.** Nanoparticle diameter (nm) profiles of iodixanol-gradient purified

EVs as quantified by TEM ExosomeAnalyser. **D.** Nanoparticle area (nm^2) profiles of iodixanol-gradient purified EVs as quantified by TEM ExosomeAnalyser. **E.** Representative nanoflow cytometry profiles as captured by the CytoFLEX platform. RNA-positive events were detected by staining samples with SYTO RNASelect prior to purification through size exclusion chromatography (SEC). Percent values represent percentage of particles detected under FITC (RNA dye). For all bar graphs, unless otherwise stated, the error bars represent the standard error of the mean (SEM) and the statistics were calculated by ordinary one-way ANOVA (where ns=$P>0.05$, *=$P\leq0.05$, **=$P\leq0.01$, ***=$P\leq0.001$, and ****= $P\leq0.0001$) on GraphPad Prism.

FIGURE S2.2

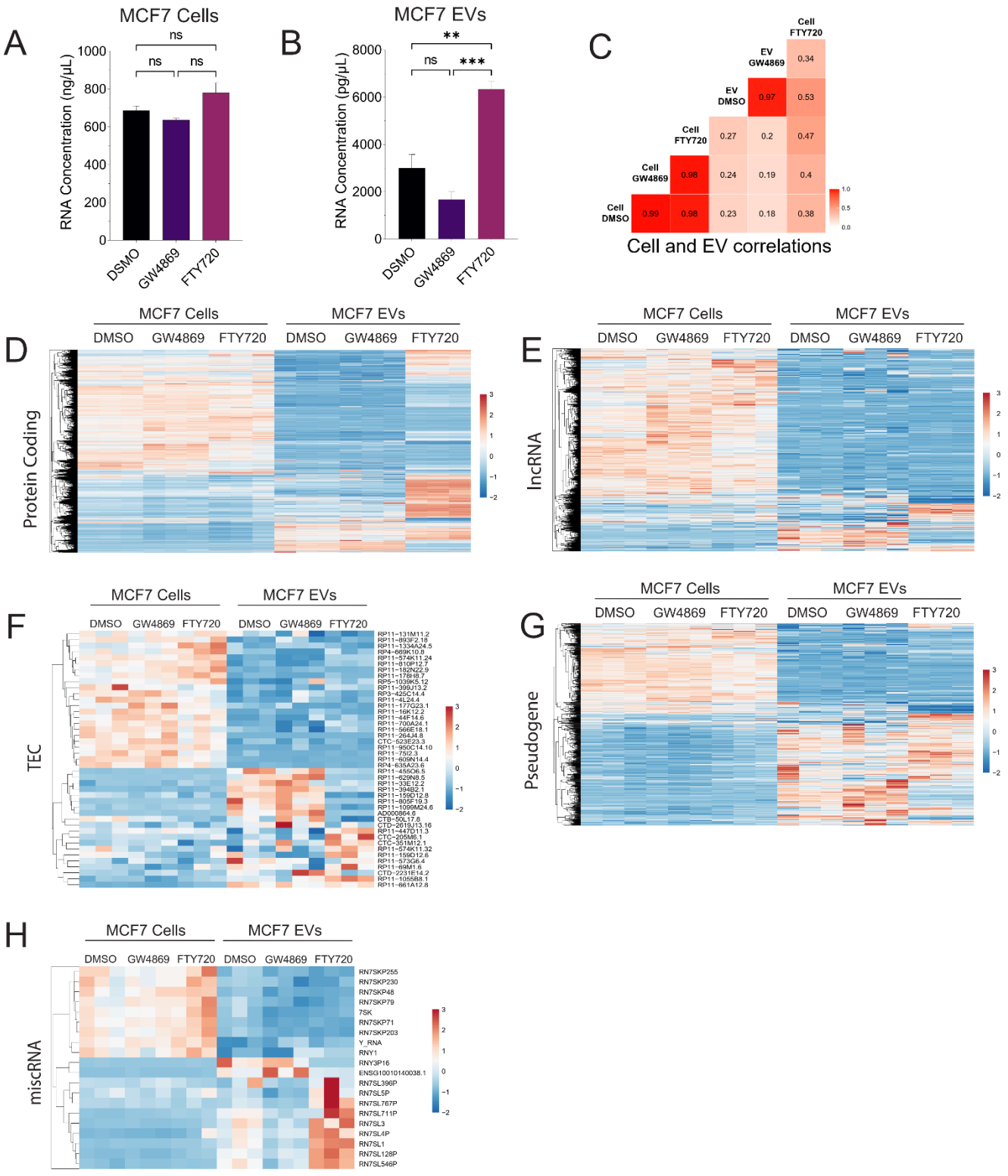
A
MCF7 Cells
RNA Concentration (ng/µL)
ns
ns
ns
DSMO
GW4869
FTY720
B
MCF7 EVs
RNA Concentration (pg/µL)
**
ns
***
C
Cell DMSO
Cell GW4869
Cell FTY720
EV DMSO
EV GW4869
Cell and EV correlations
D
Protein Coding
E
lncRNA
F
TEC
G
Pseudogene
H
miscRNA

FIGURE S2.2 Inhibition of ASM downregulates the RNA diversity of EVs. **A.** Nanodrop quantification of RNAs isolated from MCF7 cells. Statistical significance was calculated by ordinary one-way ANOVA on GraphPad Prism. **B.** Nanodrop quantification of RNAs isolated from MCF7 EV. Statistical significance was calculated by ordinary one-way ANOVA on GraphPad Prism. **C.** Global transcriptome correlations of cellular and EV specimens. **D. - F.** RNA biotype-specific clustering of cellular and EV transcriptomes with their respective identity indicated on the left.

FIGURE S2.3

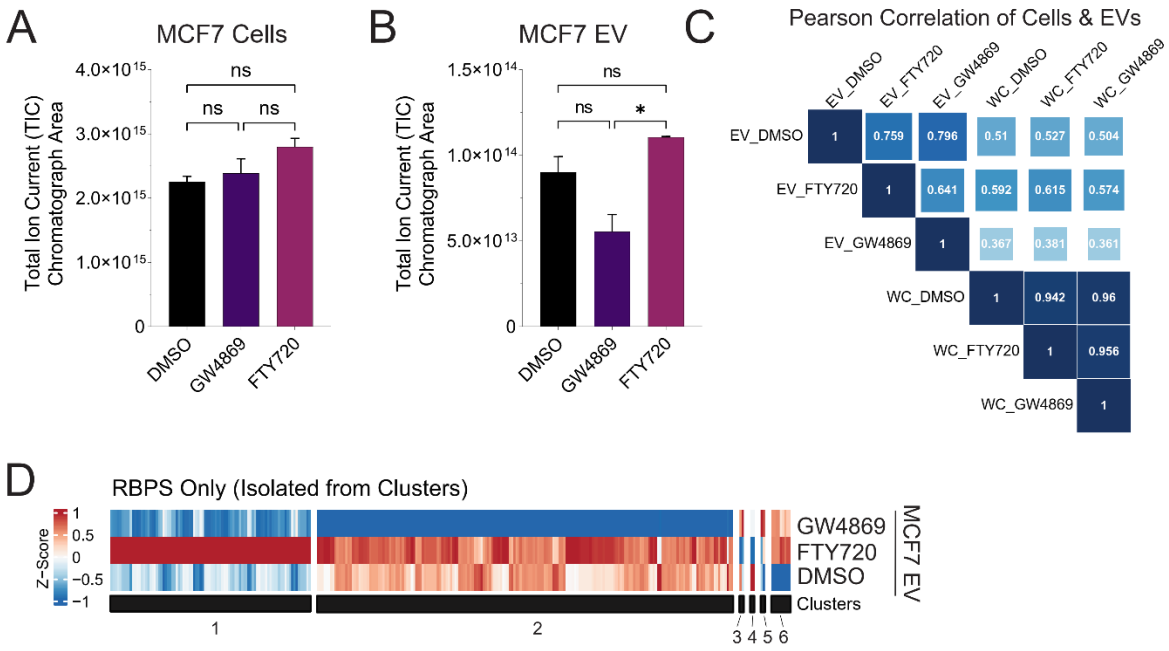

FIGURE S2.3 Neutral and acid sphingomyelinases affect different EV biogenesis pathways. **A.** Total Ion Current (TIC) chromatograph area isolated from MCF7 cells as estimated by initial injection volume and total sample volume. Statistical significance was calculated by ordinary one-way ANOVA on GraphPad Prism. **B.** Total Ion Current (TIC) chromatograph area isolated from MCF7 cells as estimated by initial injection volume and total sample volume. **C.** Pearson correlations of cellular and EV proteomes. **D.** Peptide intensities (relative Z-score) of EV RBPs retrieved from the clustered heatmap analysis showin in Figure 3 C. Blue lines denote lower association, while red lines denote higher association of each protein relative to the other two groups. For all bar graphs, unless otherwise stated, the error bars represent the standard error of the mean (SEM) and the statistics were calculated by ordinary one-way ANOVA (where ns=P>0.05, *=P≤0.05, **=P≤0.01, ***=P≤0.001, and ****= P≤0.0001) on GraphPad Prism.

FIGURE S2.4

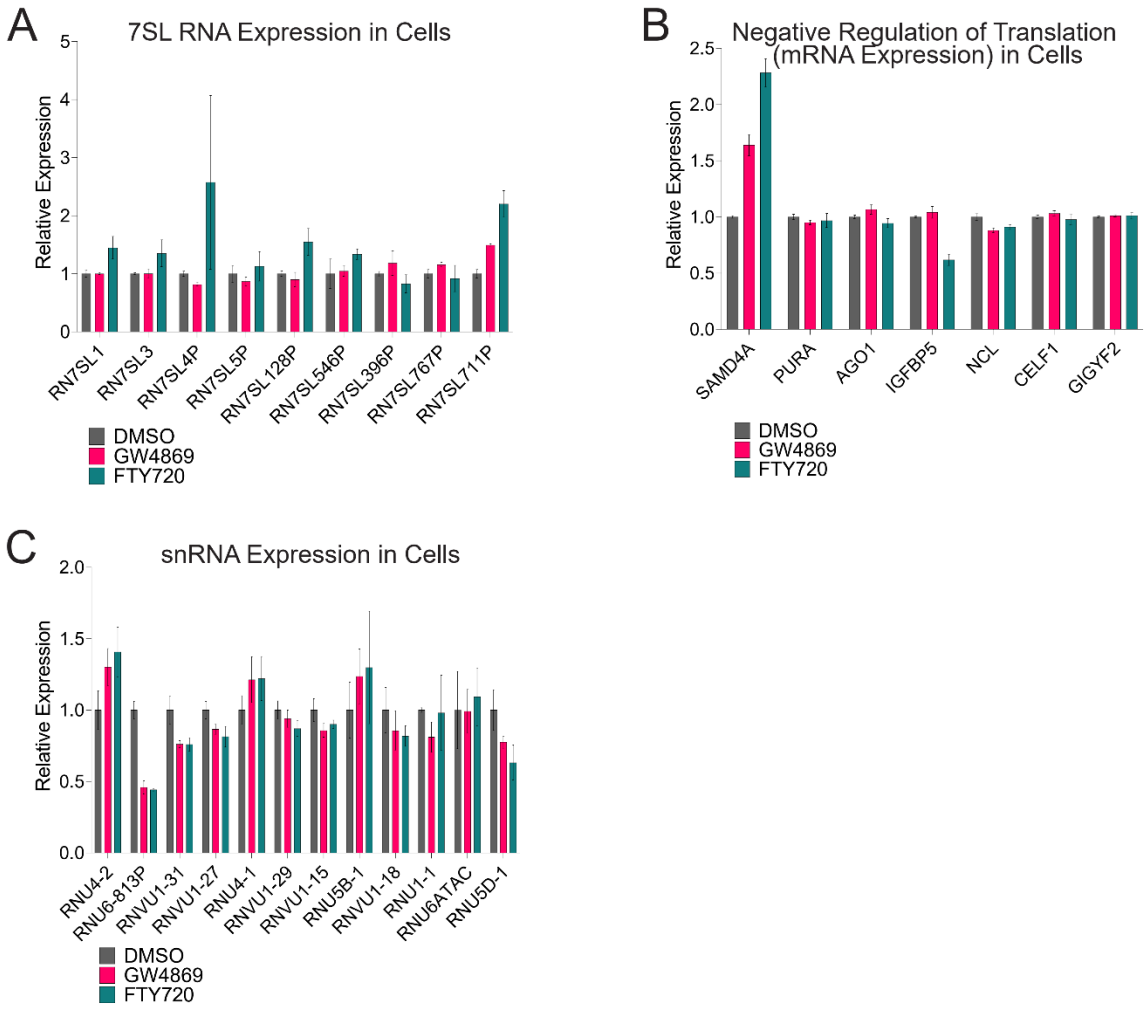

FIGURE S2.4 NSM is essential for the export of RBPs and their binding partners. **A.** Expression (TPM) of 7SL RNAs in GW4869 and FTY720 treated cells relative to the DMSO control. **B.** Expression (TPM) of RNAs associated to the negative regulation of translation in GW4869 and FTY720 treated cells relative to the DMSO control. **C.** Expression (TPM) of snRNAs in GW4869 and FTY720 treated cells relative to the DMSO control.

FIGURE S2.5

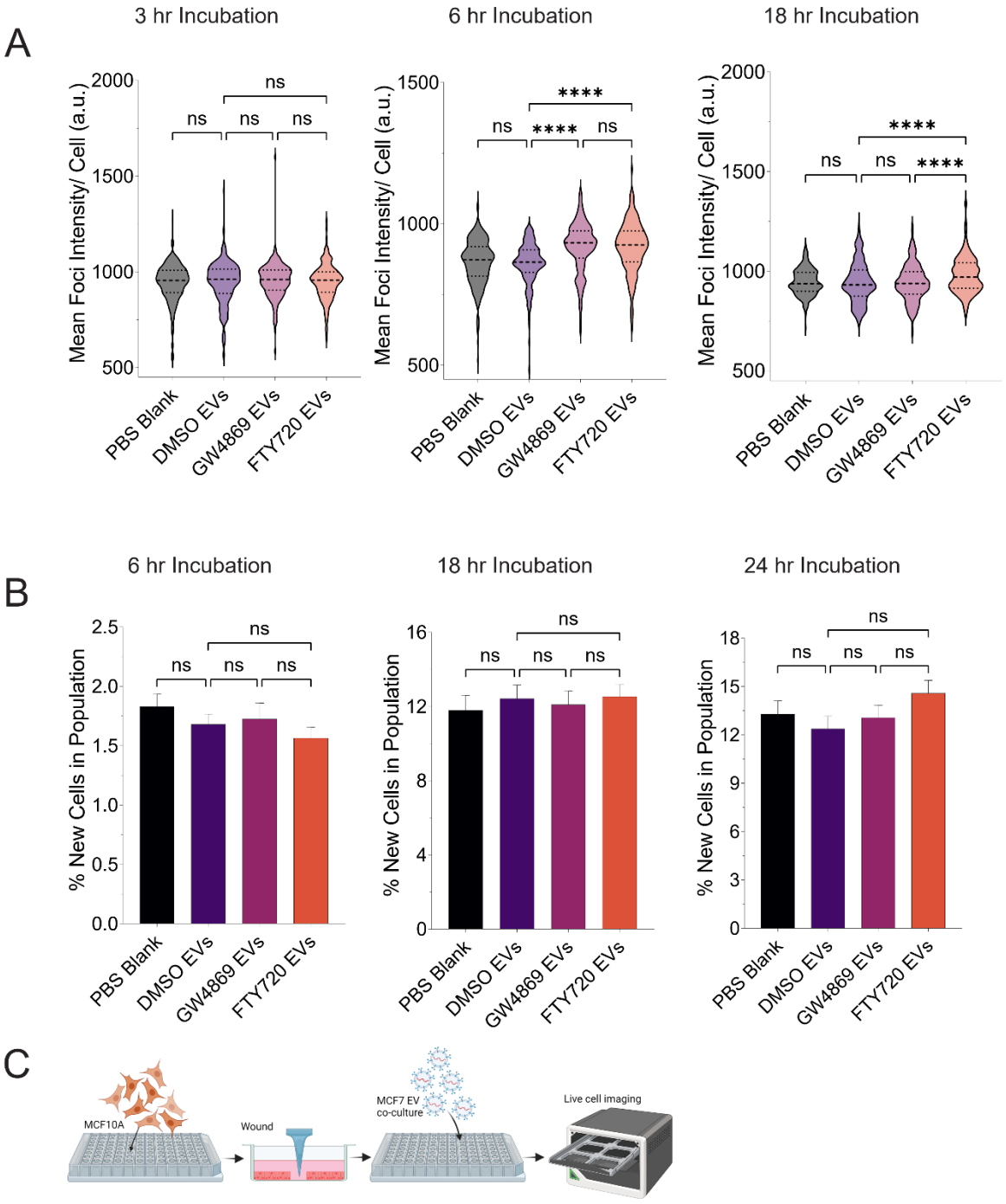
A
3 hr Incubation
6 hr Incubation
18 hr Incubation
Mean Foci Intensity/ Cell (a.u.)
2000
1500
1000
500
ns
****
PBS Blank
DMSO EVs
GW4869 EVs
FTY720 EVs
B
6 hr Incubation
18 hr Incubation
24 hr Incubation
% New Cells in Population
2.5
2.0
1.5
1.0
0.5
0.0
16
12
8
4
0
18
15
9
6
3
C
MCF10A
Wound
MCF7 EV co-culture
Live cell imaging

FIGURE S2.5 FTY720 EVs increased protein translation and induce faster migration phenotype in recipient cells. **A.** Violin plots of the distribution of intensities (a.u.) (over time) of OPP-labelled foci in MCF10A cells upon co-culture with EVs isolated from MCF7 cells treated with SMase inhibitors. **C.** Percentage of new cells (over time) as labelled by EdU in MCF10A cells upon co-culture with EVs isolated from MCF7 cells treated with SMase inhibitors. **D.** Outline of scratch wound healing assay. For all graphs, unless otherwise stated, the error bars represent the standard error of the mean (SEM) and the statistics were calculated by ordinary one-way ANOVA (where ns=$P>0.05$, *=$P\leq0.05$, **=$P\leq0.01$, ***=$P\leq0.001$, and ****= $P\leq0.0001$) on GraphPad Prism.

Bridging Text

The research presented on **Chapter II** explores the important roles of sphingolipid metabolism on the biogenesis of extracellular vesicles (EVs). Importantly, it sheds light on the differential recruitment of molecular cargoes as a response to inhibitions of neutral and acid sphingomyelinases. Our findings indicate that each sphingomyelinase variant contributes to different EV subpopulations, and further show that specific RNAs and RBPs can be exported through these distinct metabolic pathways. As discussed in **Chapter I**, the sorting of RNA molecules during EV biogenesis is multilayered and involves multiple intracellular mechanisms. These can include the modification of lipid membranes, but can also involve features intrinsic to cargoes themselves, or both.

Protein coding and non-coding RNAs are an important cargo of EVs, and numerous studies have implication them in EV-mediated intercellular communication. Interestingly, EV RNAs can display a differential enrichment relative to their cells of origin, and various EV RNA sequence motifs have been identified that appear to drive their enrichment. Furthermore, some RBPs have been identified that can regulate their incorporation (e.g. hnRNPA2B1). Currently, the sequence integrities of EV-trafficked is not clearly defined, and multiple studies suggest that mRNAs may be primarily fragmented. As the sequence features of RNAs are relevant to their communicatory potential, it is important to characterize the full-length transcripts present in EVs. To this end, we use Nanopore long-read sequencing to profile EV RNAs in their endogenous sequence lengths (**Chapter III**). This research further expands on the collective

knowledge of EV-enriched RNAs, and, importantly, shows that EVs contain full-length protein coding and non-coding RNAs.

Together, these two chapters aim to provide additional insights into the RNA and protein cargoes trafficked within the heterogenous EV population. They provide two layers of additional insights: (1) the importance of lipid metabolic pathways to cargo sorting (RNAs and proteins), and (2) the sequence features of EV-trafficked RNAs. The findings from both of these chapters are important to the burgeoning field of EV biology, and are particularly relevant in our cumulative quest to understand how to manipulate the types of cargoes that can be trafficked by EVs.

Chapter III:

Manuscript II

Profiling the Full-Length Transcriptome of Extracellular Vesicles With Oxford Nanopore Sequencing

Juan-Carlos A. Padilla[1,2], Seda Barutcu[1], Ludovic Malet[1], Gabrielle Deschamps-Francoeur[1], Virginie Calderon[1], Eunjeong Kwon[1], Eric Lécuyer[1,2,3,*]

1. Institut de Recherches Cliniques de Montréal, Montréal, QC H2W 1R7, Canada
2. Division of Experimental Medicine, McGill University, Montréal, QC H4A 3J1, Canada
3. Département de Biochimie et de Médecine Moléculaire, Université de Montréal, Montréal, QC H3T 1J4, Canada

4.1. Abstract

While numerous studies have described the transcriptomes of extracellular vesicles (EVs) in different cellular contexts, these efforts have typically relied on sequencing methods requiring RNA fragmentation, which limits interpretations on the integrity and isoform diversity of EV-targeted RNA populations. It has been assumed that mRNA signatures in EVs are likely to be fragmentation products of the cellular mRNA material, and the extent to which full-length mRNAs are present within EVs remains to be clarified. Using long-read nanopore RNA sequencing, we sought to characterize the full-length polyadenylated (poly-A) transcriptome of EVs released by human chronic myelogenous leukemia K562 cells. We detected 443 and 280 RNAs that were respectively enriched or depleted in EVs. EV-enriched poly-A transcripts consist of a variety of biotypes, including mRNAs, long non-coding RNAs, and pseudogenes. Our analysis revealed that 10.58% of all EV reads, and 18.67% of all cellular (WC) reads, corresponded to known full-length transcripts, with mRNAs representing the largest biotype for each group (EV=58.13%, WC=43.93%). We also observed that for many well-represented coding and non-coding genes, diverse full-length transcript isoforms were present in EV specimens, and these isoforms were reflective-of but often in different ratio compared to cellular samples.

4.2. Introduction

Extracellular vesicles (EVs) are a highly heterogeneous group of membrane-delimited nanoparticles of cellular origin [15, 281]. EVs can act as protective vehicles for the extracellular trafficking and delivery of bioactive cargoes, including a diverse array of protein, DNA, and RNA molecules [15, 151, 161]. The RNA transcriptome contained in EVs is reflective-of, but distinctive-from the cells of origin, and is typically comprised of transcripts belonging to diverse RNA biotypes, including mRNAs and various classes of non-coding RNAs [94, 123, 282, 283]. Upon internalization or fusion with recipient cells, EVs can release these transcripts and, consequently, induce specific biological responses in recipient cells [11, 284-287]. Indeed, the implications are wide ranging, from the promotion of tumorigenesis [288-290], to increased drug resistance in cancer [173, 291, 292]. As such, characterizing the RNA repertoire of EVs is an important feature to understand their biological properties.

The biological functions of RNAs are intrinsically tied to their sequence and structural features [293, 294]. For instance, the alternative splicing of pre-mRNAs allows the production of different mature mRNA isoforms from a single gene, substantially enhancing proteome complexity [295-297]. Moreover, different RNA isoforms may contain specific regulatory elements that modulate their functional properties in a variety of post-transcriptional regulatory processes, including RNA maturation [298], translation [299-301], stability [302], and subcellular localization [303]. As such, RNA sequence features are likely to be important determinants of secretion and of their activity in

recipient cells following EV-mediated transfer. Strikingly, multiple reports of EV transcriptomes have indicated that various classes of coding and non-coding RNAs appear as fragments within EVs [170, 283, 304, 305], with some exhibiting biological relevance [170, 306-308]. Even so, several studies have pointed to the transfer of functional mRNAs in recipient cells [59, 61, 309-311].

Recently, nanopore RNA sequencing has emerged as a powerful technology for the study of long-read RNA sequencing, allowing the detection of full-length transcripts and unambiguous mapping of isoform diversity, thereby offering a great advantage over traditional sequencing methods that require fragmentation of the starting RNA material [312-315]. Using the nanopore sequencing, we sought to compare the full-length poly-A transcriptome signatures of human K562 cells (WC) and EVs, in order to better understand the integrity and sequence features of EV transcripts. Strikingly, we show that EVs contain a high proportion of full-length mRNAs and non-coding RNAs, and further show that these transcripts can exhibit differential isoform diversity ratios in EVs versus their cells of origin. Thus, long-read RNA sequencing approaches offer an attractive approach to ascertain the sequence features of EV transcriptomes and to better predict their functional properties.

4.3. Methodology

4.3.1. Cell Culture Conditions for EV Collection

Human K562 Chronic Myelogenous Leukemia cells were routinely cultured in Roswell Park Memorial Institute (RPMI) 1640 medium with L-glutamate (Corning, 10-040-CV) supplemented with 10% foetal bovine serum (FBS), 100 U mL^{-1} penicillin and 100 µg mL^{-1} streptomycin (Wisent, 450-202-EL). The cells were grown under incubation conditions of 37 °C and humidified 5% CO_2 atmosphere.

For EV isolations, the same conditions were used, but the media contained 10% EV-depleted foetal bovine serum (dFBS), rather than 10% FBS. dFBS was prepared via tangential flow filtration (TFF) using the Labscale TFF System (Millipore-Sigma) equipped with a Pellicon XL50 ultrafiltration module with a 300 kDa Ultracell membrane (Millipore-Sigma, PXC300C50). K562 cells were plated starting at 1.75×10^7 cells per T-175 flask in 35 mL of media ($0.5x10^6$ cells/mL) in a total of 5 flasks per replicate (n=3). The cells were incubated for 36 h at 37 °C in humidified 5% CO_2 atmosphere. After 36 h, the cell-conditioned media was collected, along with representative cellular samples. The cells were assessed for ≥95% cell viability by Trypan blue exclusion assay. The cell-conditioned media was used for purification of EVs.

4.3.2. EV Purification Approach

The purification of K562 EVs was conducted with size exclusion chromatography. The collected cell-conditioned media was pre-processed to clear it of cells and large

debris by centrifugation at 500 × *g* for 10 min, and 2000 × *g* for 20 min, respectively. The cleared supernatant was collected and then concentrated by centrifugation at 2000 × *g* with a 100 kDa NMWL Amicon Ultra-15 centrifugal filter unit (Millipore-Sigma, UFC910024) to a volume of 0.5 mL. The samples were collected and then concentrated further to 100 µL using 100 kDa NMWL Amicon Ultra-0.5 centrifugal filter unit (Millipore-Sigma, UFC510096). The final concentrated samples were recovered and used for the purification of EVs through size exclusion chromatography (SEC) with qEVsingle 70 nm columns (Izon Science, SP2-USD) following the manufacturer's recommendations. Briefly, 100 µL of concentrated media was loaded on the column and allowed to elute. Next, 900 µL of 0.1 µm-filtered phosphate-buffered saline (PBS) 1x was loaded and allowed to elute, for a combined 1 mL void volume. Finally, 600 µL of 0.1 µm-filtered phosphate-buffered saline (PBS) 1x was loaded to the SEC column, and the eluted 600 µL was kept as the EV-enriched fraction. Purifications of EVs was conducted in biological triplicates.

4.3.3. Characterisations of Purified EV Samples

The eluted SEC samples (n=3) were subjected to validation experiments to assess the presence and features of purified EVs. First, nanoparticle tracking analysis (NTA) was performed to verify the presence of nanoparticles of the size range in the EV preparations. NTA was conducted using a NanoSight NS500 system (Malvern Panalytical) equipped with the 532 nm laser, and by way of three 30 s recordings at 37 °C. Data processing and analysis was performed automatically by the NanoSight NTA software v3.0 (Malvern

Panalytical). The data were exported and further analysed on Microsoft Excel (Microsoft Corporation) and visualized on GraphPad Prism (GraphPad Software Inc). Next, the samples were subject to transmission electron microscopy (TEM) to corroborate the presence of EVs. Samples from the SEC-recovered eluates were combined 1:1 with a 5% glutaraldehyde solution (2.5% final concentration) for fixation. 5 µL of the fixed samples were then loaded to previously discharged formvar-coated copper grids and allowed to adhere for 3 min. The sample-containing grids were washed 3 times with water, and then placed in droplets of 2% uranyl acetate and incubated for 1 min. The grids were then washed 3 more times with water, blotted to remove excess water, and air dried for 30 mins. The grids were then imaged on the FEI Tecnai T12 120kV (Field Electron and Ion Company) transmission electron microscope. Sample preparation and imaging was carried out at the Facility for Electron Microscopy Research (FEMR) at McGill University.

4.3.4. RNA Isolation

For each of the experimental replicates, representative K562 cells were collected and pelleted at 500 × *g* for 5 min. The cellular pellets were resuspended in TRIzol reagent (Thermo Fisher, 15596018) to isolate RNA as per the manufacturer's recommendations. Briefly, the samples were homogenized in 500 µL of TRIzol reagent, after which 100 µL of chloroform was added (VWR, BDH1109-4LG). The samples were then centrifuged at 12,000 × *g* for 15 min. Following the centrifugation, the aqueous phase was used for RNA purification using the RNA Clean & Concentrator-5 system (Zymo Research, R1013) with in-column DNaseI treatment. All steps were performed according to the manufacturers'

protocols. K562 EV samples were processed using TRIzol LS reagent (Thermo Fisher, 10296028), as it would prevent the need to pellet the samples and reduce loss of materials.. For RNA purification, the SEC-eluted EV samples were homogenized in 1.8 mL of TRIzol LS reagent, after which 480 µL of chloroform was added (VWR, BDH1109-4LG). The samples were then centrifuged at 12,000 × *g* for 15 min. The aqueous phase was processed for RNA purification as described above, using the RNA Clean & Concentrator-5 system (Zymo Research, R1013) with in-column DNaseI treatment. All RNA samples were eluted in nuclease-free water and assessed for quality and concentration with Nanodrop and Bioanalyzer.

4.3.5. Preparation of RNA Sequencing Library

The purified cellular and EV RNA samples were utilized for preparation of sequencing libraries using the PCR-cDNA Barcoding Kit (Oxford Nanopore Technologies, SQK-PCB109), as per the manufacturer's guidelines, with some modifications. Briefly, cellular and EV samples were used for the preparation of cDNA starting with 50 ng of total RNA, followed by PCR amplification of each of the six libraries using a unique barcode per sample. The samples were subjected to 14 cycles of denaturation, annealing, and extension, and the products were purified using RNAClean XP beads (Beckman-Coulter, A66514), which can be used for both RNA and DNA purification. The purification of PCR products was conducted using the methods outlined by Oxford Nanopore. The bead-bound libraries were then eluted with 12 µL of Elution Buffer (EB) and quantified using the Qubit RNA Broad Range (BR) kit (Thermo Fisher, Q10211), as per the manufacturer's

recommendations. The samples were further analysed with Bioanalyzer to assess the library quality.

4.3.6. Loading and Sequencing of PCR-cDNA Libraries

The sequencing of PCR-cDNA libraries was carried out using a MinION device (Oxford Nanopore Technologies, MIN-101B) equipped with a compatible Flow Cell R9.4.1 (Oxford Nanopore Technologies, FLO-MIN106D). Each loading library consisted of one cellular library and one EV library in a 2:1 ratio, respectively, and to a final loading concentration of ~100 fmol. This ratio was chosen as cellular sequencing libraries were expected to be comparatively more complex to EV sequencing libraries. Briefly, 66.66 fmol of cell library was combined with 33.33 fmol of EV library, and the volume was adjusted to 11 µL of Elution Buffer (EB). Next, 1 µL of Rapid Adapter (RAP) was added to the combined libraries, followed by a room temperature incubation of 5 min. The flow cell was then primed and loaded following the manufacturer's recommendations. Primary data acquisition was performed using the MinION Software (Oxford Nanopore Technologies, MinION Release 22.05.5) with default parameters, but no local basecalling. The sequencing of the loaded libraries was allowed to proceed for 72 h, after which the resulting FAST5 files were further processed bioinformatically.

4.3.7. Transcriptomics and Bioinformatics Analyses

To analyse the resulting FAST5 files, the nfcore/nanoseq pipeline was used as described previously [316]. Briefly, basecalling was performed on FAST5 files for each

replicate with Guppy base caller software (Oxford Nanopore Technologies, v6.2.1) using a quality threshold of 7. Passing reads were then demultiplexed into individual barcodes using the FASTQ barcoding pipeline (demux_fast5) of the Oxford Nanopore Technologies Bioinformatics Platform. Demultiplexed FASTQ files were mapped to the human reference genome GENCODE v41 using minimap2 [317]. Counts per million reads mapped (CPM)-normalized BedGraph files were generated from Binary Alignment/Map (BAM) files using the bamCoverage tool from the deepTools suite [318]. BAM files were used as input to featureCounts from Rsubreads [319] for gene count and transcript quantifications in long-read mode using the GENCODE v41 annotation file. Next, differential expression analysis was performed with the DEseq2 R package [231] to identify significant EV-enriched or EV-depleted genes and transcripts.

The web-based integrated Differential Expression and Pathway analysis (iDEP) tool [320] was used to generate a k-Means heatmap of the normalized read count data. GraphPad Prism (GraphPad Software Inc.) was used to generate a volcano plot depicting the differentially expressed EV RNAs. Overrepresentation analyses (ORA) of gene ontology (GO) terms were executed on g:Profiler [321] (version e107_eg54_p17_bf42210) with the Benjamini-Hochberg false discovery rate multiple testing correction method and while applying significance threshold of 0.05. The sequenced lncRNAs were investigated for enrichment profiles using the LncSEA platform [322]. Gene lists included in these analyses were filtered for EV-enrichment [Log_2 fold change ≥2, *Padj*≤0.01] or EV-depletion (i.e. cell-enriched) [Log_2 fold change ≤-2, *Padj*≤0.01]. Svist4get [323] was used to visualize genomic signal tracks of selected EV-

enriched genes. Sequence length statistics were computed using the BamSlam script (https://github.com/josiegleeson/BamSlam) [324], requesting to re-run mapping steps with specific parameters for minimap2. For representation purposes, BAM files were then sorted and indexed with SAMtools before merging by condition (cells and EV). Read coverage scores >95% of the annotated transcript was considered as full-length. Differential splicing and isoform analyses were conducted by using the Full-Length Alternative Isoform Analysis of RNA (FLAIR) tool [325]. FLAIR modules *align*, *correct* and *collapse* were successively used for mapping FASTQ files to GENCODE v41, identifying splice junctions. Next, isoform quantifications were made with the *quantify* module, and the output count matrix was used to plot isoform structures and the percent usage of each isoform in each sample for a given gene. Finally, *predictProductivity* was utilized to predict isoform productivity with output definitions as PRO (productive), PTC (premature termination codon), NGO (no start codon), or NST (has start codon but no stop codon).

4.4. Results

4.4.1. Nanopore Sequencing Exposes a Variety of RNAs in Cells and EVs

To investigate the sequence features of an EV-targeted transcriptome, we herein sought to apply nanopore long-read sequencing to RNA purified from whole cells (WC) or EVs of the human chronic myelogenous leukemia cell line K562. For this, we employed a poly-A priming approach utilizing a PCR-cDNA barcoding strategy, which enables one to sequence full-length transcripts generated through reverse-transcription of poly-A+ material (**Figure 1A**). EVs were purified from K562 cell conditioned media through centrifugation-based filtering and size exclusion chromatography using qEVsingle 70 nm columns. Nanoparticle tracking analysis (NTA) was performed on purified EV material, which revealed the presence of nanoparticles ranging from 100-600 nm in diameter (**Figure 1B**). Furthermore, transmission electron micrographs of the recovered material revealed circular structures displaying the biconcave morphologies typically associated with EVs (**Figure 1C**). RNA isolated from EV and cellular samples was subjected to Bioanalyzer automated electrophoresis to assess the concentration and quality of the preparations, revealing standard RNA integrity values typical of such specimens (**Figure S1A**). Similar analysis of PCR-cDNA sequencing libraries showed that EVs cDNA specimens display a biphasic size distribution, with a broader population >700nt similar to cellular samples, as well as a weaker population in the ~150-200nt size range (**Figure S1B**). Initial analysis of sequencing data demonstrated an average of ~8M reads per sequencing run, with that an average of 62% of the raw reads passing the minimum

quality score during base-calling (**Figure S1C**). For sequencing, WC and EV libraries from the same replicate specimen were combined in the same flow cell at a ratio of 2:1. Consistent with this loading scheme, we obtained averages of 66.3% and 31.4% barcoded reads representing WC and EV, respectively (**Figure S1D**).

Among the reads that passed quality control, a higher proportion of mappable reads were obtained for WC (~88%) comparted to EV (~56%) specimens, with unmappable reads presenting characteristics of repetitive sequences (**Figure S1E**). Further interrogation of mappable reads revealed a similar proportion (~65%) of assigned versus unassigned reads across all samples (**Figure 1D**), with ~15% of unassigned reads respectively being classified as either ambiguous (i.e. deriving from regions overlapping multiple genes) or NoFeatures (i.e. mapping to a region of the genome that does not contain any known gene). Principal component analysis (PCA) was performed on both cellular and EV triplicate libraries, revealing a segmentation based on library types (**Figure S1G**). To evaluate the overall diversity of RNAs present in the sequencing data, their biotype assignations were assessed in transcripts per million (TPM). The groupings included 3 major classes: mRNA, lncRNA, and all RNA with a 'pseudogene' designation, while all minor classes of RNAs (e.g. miRNA, snoRNA, snRNA, miscRNA) were grouped as 'other' and accounted for <1% of all assigned reads. These results showed that, in both cells and EVs, most transcripts detected were mRNAs or pseudogene transcripts, with a smaller number representing lncRNAs (2-3%). While EVs had similar proportions of mRNAs to pseudogene-derived transcripts (~48% each), cellular samples contained a higher proportion of mRNA (~56%) mRNAs versions pseudogene (~40%) transcripts

(**Figure 1E**). Next, DESeq2 normalized counts were subject to iDEP differential expression and pathway analysis. A k-Means heatmap was made of the top 4000 most variable coding genes, and their associated gene ontology (GO) enrichments for cellular components (CC) was determined. Unsupervised clustering revealed that EV mRNAs were enriched for functional classes associated with extracellular vesicles, ribosomal subunits, and ribonucleoprotein complexes, while WC-enriched mRNAs had functional signatures associated with varied intracellular compartments (**Figure 1F**).

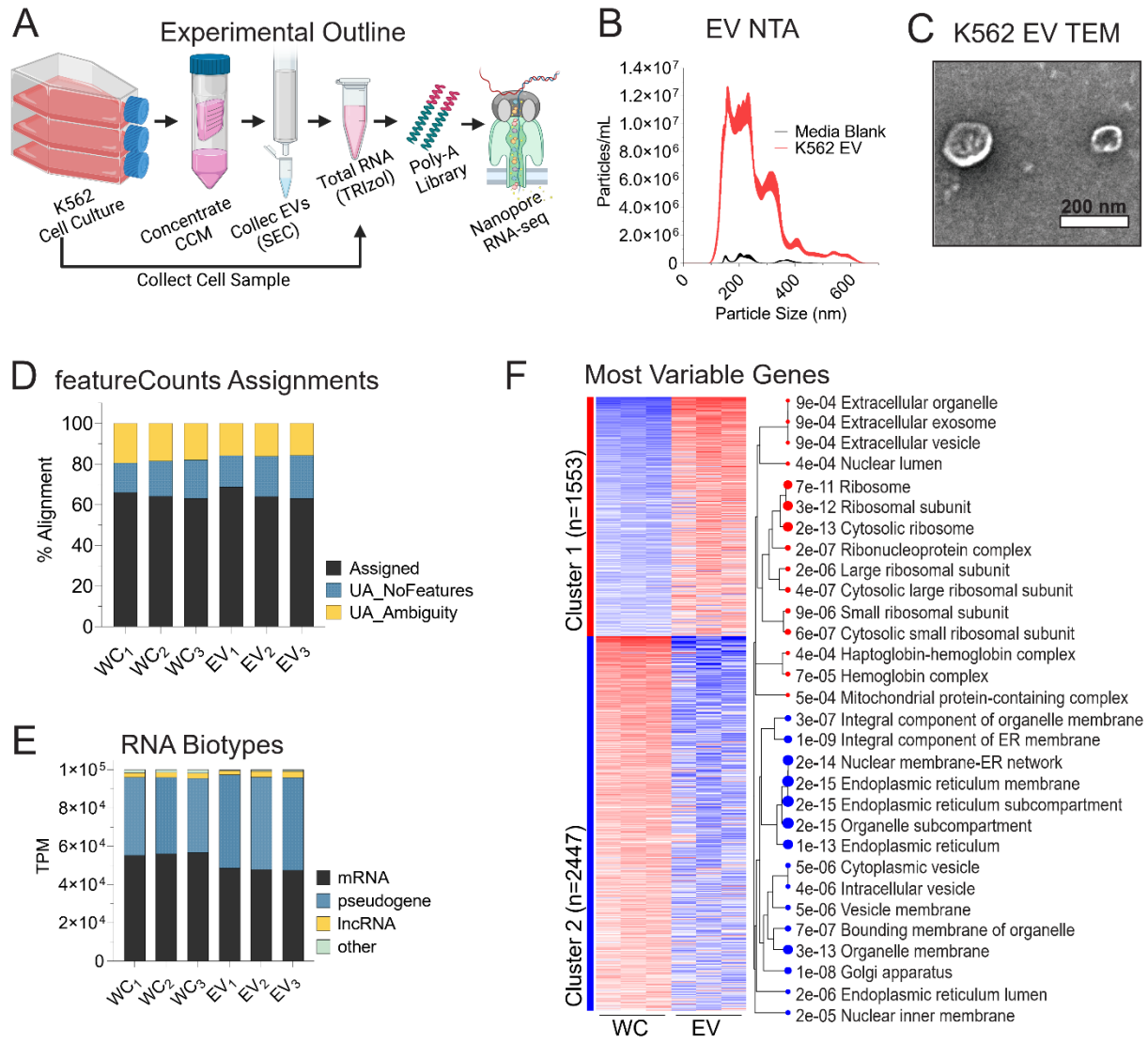

FIGURE 3.1 Nanopore sequencing identifies a variety of RNA biotypes. **A.** Graphical experimental outline of the isolation of K562 cellular and extracellular vesicles (EV) total RNA, library preparation, and nanopore sequencing. **B.** Nanoparticle Tracking Analysis (NTA) of cleared cell-conditioned media. Border thickness defines the standard error. **C.** Transmission electron micrographs of iodixanol gradient-purified EVs. EVs were negatively stained with 2% uranyl acetate and imaged on the FEI Tecnai T12 120kV transmission electron microscope. **D.** Stalked bar graphs of the percentage of input cellular and EV sequencing reads with assigned or unassigned (UA) features as

determined by featureCounts. **E.** RNA biotype distributions of cellular and EV transcriptomes. ‘Other’ includes a varied group of minor transcripts including, but not limited to, miscRNA, snRNA, snoRNA, etc. **F.** iDEP unsupervised clustering heatmap of the top 4000 most variable genes in cellular and EV transcriptomes. Cellular component gene ontology (GO) terms associated with each cluster are represented on the right. Red lines denote enrichment in EVs, blue lines denote enrichment in cells.

4.4.2. Nanopore sequencing reveals EV-enriched transcripts

A deeper analysis of differentially expressed transcripts between WC and EV samples revealed a total of 280 and 443 transcripts that were respectively enriched within WC or EV samples, while 10865 RNA were similarly detected in both specimen types (**Figure 2A-B**). EV-enriched RNAs included various RNA biotypes, with lncRNA (42.9%), pseudogenes (35.5%), and mRNA (13.7%) representing the major classes [%TPM]. In WC specimens, enriched RNAs included mostly lncRNA (78.6%), with pseudogenes (15.6%) and mRNA (5.6%) representing smaller populations [%TPM] (**Figure 2B**). Although transcriptomic signatures across various biotypes were recorded for both cellular and EV specimens, the EV groups were the only class that demonstrated enrichment for other biotype classes, including snRNA, 5S rRNA, and Y-RNA.

The top EV-enriched RNAs included both coding and non-coding species, which included 105 mRNA and 14 lncRNA (**Figure 2C-D**). By contrast, the top cell-enriched RNAs included 198 mRNA and 47 lncRNA (**Figure 2F-G**), marked by the presence of mRNAs encoding various members of the Speedy/RINGO family, which have been associated with the mammalian cell cycle regulation through the activation of Cyclin-dependent kinases [326]. To determine whether the EV- or WC-enriched transcripts were associated to known gene ontology molecular functions, they were subjected to over-representation analyses (ORA) with g:Profiler. Our results showed that these EV-enriched transcripts were associated to various molecular functions relating to RNA metabolism, including structural constituent of the ribosome, pre-mRNA splicing and RNA binding

protein mRNAs (**Figure 2E**, **Figure S2B-C**). By contrast, cell-enriched mRNAs associated to varied gene ontology terms relating to molecular function, including kinase binding, enzyme binding, and protein binding (**Figure 2H, Figure S2B-C**). To further investigate the functional attributes of WC- and EV-enriched lncRNA, analysis was conducted using LncSEA, a platform that combines numerous human lncRNA databases for enrichment analyses [322]. Our results suggest that various EV-enriched lncRNA have been associated with RNA binding proteins (RBPs) (**Table S2.1**). Interestingly, these RBPs were also associated to WC-enriched specimens, suggesting that they can interact with multiple lncRNA.

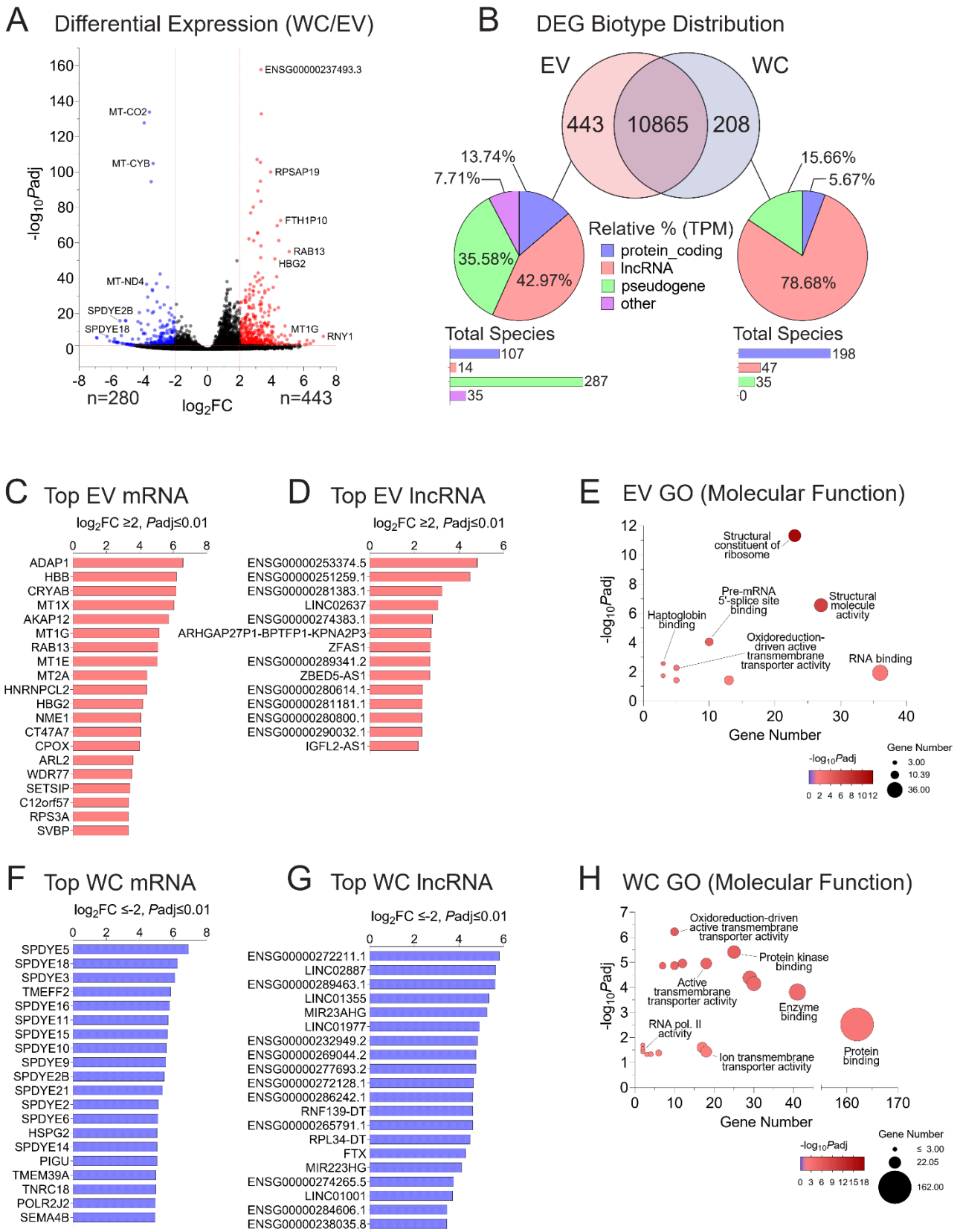
A
Differential Expression (WC/EV)
ENSG00000237493.3
MT-CO2
MT-CYB
RPSAP19
FTH1P10
RAB13
HBG2
MT-ND4
SPDYE2B
SPDYE18
MT1G
RNY1
-log10Padj
log2FC
n=280
n=443
B
DEG Biotype Distribution
EV
WC
443
10865
208
13.74%
7.71%
15.66%
5.67%
35.58%
42.97%
78.68%
Relative % (TPM)
protein_coding
lncRNA
pseudogene
other
Total Species
107
14
287
35
198
47
35
0
C
Top EV mRNA
log2FC ≥2, Padj≤0.01
ADAP1
HBB
CRYAB
MT1X
AKAP12
MT1G
RAB13
MT1E
MT2A
HNRNPCL2
HBG2
NME1
CT47A7
CPOX
ARL2
WDR77
SETSIP
C12orf57
RPS3A
SVBP
D
Top EV lncRNA
log2FC ≥2, Padj≤0.01
ENSG00000253374.5
ENSG00000251259.1
ENSG00000281383.1
LINC02637
ENSG00000274383.1
ARHGAP27P1-BPTFP1-KPNA2P3
ZFAS1
ENSG00000289341.2
ZBED5-AS1
ENSG00000280614.1
ENSG00000281181.1
ENSG00000280800.1
ENSG00000290032.1
IGFL2-AS1
E
EV GO (Molecular Function)
Structural constituent of ribosome
Pre-mRNA 5'-splice site binding
Structural molecule activity
Haptoglobin binding
Oxidoreduction-driven active transmembrane transporter activity
RNA binding
-log10Padj
Gene Number
Gene Number
3.00
10.39
36.00
F
Top WC mRNA
log2FC ≤-2, Padj≤0.01
SPDYE5
SPDYE18
SPDYE3
TMEFF2
SPDYE16
SPDYE11
SPDYE15
SPDYE10
SPDYE9
SPDYE2B
SPDYE21
SPDYE2
SPDYE6
HSPG2
SPDYE14
PIGU
TMEM39A
TNRC18
POLR2J2
SEMA4B
G
Top WC lncRNA
log2FC ≤-2, Padj≤0.01
ENSG00000272211.1
LINC02887
ENSG00000289463.1
LINC01355
MIR23AHG
LINC01977
ENSG00000232949.2
ENSG00000269044.2
ENSG00000277693.2
ENSG00000272128.1
ENSG00000286242.1
RNF139-DT
ENSG00000265791.1
RPL34-DT
FTX
MIR223HG
ENSG00000274265.5
LINC01001
ENSG00000284606.1
ENSG00000238035.8
H
WC GO (Molecular Function)
Oxidoreduction-driven active transmembrane transporter activity
Protein kinase binding
Active transmembrane transporter activity
Enzyme binding
RNA pol. II activity
Protein binding
Ion transmembrane transporter activity
-log10Padj
Gene Number
Gene Number
≤ 3.00
22.05
162.00

FIGURE 3.2 EV-enriched RNAs display GO associations to ribonucleoprotein complexes. **A.** Volcano plot of cellular and EV transcriptomes signifying the shift in transcript expression levels. Blue dots represent statistically significant downregulated EV-transcripts (Log_2 fold change ≤-2, *Padj*≤0.01). Red dots represent statistically significant upregulated EV-transcripts (Log_2 fold change ≥2, *Padj*≤0.01). **B.** Venn diagram of differentially expressed RNAs in EV vs WC (Log_2 fold change ≤-2, *Padj*≤0.01). In the center are RNAs which displayed similar expression profiles in either group. Inclusion to this group was limited to transcripts with an average of ≥5 reads (triplicates). Differentially expressed RNAs are further categorized into pie charts and bar graphs, denoting their relative percentages in transcripts per million and their contributing RNAs, respectively. **C-D.** Bar graphs of the top 20 and top 14 EV-enriched (Log_2 fold change ≥2, *Padj*≤0.01) mRNA and lncRNA, respectively. **E.** Bubble plot of GO molecular function of EV-enriched mRNA as determined with g:Profiler. All enriched (Log_2 fold change ≥2, *Padj*≤0.01) RNA considered. **F-G.** Bar graphs of the top 20 cell-enriched/EV-depleted (Log_2 fold change ≤-2, *Padj*≤0.01) mRNA and lncRNA, respectively. **H.** Bubble plot of GO molecular function of cell-enriched mRNA as determined with g:Profiler. All enriched (Log_2 fold change ≤-2, *Padj*≤0.01) RNA considered.

4.4.3. EVs contain full-length RNAs and display preferential isoform recruitment

We next sought to interrogate our nanopore sequencing data to evaluate the presence of full-length RNA molecules across different biotypes, versus those which could represent shorter transcription or degradation products. To clarify these questions, we next used BamSlam, a tool developed to analyse sequence length statistics of nanopore long-read sequencing data [324]. Mapping to the GENCODE v41 human transcriptome, sequenced transcripts displayed a median primary alignment >91% for both cell and EV libraries (**Figure 3A**). Following recommendations made by BamSlam's authors, we considered transcripts as "full-length" if they aligned to >95% of their annotated transcript. Applying these criteria revealed that ~10.6% of all identified EV transcripts were full-length, whereas ~18.7% of cellular RNAs were full-length (**Figure 3B,E**). Moreover, the coverage fraction of the identified RNAs, relative to their isoform size averages, were relatively similar for WC and EV populations (**Figure 3C-E**). Indeed, most full-length transcripts fell below 5000 nt in EVs, while cellular transcripts could be up to 10,000 nt in length but often under 7000 nt. Notably, the median length of all unique EV transcripts identified was 2050 nt, while their cellular counterparts were 1683 nt (**Figure 3C-E**). These findings were reflective of the GENCODE v41-mapped reads (**Figure S3A-B**), which displayed similar size distribution profiles to those identified by BamSlam. This suggests that while the EV RNA repertoire may be composed of smaller transcripts, in comparison to the diversity of sizes displayed in cellular specimens, the relative occurrence of longer RNAs is more common within the EV transcriptome.

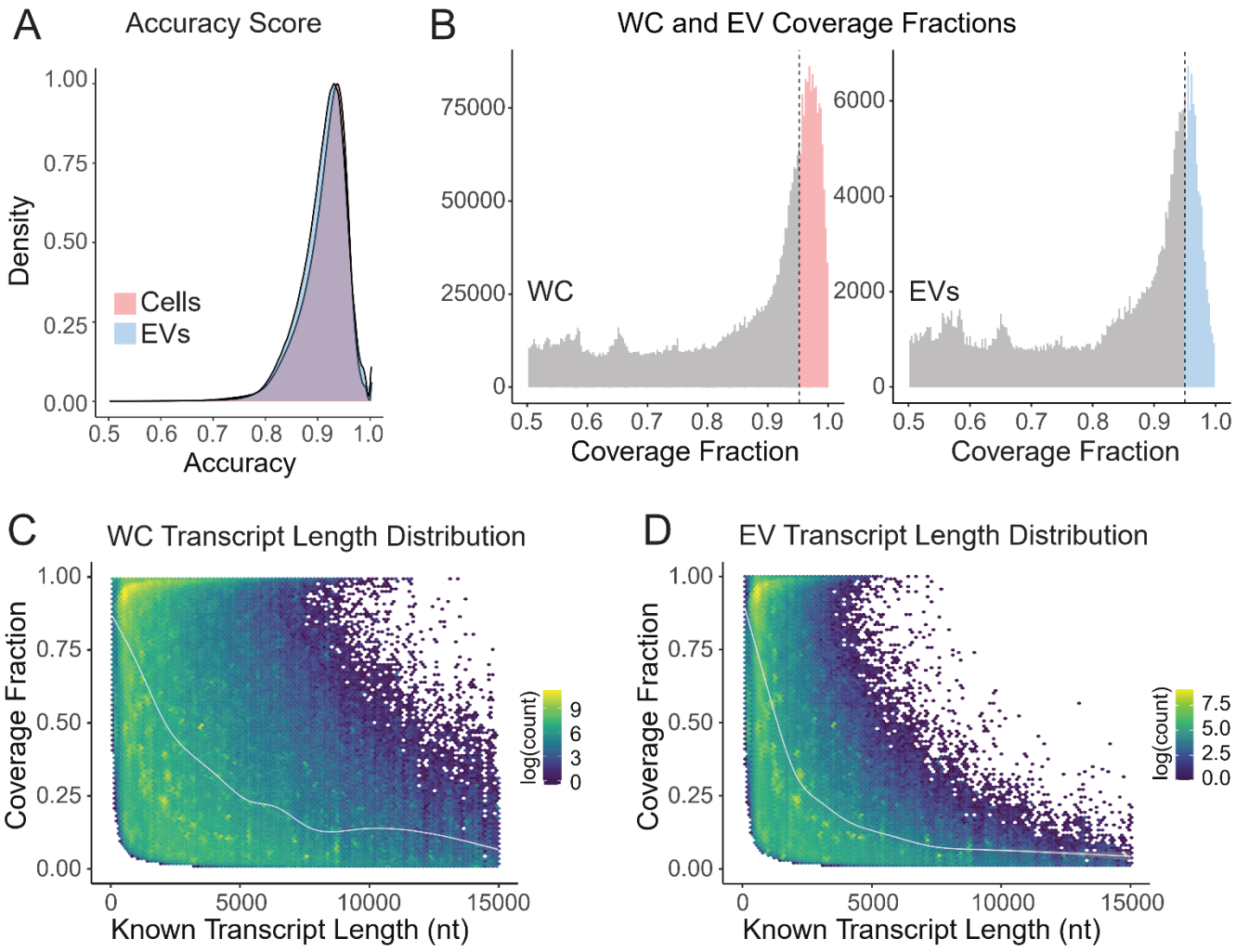

E

Full-Length Coverage Statistics Summary

Sample	WC Reads	EV Reads
Number of reads representing full-length transcripts	1285568	149243
Out of total number of reads	6887456	1410601
Median alignment length of primary alignments	618	459
Percentage of reads representing full-length transcripts	18.67	10.58
Median coverage fraction of transcripts (primary alignments)	0.57	0.45
Median accuracy of primary alignments	91.86	91.54
Number of reads with no secondary alignments	1384348	188554
Percentage of reads with no secondary alignments	20.10	13.37
Number of unique transcripts identified	110919	53975
Median coverage fraction of all unique transcripts	0.34	0.22
Median length of all unique transcripts identified	1683.0	2050.0

FIGURE 3.3 EVs contain full-length RNAs. **A.** Median accuracy of primary alignment score determined using the BamSlam algorithm. **B.** Histogram distribution of full-length reads in cells and EVs. Represented are the coverage fractions of known transcript length covered by each read (truncated at 0.5). The dotted lines represent the >95% coverage denoting full-length. Full-length cellular transcripts shown in red, full-length EV transcripts shown in blue. **C.** Density plot of cellular transcripts displaying their coverage fractions against known transcript lengths. The trend line represents a generalized additive model. **D.** Density plot of EV transcripts displaying their coverage fractions against known transcript lengths. The trend line represents a generalized additive model. **E.** Summary of statistical information as determined by BamSlam.

Next, we assessed whether full-length read coverage displayed differences between different RNA biotypes. As shown in **Figure 4A**, comparison of transcript coverage percentage sorted according to RNA biotypes revealed a general similarity in coverage scores between WC and EV specimens for biotypes including mRNAs, lncRNAs, snRNAs, snoRNAs and pseudogene-derived transcripts. However, we also observed fragmented RNAs across various categories, with some biotypes being more strongly populated by these products. Notably, RNA families made up of shorter RNA molecules, such as snRNAs and snoRNAs, had a higher proportion of longer full-length transcripts compared to mRNAs, snRNAs and pseudogene RNAs. Focusing our analyses on full-length RNAs across all RNA biotypes revealed that the diversity of full-length RNAs is markedly different between WC and EV specimens, with cells having a larger proportion of full-length pseudogenes (10.3%), while EVs had a higher proportion of full-length mRNA transcripts (58.1%) (**Figure 4B-C**). These findings differ from the overall BamSlam-identified population (**Figure 4D-E**), which displayed the presence of large proportions of transcripts corresponding to mRNA in cells and “other” RNA in EVs, but whose values were reduced in the full-length population, suggesting fragmented products.

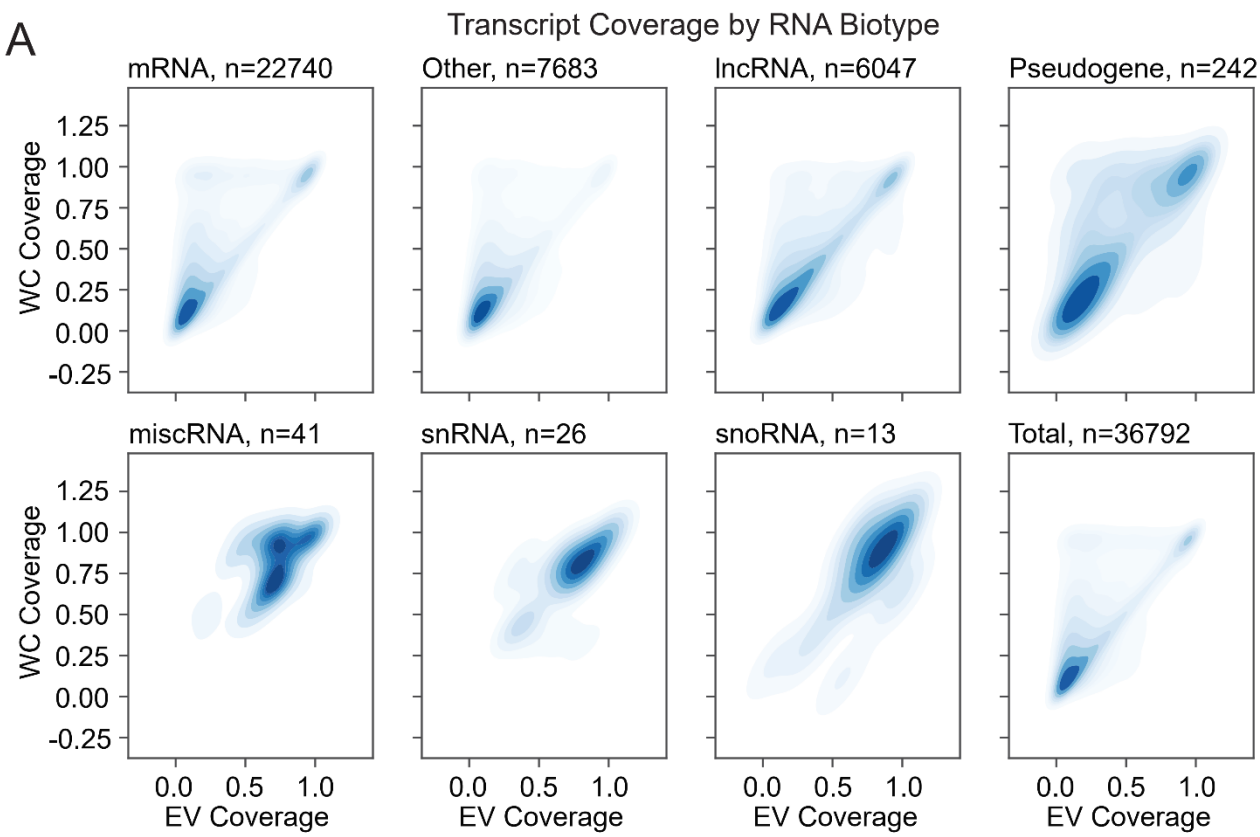
A
Transcript Coverage by RNA Biotype
mRNA, n=22740
Other, n=7683
lncRNA, n=6047
Pseudogene, n=242
miscRNA, n=41
snRNA, n=26
snoRNA, n=13
Total, n=36792
WC Coverage
1.25
1.00
0.75
0.50
0.25
0.00
-0.25
0.0
0.5
1.0
EV Coverage

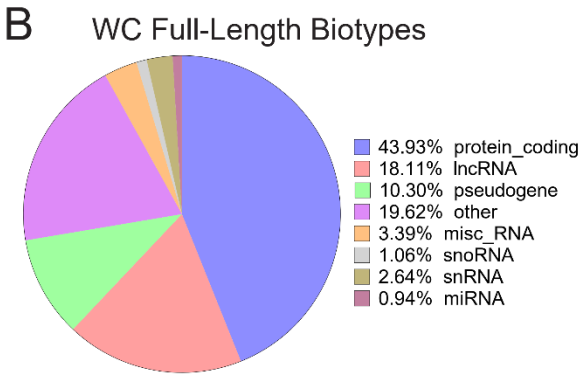
B
WC Full-Length Biotypes
43.93% protein_coding
18.11% lncRNA
10.30% pseudogene
19.62% other
3.39% misc_RNA
1.06% snoRNA
2.64% snRNA
0.94% miRNA

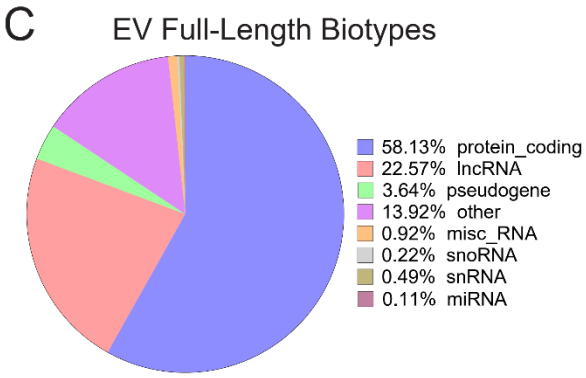
C
EV Full-Length Biotypes
58.13% protein_coding
22.57% lncRNA
3.64% pseudogene
13.92% other
0.92% misc_RNA
0.22% snoRNA
0.49% snRNA
0.11% miRNA

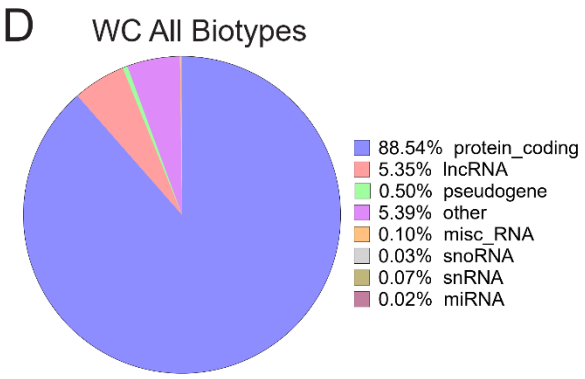
D
WC All Biotypes
88.54% protein_coding
5.35% lncRNA
0.50% pseudogene
5.39% other
0.10% misc_RNA
0.03% snoRNA
0.07% snRNA
0.02% miRNA

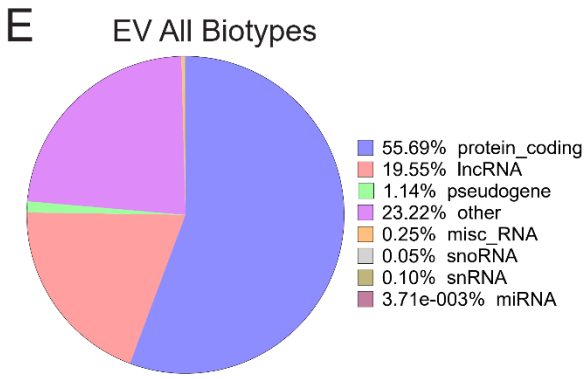
E
EV All Biotypes
55.69% protein_coding
19.55% lncRNA
1.14% pseudogene
23.22% other
0.25% misc_RNA
0.05% snoRNA
0.10% snRNA
3.71e-003% miRNA

FIGURE 3.4 EVs contain full-length RNAs of different biotypes. **A.** Density plots of RNA biotypes displaying the transcript coverage EVs RNAs relative to cells. **B-C.** Pie charts displaying the RNA biotype percentages of BamSlam-identified full-length RNAs identified in cells and EVs. **C-D.** Pie charts displaying the RNA biotype percentages of all BamSlam-identified RNAs (full-length and non-full-length) identified in cells and EVs.

Finally, we investigated whether EV specimens display differential recruitment of transcript isoforms relative to their cells of origin. Using the Full-Length Alternative Isoform Analysis of RNA (FLAIR) tool [325], we conducted differential splicing and isoform analyses of the WC and EV transcriptomes. Strikingly, various RNAs identified included transcript isoforms that displayed simultaneous up- and downregulation in EV or WC specimens, demonstrating the occurrence of transcript isoform-specific recruitments in the EV population (**Figure S5A-B**). Our results show that, depending on the gene, WC and EV transcript populations can exhibit different levels of similarity. I some cases, the isoform distributions were very similarly between WC and EV specimens, as exemplified by the case of RPL10 mRNA isoforms (**Figure 5C**). By contrast, analysis of mRNA isoforms derived from the ELOVL5 and HSPA9 genes revealed a striking shift in isoform representation in EV versus cellular specimens (**Figure 5B-C**). Altogether, these results demonstrate that EVs can carry a diversity of full-length RNAs, displaying enrichments for a subset of these, and can further incorporate preferred isoforms relative to their cells of origin.

A *ELOVL5* Read and Transcript Isoform Overview

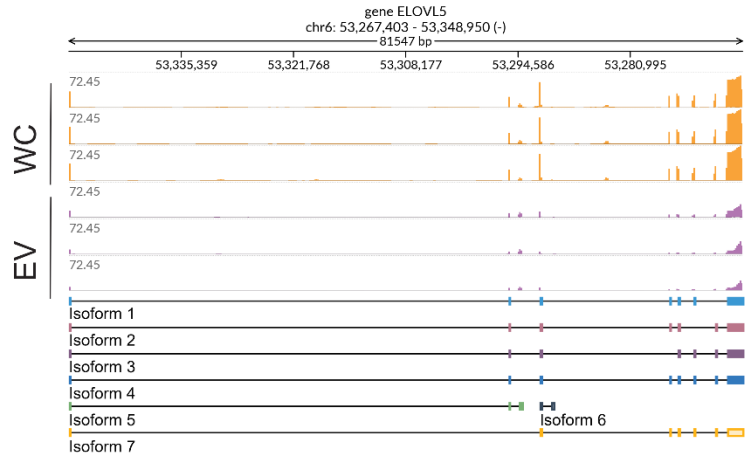

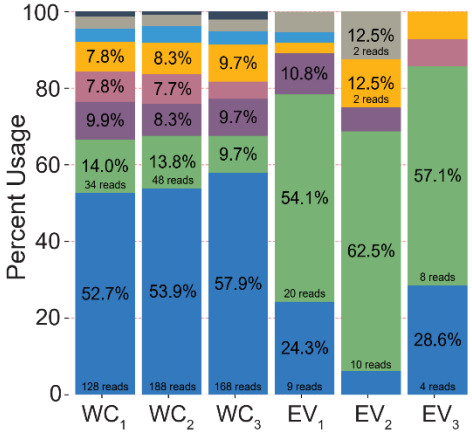

B *HSPA9* Read and Transcript Isoform Overview

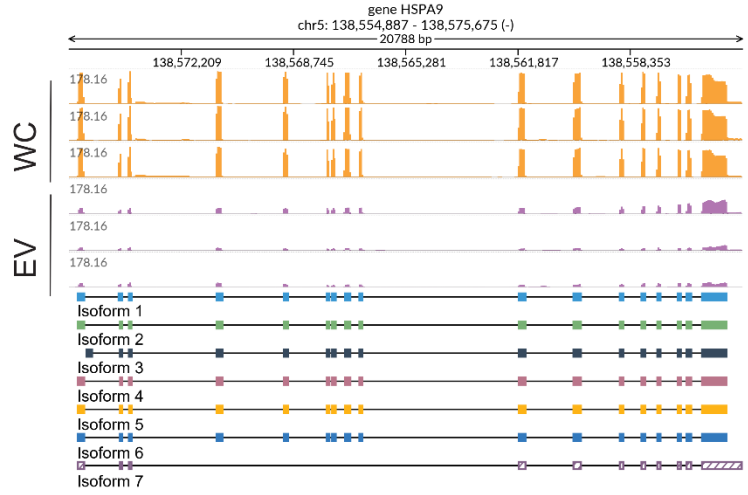

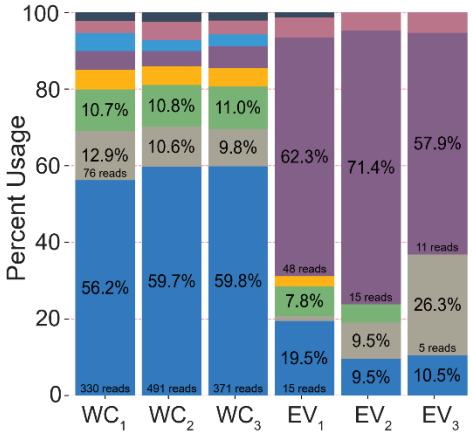

C *RPL10* Read and Transcript Isoform Overview

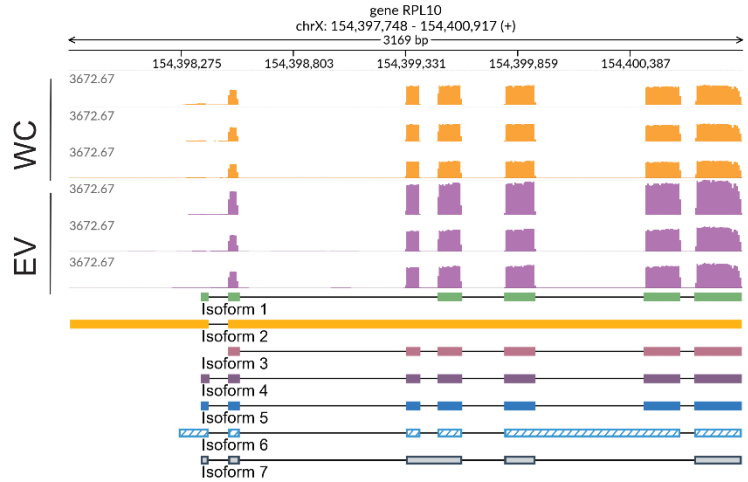

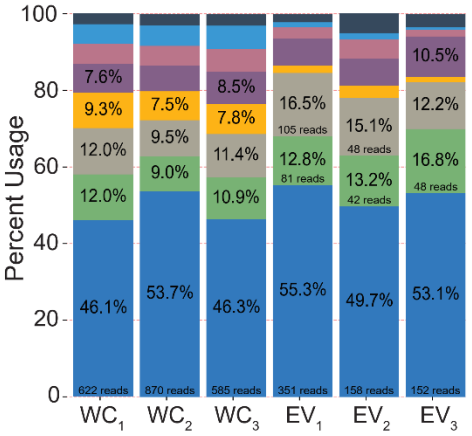

FIGURE 3.5 EVs carry differentially expressed transcript isoforms. **A.** Isoform usage analysis of *ELOVL5* displaying preference for the recruitment of isoform variants in EVs relative to cells of origin, with variant *ENST00000370913.5* showing enrichment in EVs. Isoform identities (as defined by FLAIR): Isoform 1: *9d9223d4-0463-4bdf-ae2c-603abfbc8fae*, Isoform 2: *ENST00000542638.5*, Isoform 3: *a987f2f6-fdb0-4501-87c3-9b457392a133*, Isoform 4: *ENST00000304434.11*, Isoform 5: *ENST00000370913.5*, Isoform 6: *03f316c6-1d4c-48e5-ab63-57acbaaf3126*, Isoform 7: *4a5f7dbd-8838-4359-af96-63e1ff580847*. **B.** Isoform usage analysis of *HSPA9* displaying preference for the recruitment of isoform variants in EVs relative to cells of origin, with variant *4671fbc1-2c63-4c88-af4b-90b6b1aa4277* showing enrichment in EVs. Isoform identities (as defined by FLAIR): Isoform 1: *ENST00000677988.1*, Isoform 2: *ENST00000678794.1*, Isoform 3: *ENST00000678384.1*, Isoform 4: *ENST00000678300.1*, Isoform 5: *ENST00000677553.1*, Isoform 6: *ENST00000297185.9*, Isoform 7: *4671fbc1-2c63-4c88-af4b-90b6b1aa4277*. **C.** Isoform usage analysis of *RPL10* displaying recruitment of similar isoform types in EVs relative to cells of origin. Legend: Isoform productivity analysis showing ‘Productive’ (solid color), ‘Premature Termination Codon/ Unproductive’ (hatched color), ‘No Start or Stop Codon’ (faded color). Isoform identities (as defined by FLAIR): Isoform 1: *6eee3e78-fe04-4ee6-90d4-ecc361ca6e05*, Isoform 2: *415620e2-1272-483b-86eb-7d7532fe4780*, Isoform 3: *ENST00000344746.8*, Isoform 4: *ENST00000436473.5*, Isoform 5: *ENST00000369817.7*, Isoform 6: *07d5ac1f-db7c-47ab-a5e8-04a78777867e*, Isoform 7: *40708139-1f87-49ca-a99a-5f5e1e0422c9*. For all figures, isoform shading corresponds to: solid color (productive), hatched color (premature termination codon), or faded color (no start codon or has start codon but no stop codon).

4.5. Discussion

Extracellular vesicles have gained prominence as novel mediators of the exchange of information between cells [1, 5]. This ability is bestowed by their loading with bioactive molecules, including RNAs, which can influence the behaviour of recipient cells [18-21]. While the transcripts that can be identified in EVs generally represent the RNAs found in parental cells, there is a marked specificity in the recruitment of particular RNA species to the EV population [94, 122, 123]. Indeed, our results show that EV-enriched RNAs included various classes of RNA biotypes including coding and non-coding varieties (**Figure 2A-D**). Interestingly, while these transcripts demonstrated GO-enrichments to extracellular vesicles and the extracellular space (**Figure 1F**, **Figure S2B**), they were also highly associated to various ribonucleoprotein complexes and included structural components of the ribosome and the U1 spliceosome (**Figure S2B**). The associated ribosome components included various rRNA species (e.g. *RNA5S1*, *RNA5S2*, *RNA5S4*), but also protein coding transcripts such as *RPL26* and *RPL23A*. While 18S and 28S rRNAs have been previously associated extracellular vesicles [122, 327], we did not detect either 18S or 28S rRNA by poly-A long-read nanopore sequencing, although we did observe their corresponding peaks with Bioanalyzer analysis of EV-isolated RNAs (**Figure S1A**). Our results, however, show the enrichment for various 5S rRNAs. Of note, 5S rRNAs have been previously identified as a major component of the transcriptome of CD24 cell surface receptor-presenting extracellular vesicles [328]. Contrastingly, transcripts enriched in parental cells displayed an association with various intracellular compartments (**Figure 1F**, **Figure S2B**).

Differential expression analysis of EV RNAs, relative to parental cells, uncovered over 443 EV-enriched and 280 cell-enriched transcripts. Various coding, non-coding, and pseudogene RNAs were highly enriched in EVs (Log_2 fold change ≥2, *Padj*≤0.01). These included *RNY1*, *ADAP1*, *HMGB1P26*, *RNU1-28P*, *RAB13*, and *MT1X*, with *RNY1* being the most enriched (**Figure S2A**). This is consistent with previous reports, including our own, that EVs are enrichment for various RNA biotypes such as Y-RNAs, mRNAs, spliceosomal RNAs, and pseudogenes transcripts [94, 170, 283, 311, 329-331]. In contrast, the cellular transcriptome displayed an enrichment for various members of the Speedy/RINGO family of non-canonical Cyclin-dependent kinases (CDKs) (**Figure S2A**). Proteins of this family have been associated with the activation of CDKs during cell cycle regulation and cell proliferation, moreover they may be overexpressed in various cancers [326, 332-334]. Although Speedy/RINGO mRNAs are detected in our K562 EV transcriptomes, their enrichment lies with the cellular specimens.

There is currently no consensus as to the full nature of the RNA repertoire present within EVs. Moreover, various reports have pointed to populations of fragmented coding and non-coding transcripts [170, 283, 304-308]. However, the true extent to which full-length transcripts may be incorporated into EVs remains unclear. Recently, Li *et al*. provided some insight into this pervasive question [155]. They developed the extracellular vesicle long RNA sequencing (exLR-seq) technique, whereby EV RNAs were used to generate sequencing libraries using the SMARTer® Stranded Total RNA-Seq Kit (Clontech) followed by the sequencing of 150 bp pair-end reads on the Illumina platform [155]. Using bioinformatic tools, they were able to show that numerous EV mRNAs

displayed coverage reads spanning equally along the UTRs and CDS regions, suggesting full-length coverage [155]. The approach here described provides more pointed evidence, as it employs the use of long-read sequencing technology that allowed us to investigate EV RNAs in their endogenous state. To investigate the proportion of full-length transcripts present in our sequencing data, we utilized the bioinformatic tool, BamSlam [324]. This allowed us to calculate sequence length statistics by mapping the sequencing reads to the human transcriptome (GRCh38.p13, Transcript sequences [GENCODE v41]). This analysis revealed that 10.58% of all reads in EVs spanned across the reported full-length transcript to which they mapped (**Figure 3B,E**). Strikingly, this was only ~8% lower than the population of full-length transcripts identified in their parental cells, which were 18.67% (**Figure 3B,E**). Interestingly, WC transcripts were more diverse in their sequence lengths relative to EV transcripts (**Figure 3C-D**). Nevertheless, the median length of EV full-length transcripts was longer than their cellular counterparts (**Figure 3E**), which may be attributed to mRNA and lncRNA making up the largest proportion biotypes in EVs, while cellular biotypes were more diverse (**Figure 4B-C**). We further analysed our data to focus on the identification of transcript isoforms, and whether recruitment of isoforms is differential in the EV transcriptome. To this end, various possible approaches have been recently reported in the literature [325, 335, 336]. Our analysis shows that EVs RNAs may reflect the isoform diversity present in their parental cells (**Figure 5C**), but they may also carry preferred isoform variants (**Figure 5 A-B**). Moreover, various mRNAs can display differential isoform enrichment in the EV population (**Figure S5A-B**).

Taken together, these data provide compelling evidence demonstrating the existence of full-length RNAs within EVs derived from human cells. Furthermore, these RNAs can exhibit differential expression relative to their parental cells, with some displaying isoform-specific enrichments. These findings further highlight the selective mechanisms of RNA incorporation during EV biogenesis, adding additional insights to our current understanding of nucleic acid trafficking outside of the cell.

4.6. Chapter III References

1. Fafián-Labora, J.A. and A. O'Loghlen, *Classical and Nonclassical Intercellular Communication in Senescence and Ageing.* Trends in Cell Biology, 2020. **30**(8): p. 628-639.

5. Andaloussi, S.E., et al., *Extracellular vesicles: biology and emerging therapeutic opportunities.* Nat Rev Drug Discov, 2013. **12**(5): p. 347-57.

11. Haderk, F., et al., *Tumor-derived exosomes modulate PD-L1 expression in monocytes.* Sci Immunol, 2017. **2**(13).

15. van Niel, G., G. D'Angelo, and G. Raposo, *Shedding light on the cell biology of extracellular vesicles.* Nat Rev Mol Cell Biol, 2018. **19**(4): p. 213-228.

18. Lo Cicero, A., P.D. Stahl, and G. Raposo, *Extracellular vesicles shuffling intercellular messages: for good or for bad.* Current Opinion in Cell Biology, 2015. **35**: p. 69-77.

19. Yoon, Y.J., O.Y. Kim, and Y.S. Gho, *Extracellular vesicles as emerging intercellular communicasomes.* BMB Rep, 2014. **47**(10): p. 531-9.

20. Robbins, P.D. and A.E. Morelli, *Regulation of immune responses by extracellular vesicles.* Nature Reviews Immunology, 2014. **14**(3): p. 195-208.

21. Yáñez-Mó, M., et al., *Biological properties of extracellular vesicles and their physiological functions.* Journal of Extracellular Vesicles, 2015. **4**(1): p. 27066.

59. Ratajczak, J., et al., *Embryonic stem cell-derived microvesicles reprogram hematopoietic progenitors: evidence for horizontal transfer of mRNA and protein delivery.* Leukemia, 2006. **20**(5): p. 847-56.

61. Skog, J., et al., *Glioblastoma microvesicles transport RNA and proteins that promote tumour growth and provide diagnostic biomarkers.* Nat Cell Biol, 2008. **10**(12): p. 1470-6.

94. Lefebvre, F.A., et al., *Comparative transcriptomic analysis of human and Drosophila extracellular vesicles.* Sci Rep, 2016. **6**: p. 27680.

122. Crescitelli, R., et al., *Distinct RNA profiles in subpopulations of extracellular vesicles: apoptotic bodies, microvesicles and exosomes.* J Extracell Vesicles, 2013. **2**.

123. Baglio, S.R., et al., *Human bone marrow- and adipose-mesenchymal stem cells secrete exosomes enriched in distinctive miRNA and tRNA species.* Stem Cell Res Ther, 2015. **6**(1): p. 127.

151. O'Brien, K., et al., *RNA delivery by extracellular vesicles in mammalian cells and its applications.* Nat Rev Mol Cell Biol, 2020. **21**(10): p. 585-606.

155. Li, Y., et al., *Extracellular Vesicles Long RNA Sequencing Reveals Abundant mRNA, circRNA, and lncRNA in Human Blood as Potential Biomarkers for Cancer Diagnosis.* Clin Chem, 2019. **65**(6): p. 798-808.

161. Maacha, S., et al., *Extracellular vesicles-mediated intercellular communication: roles in the tumor microenvironment and anti-cancer drug resistance.* Molecular Cancer, 2019. **18**(1): p. 55.

170. Chakrabortty, S.K., et al., *Extracellular vesicle-mediated transfer of processed and functional RNY5 RNA.* RNA, 2015. **21**(11): p. 1966-1979.

173. Au Yeung, C.L., et al., *Exosomal transfer of stroma-derived miR21 confers paclitaxel resistance in ovarian cancer cells through targeting APAF1.* Nat Commun, 2016. **7**: p. 11150.

231. Love, M.I., W. Huber, and S. Anders, *Moderated estimation of fold change and dispersion for RNA-seq data with DESeq2.* Genome Biology, 2014. **15**(12): p. 550.

281. Théry, C., et al., *Minimal information for studies of extracellular vesicles 2018 (MISEV2018): a position statement of the International Society for Extracellular Vesicles and update of the MISEV2014 guidelines.* J Extracell Vesicles, 2018. **7**(1): p. 1535750.

282. Skog, J., et al., *Glioblastoma microvesicles transport RNA and proteins that promote tumour growth and provide diagnostic biomarkers.* Nat Cell Biol, 2008. **10**(12): p. 1470-6.

283. Nolte-'t Hoen, E.N., et al., *Deep sequencing of RNA from immune cell-derived vesicles uncovers the selective incorporation of small non-coding RNA biotypes with potential regulatory functions.* Nucleic Acids Res, 2012. **40**(18): p. 9272-85.

284. Wang, L., et al., *Role of cardiac progenitor cell-derived exosome-mediated microRNA-210 in cardiovascular disease.* Journal of Cellular and Molecular Medicine, 2019. **23**(11): p. 7124-7131.

285. Shen, M., et al., *Chemotherapy-Induced Extracellular Vesicle miRNAs Promote Breast Cancer Stemness by Targeting ONECUT2.* Cancer Research, 2019. **79**(14): p. 3608-3621.

286. Zhao, S., et al., *Tumor-derived exosomal miR-934 induces macrophage M2 polarization to promote liver metastasis of colorectal cancer.* J Hematol Oncol, 2020. **13**(1): p. 156.

287. Chen, S., et al., *Exosomes derived from miR-375-overexpressing human adipose mesenchymal stem cells promote bone regeneration.* Cell Proliferation, 2019. **52**(5): p. e12669.

288. Zhou, W., et al., *Cancer-secreted miR-105 destroys vascular endothelial barriers to promote metastasis.* Cancer Cell, 2014. **25**(4): p. 501-15.

289. Li, L., et al., *Exosomes Derived from Hypoxic Oral Squamous Cell Carcinoma Cells Deliver miR-21 to Normoxic Cells to Elicit a Prometastatic Phenotype.* Cancer Res, 2016. **76**(7): p. 1770-80.

290. Fang, J.H., et al., *Hepatoma cell-secreted exosomal microRNA-103 increases vascular permeability and promotes metastasis by targeting junction proteins.* Hepatology, 2018. **68**(4): p. 1459-1475.

291. Binenbaum, Y., et al., *Transfer of miRNA in Macrophage-Derived Exosomes Induces Drug Resistance in Pancreatic Adenocarcinoma.* Cancer Res, 2018. **78**(18): p. 5287-5299.

292. Ren, J., et al., *Carcinoma-associated fibroblasts promote the stemness and chemoresistance of colorectal cancer by transferring exosomal lncRNA H19.* Theranostics, 2018. **8**(14): p. 3932-3948.

293. Wang, E. and I. Aifantis, *RNA Splicing and Cancer.* Trends Cancer, 2020. **6**(8): p. 631-644.

294. Wang, X.W., et al., *RNA structure probing uncovers RNA structure-dependent biological functions.* Nat Chem Biol, 2021. **17**(7): p. 755-766.

295. Roth, M.J., et al., *Precise and parallel characterization of coding polymorphisms, alternative splicing, and modifications in human proteins by mass spectrometry.* Mol Cell Proteomics, 2005. **4**(7): p. 1002-8.

296. Nilsen, T.W. and B.R. Graveley, *Expansion of the eukaryotic proteome by alternative splicing.* Nature, 2010. **463**(7280): p. 457-63.

297. Kim, M.S., et al., *A draft map of the human proteome.* Nature, 2014. **509**(7502): p. 575-81.

298. Wilkinson, M.E., C. Charenton, and K. Nagai, *RNA Splicing by the Spliceosome.* Annu Rev Biochem, 2020. **89**: p. 359-388.

299. Kuhn, C.D., *RNA versatility governs tRNA function: Why tRNA flexibility is essential beyond the translation cycle.* Bioessays, 2016. **38**(5): p. 465-73.

300. Baßler, J. and E. Hurt, *Eukaryotic Ribosome Assembly.* Annu Rev Biochem, 2019. **88**: p. 281-306.

301. Leppek, K., R. Das, and M. Barna, *Functional 5' UTR mRNA structures in eukaryotic translation regulation and how to find them.* Nat Rev Mol Cell Biol, 2018. **19**(3): p. 158-174.

302. Quévillon Huberdeau, M. and M.J. Simard, *A guide to microRNA-mediated gene silencing.* Febs j, 2019. **286**(4): p. 642-652.

303. Flores, J.K. and S.F. Ataide, *Structural Changes of RNA in Complex with Proteins in the SRP.* Front Mol Biosci, 2018. **5**: p. 7.

304. Batagov, A.O. and I.V. Kurochkin, *Exosomes secreted by human cells transport largely mRNA fragments that are enriched in the 3'-untranslated regions.* Biol Direct, 2013. **8**: p. 12.

305. Tosar, J.P., et al., *Assessment of small RNA sorting into different extracellular fractions revealed by high-throughput sequencing of breast cell lines.* Nucleic Acids Res, 2015. **43**(11): p. 5601-16.

306. Chen, Q., et al., *Sperm tsRNAs contribute to intergenerational inheritance of an acquired metabolic disorder.* Science, 2016. **351**(6271): p. 397-400.

307. Sharma, U., et al., *Biogenesis and function of tRNA fragments during sperm maturation and fertilization in mammals.* Science, 2016. **351**(6271): p. 391-396.

308. Cambier, L., et al., *Y RNA fragment in extracellular vesicles confers cardioprotection via modulation of IL-10 expression and secretion.* EMBO Mol Med, 2017. **9**(3): p. 337-352.

309. Valadi, H., et al., *Exosome-mediated transfer of mRNAs and microRNAs is a novel mechanism of genetic exchange between cells.* Nat Cell Biol, 2007. **9**(6): p. 654-9.

310. Zomer, A., et al., *In Vivo imaging reveals extracellular vesicle-mediated phenocopying of metastatic behavior.* Cell, 2015. **161**(5): p. 1046-1057.

311. Hinger, S.A., et al., *Diverse Long RNAs Are Differentially Sorted into Extracellular Vesicles Secreted by Colorectal Cancer Cells.* Cell Rep, 2018. **25**(3): p. 715-725.e4.

312. van Dijk, E.L., et al., *The Third Revolution in Sequencing Technology.* Trends Genet, 2018. **34**(9): p. 666-681.

313. Deamer, D., M. Akeson, and D. Branton, *Three decades of nanopore sequencing.* Nat Biotechnol, 2016. **34**(5): p. 518-24.

314. Wang, Y., et al., *Nanopore sequencing technology, bioinformatics and applications.* Nat Biotechnol, 2021. **39**(11): p. 1348-1365.

315. Grünberger, F., S. Ferreira-Cerca, and D. Grohmann, *Nanopore sequencing of RNA and cDNA molecules in Escherichia coli.* RNA, 2022. **28**(3): p. 400-417.

316. Ewels, P.A., et al., *The nf-core framework for community-curated bioinformatics pipelines.* Nature Biotechnology, 2020. **38**(3): p. 276-278.

317. Li, H., *Minimap2: pairwise alignment for nucleotide sequences.* Bioinformatics, 2018. **34**(18): p. 3094-3100.

318. Ramírez, F., et al., *deepTools2: a next generation web server for deep-sequencing data analysis.* Nucleic Acids Research, 2016. **44**(W1): p. W160-W165.

319. Liao, Y., G.K. Smyth, and W. Shi, *The R package Rsubread is easier, faster, cheaper and better for alignment and quantification of RNA sequencing reads.* Nucleic Acids Research, 2019. **47**(8): p. e47-e47.

320. Ge, S.X., E.W. Son, and R. Yao, *iDEP: an integrated web application for differential expression and pathway analysis of RNA-Seq data.* BMC Bioinformatics, 2018. **19**(1): p. 534.

321. Raudvere, U., et al., *g:Profiler: a web server for functional enrichment analysis and conversions of gene lists (2019 update).* Nucleic Acids Res, 2019. **47**(W1): p. W191-w198.

322. Chen, J., et al., *LncSEA: a platform for long non-coding RNA related sets and enrichment analysis.* Nucleic Acids Research, 2020. **49**(D1): p. D969-D980.

323. Egorov, A.A., et al., *svist4get: a simple visualization tool for genomic tracks from sequencing experiments.* BMC Bioinformatics, 2019. **20**(1): p. 113.

324. Gleeson, J., et al., *Accurate expression quantification from nanopore direct RNA sequencing with NanoCount.* Nucleic Acids Research, 2021. **50**(4): p. e19-e19.

325. Tang, A.D., et al., *Full-length transcript characterization of SF3B1 mutation in chronic lymphocytic leukemia reveals downregulation of retained introns.* Nat Commun, 2020. **11**(1): p. 1438.

326. Gonzalez, L. and A.R. Nebreda, *RINGO/Speedy proteins, a family of non-canonical activators of CDK1 and CDK2.* Semin Cell Dev Biol, 2020. **107**: p. 21-27.

327. Crescitelli, R., et al., *Subpopulations of extracellular vesicles from human metastatic melanoma tissue identified by quantitative proteomics after optimized isolation.* J Extracell Vesicles, 2020. **9**(1): p. 1722433.

328. Ayre, D.C., et al., *CD24 induces changes to the surface receptors of B cell microvesicles with variable effects on their RNA and protein cargo.* Sci Rep, 2017. **7**(1): p. 8642.

329. Herrera, M., et al., *Differential distribution and enrichment of non-coding RNAs in exosomes from normal and Cancer-associated fibroblasts in colorectal cancer.* Mol Cancer, 2018. **17**(1): p. 114.

330. Magaña, S.M., et al., *Pediatric brain tumor cell lines exhibit miRNA-depleted, Y RNA-enriched extracellular vesicles.* J Neurooncol, 2022. **156**(2): p. 269-279.

331. Sousa, D., et al., *Deep Sequencing Analysis Reveals Distinctive Non-Coding RNAs When Comparing Tumor Multidrug-Resistant Cells and Extracellular Vesicles with Drug-Sensitive Counterparts.* Cancers (Basel), 2020. **12**(1).

332. Porter, L.A., et al., *Human Speedy: a novel cell cycle regulator that enhances proliferation through activation of Cdk2.* J Cell Biol, 2002. **157**(3): p. 357-66.

333. Gastwirt, R.F., C.W. McAndrew, and D.J. Donoghue, *Speedy/RINGO regulation of CDKs in cell cycle, checkpoint activation and apoptosis.* Cell Cycle, 2007. **6**(10): p. 1188-93.

334. Cheng, A. and M.J. Solomon, *Speedy/Ringo C regulates S and G2 phase progression in human cells.* Cell Cycle, 2008. **7**(19): p. 3037-47.

335. Byrne, A., et al., *Nanopore long-read RNAseq reveals widespread transcriptional variation among the surface receptors of individual B cells.* Nat Commun, 2017. **8**: p. 16027.

336. Hu, Y., et al., *LIQA: long-read isoform quantification and analysis.* Genome Biol, 2021. **22**(1): p. 182.

4.7. Supplementary Figures

FIGURE S3.1

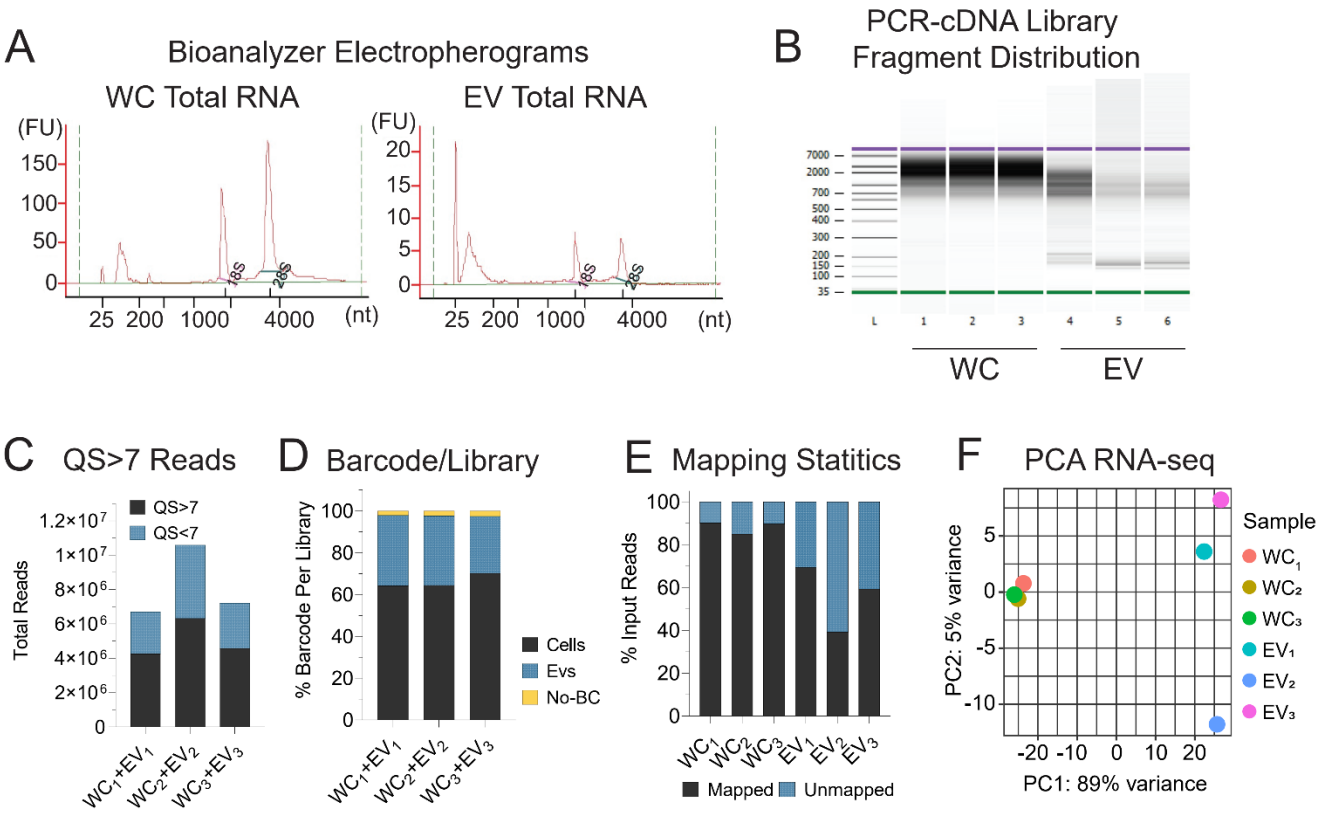

FIGURE S3.1 **Library preparation and initial analyses**. **A.** Representative Bioanalyzer electropherograms of purified total cellular and EV RNA displaying size distribution. **B.** Bioanalyzer densitometry plot of purified barcoded sequencing cellular and EV libraries. **C.** Stacked bar graphs of the total number of raw reads, in mixed, libraries passing (QS>7) or failing (QS<7) quality control steps as determined by Guppy basecalling. **D.** Stacked bar graphs representing the percentage of cellular and EV barcodes detected per sequenced library, after initial quality control steps. **E.** Stalked bar graphs of the percentage of input mapped and unmapped reads (to GENCODE v41) in EV and cellular transcriptomes. **F.** Principal Component Analysis (PCA) of RNA-sequencing data derived from cellular and EV RNA libraries.

FIGURE S3.2.1

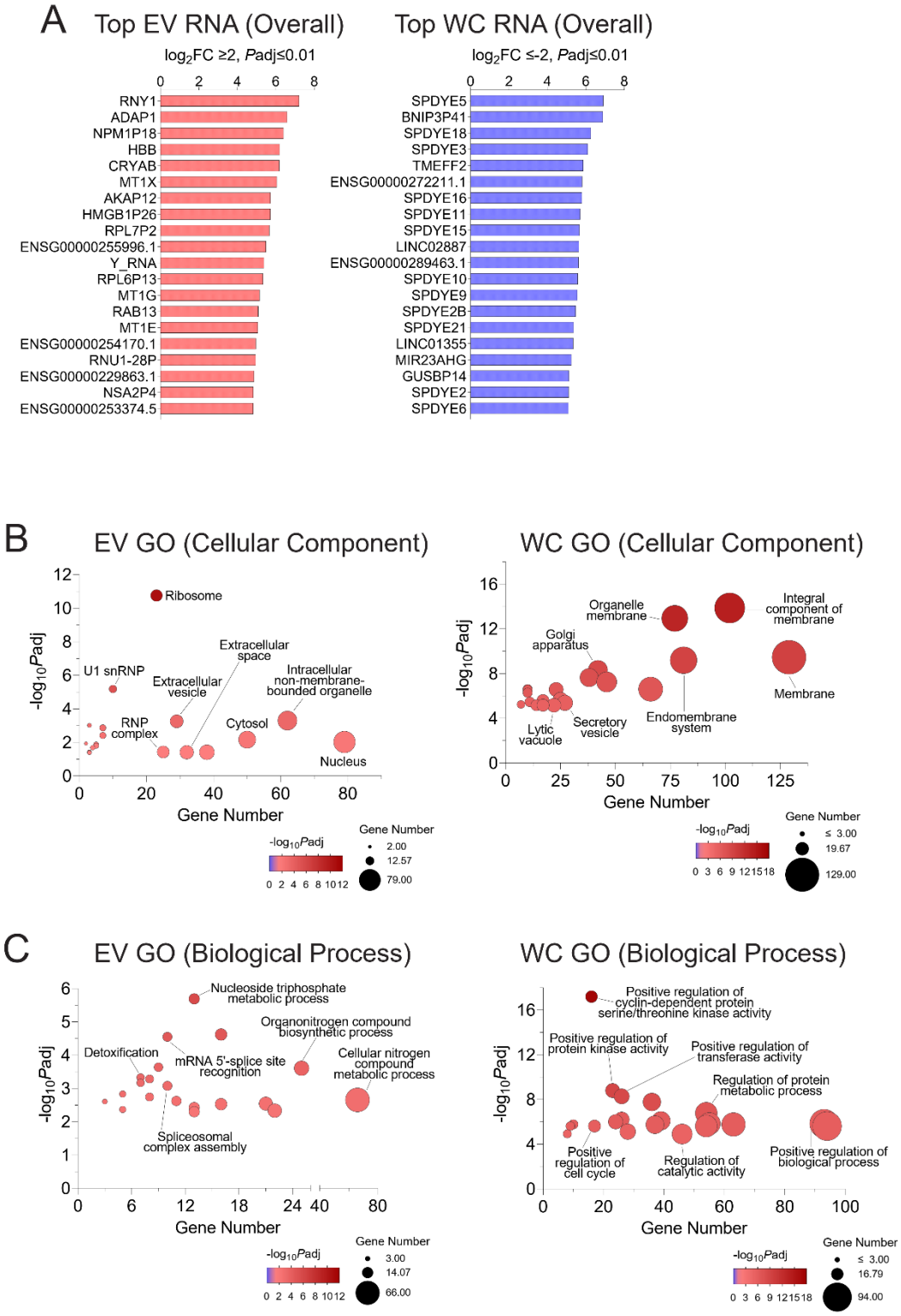
A
Top EV RNA (Overall)
log2FC ≥2, Padj≤0.01
RNY1
ADAP1
NPM1P18
HBB
CRYAB
MT1X
AKAP12
HMGB1P26
RPL7P2
ENSG00000255996.1
Y_RNA
RPL6P13
MT1G
RAB13
MT1E
ENSG00000254170.1
RNU1-28P
ENSG00000229863.1
NSA2P4
ENSG00000253374.5
Top WC RNA (Overall)
log2FC ≤-2, Padj≤0.01
SPDYE5
BNIP3P41
SPDYE18
SPDYE3
TMEFF2
ENSG00000272211.1
SPDYE16
SPDYE11
SPDYE15
LINC02887
ENSG00000289463.1
SPDYE10
SPDYE9
SPDYE2B
SPDYE21
LINC01355
MIR23AHG
GUSBP14
SPDYE2
SPDYE6
B
EV GO (Cellular Component)
Ribosome
U1 snRNP
Extracellular vesicle
Extracellular space
Intracellular non-membrane-bounded organelle
RNP complex
Cytosol
Nucleus
-log10Padj
Gene Number
WC GO (Cellular Component)
Organelle membrane
Integral component of membrane
Golgi apparatus
Membrane
Lytic vacuole
Secretory vesicle
Endomembrane system
C
EV GO (Biological Process)
Nucleoside triphosphate metabolic process
Organonitrogen compound biosynthetic process
Detoxification
mRNA 5'-splice site recognition
Cellular nitrogen compound metabolic process
Spliceosomal complex assembly
WC GO (Biological Process)
Positive regulation of cyclin-dependent protein serine/threonine kinase activity
Positive regulation of protein kinase activity
Positive regulation of transferase activity
Regulation of protein metabolic process
Positive regulation of cell cycle
Regulation of catalytic activity
Positive regulation of biological process

FIGURE S3.2.1 EV-enriched RNAs display gene ontology associations to ribonucleoprotein complexes. **A.** Bar graphs of the top 20 EV-enriched (Log_2 fold change ≥2, *Padj*≤0.01) and cell-enriched/EV-depleted (Log_2 fold change ≤-2, *Padj*≤0.01) RNA. **B.** Bubble plot of GO cellular component of EV-enriched (Log_2 fold change ≥2, *Padj*≤0.01) and cell-enriched/EV-depleted (Log_2 fold change ≤-2, *Padj*≤0.01) RNA. All enriched RNA considered. **C.** Bubble plot of GO biological process of EV-enriched (Log_2 fold change ≥2, *Padj*≤0.01) and cell-enriched/EV-depleted (Log_2 fold change ≤-2, *Padj*≤0.01) RNA. All enriched RNA considered.

FIGURE S3.2.1

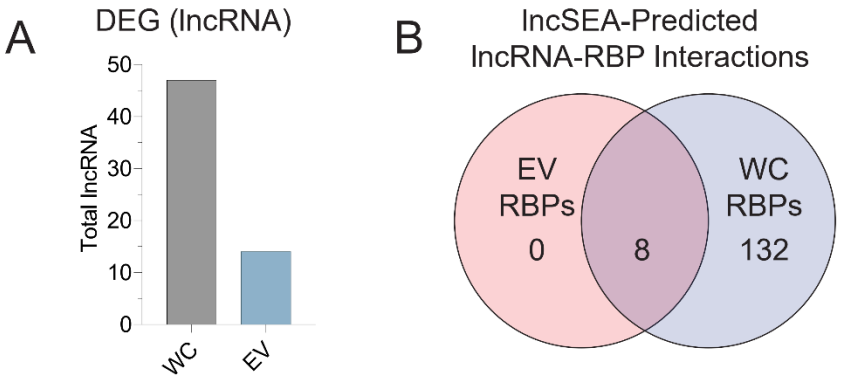

C

Table S2.1 lncSEA-Predicted lncRNA-RBP Interactions (EV/WC Overlap)

EV-Enriched lncRNA (Predicted RBP Interaction)									
Set	**Sub Class**	**lncRNA count**	**Simpson**	**P-value**	**FDR**	**Bonferroni**	**Jaccard**	**%**	**Input number**
RO60	RNAInter	4	0.286	8.98E-07	0.00971	0.0166	0.0119	4/325	14
TRA2A	RNAInter	4	0.286	1.05E-06	0.00971	0.0194	0.0115	4/338	14
EXOSC5	EuRBPDB	2	0.143	0.000245	0.0116	0.0252	0.0183	2/97	14
FMR1	starBasev2.0	2	0.143	0.000688	0.00697	0.0186	0.0114	2/163	14
CSTF2T	starBasev2.0	2	0.143	0.000748	0.00697	0.0202	0.011	2/170	14
DDX54	starBasev2.0	2	0.143	0.00105	0.00697	0.0283	0.00935	2/202	14
HNRNPA2B1	starBasev2.0	2	0.143	0.00109	0.00697	0.0294	0.00917	2/206	14
U2AF2	starBasev2.0	3	0.214	0.00129	0.00697	0.0348	0.00318	3/932	14
WC-Enriched lncRNA (Predicted RBP Interaction)									
Set	**Sub Class**	**lncRNA count**	**Simpson**	**P-value**	**FDR**	**Bonferroni**	**Jaccard**	**%**	**Input number**
U2AF2	starBasev2.0	12	0.255	7.87e-12	2.12e-10	2.12e-10	0.0124	12/932	47
TRA2A	RNAInter	8	0.17	2.97e-10	2.61e-07	5.49e-06	0.0212	8/338	47
U2AF2	RNAInter	16	0.34	7.66e-10	5.9e-07	1.42e-05	0.00526	16/3010	47
FMR1	RNAInter	11	0.234	2.14e-09	1.52e-06	3.96e-05	0.00896	11/1191	47
RO60	RNAInter	7	0.149	8e-09	4.23e-06	0.000148	0.0192	7/325	47
CSTF2T	RNAInter	15	0.319	9.25e-09	4.75e-06	0.000171	0.00484	15/3068	47
HNRNPA2B1	RNAInter	7	0.149	1.98e-07	6.91e-05	0.00366	0.0125	7/521	47
CSTF2T	starBasev2.0	5	0.106	2.72e-07	1.22e-06	7.34e-06	0.0236	5/170	47
DDX54	starBasev2.0	5	0.106	6.39e-07	2.11e-06	1.73e-05	0.0205	5/202	47
HNRNPA2B1	starBasev2.0	5	0.106	7.04e-07	2.11e-06	1.9e-05	0.0202	5/206	47
EXOSC5	EuRBPDB	4	0.0851	1.2e-06	2.28e-05	0.000124	0.0286	4/97	47
TRA2A	EuRBPDB	4	0.0851	1.22e-05	4.49e-05	0.00126	0.0184	4/174	47
U2AF2	EuRBPDB	4	0.0851	0.000198	0.00024	0.0204	0.01	4/357	47
CSTF2T	EuRBPDB	4	0.0851	0.00028	0.000317	0.0288	0.00922	4/391	47

FIGURE S3.2.2 LncSEA enrichment analysis of EV and WC enriched lncRNA. **A.** Bar graph of all EV-enriched (Log_2 fold change ≥2, *Padj*≤0.01) and cell-enriched/EV-depleted (Log_2 fold change ≤-2, *Padj*≤0.01) lncRNA. **B.** Venn diagram of RBPs associated to EV- and WC-enriched lncRNA as determined by LncSEA. **C.** Table S2.1 displaying lncSEA-predicted lncRNA-RBP Interactions (overlap only).

FIGURE S3.3

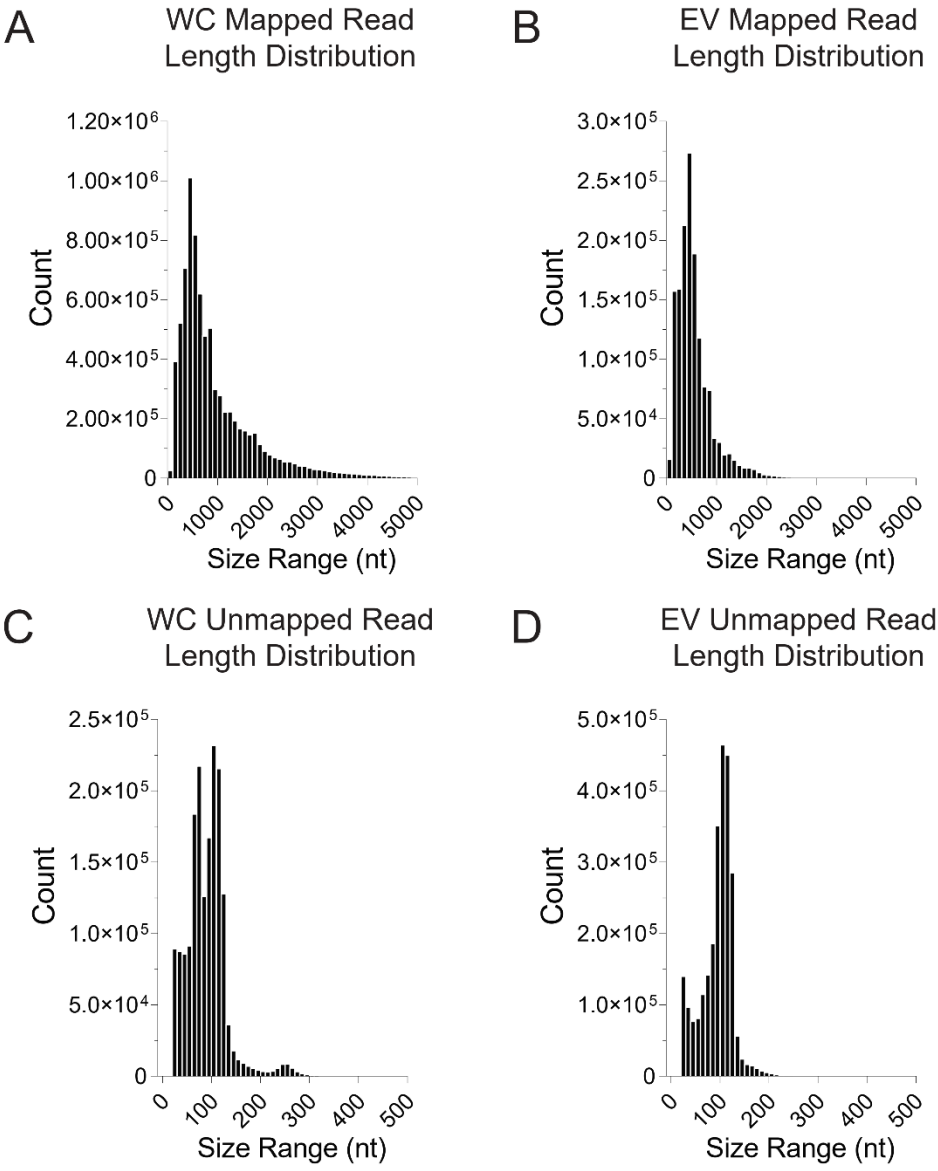

E Length Distribution Statistics Summary

Sample	Total number of values	Number of excluded values	Number of binned values	Minimum	25% Percentile	Median	75% Percentile	Maximum
Mapped WC	8012682	0	8012682	80	441	685	1258	23192
Mapped EV	1463222	0	1463222	80	318	472	674	12633
Unmapped WC	1778223	0	1778223	20	65	90	112	5137
Unmapped EV	2557415	0	2557415	20	78	101	115	2014

FIGURE S3.3 Size distribution of EV-derived RNAs. **A-B.** Histograms of cell and EV mapped reads displaying sequence lengths distribution frequencies. Cell and EV reads binned at intervals of 100. **C-D.** Histograms of cell and EV unmapped reads displaying sequence lengths distribution frequencies. Cell and EV reads binned at intervals of 10. **E.** Summary of length distribution statistics of binned values of mapped and unmapped reads.

FIGURE S3.5

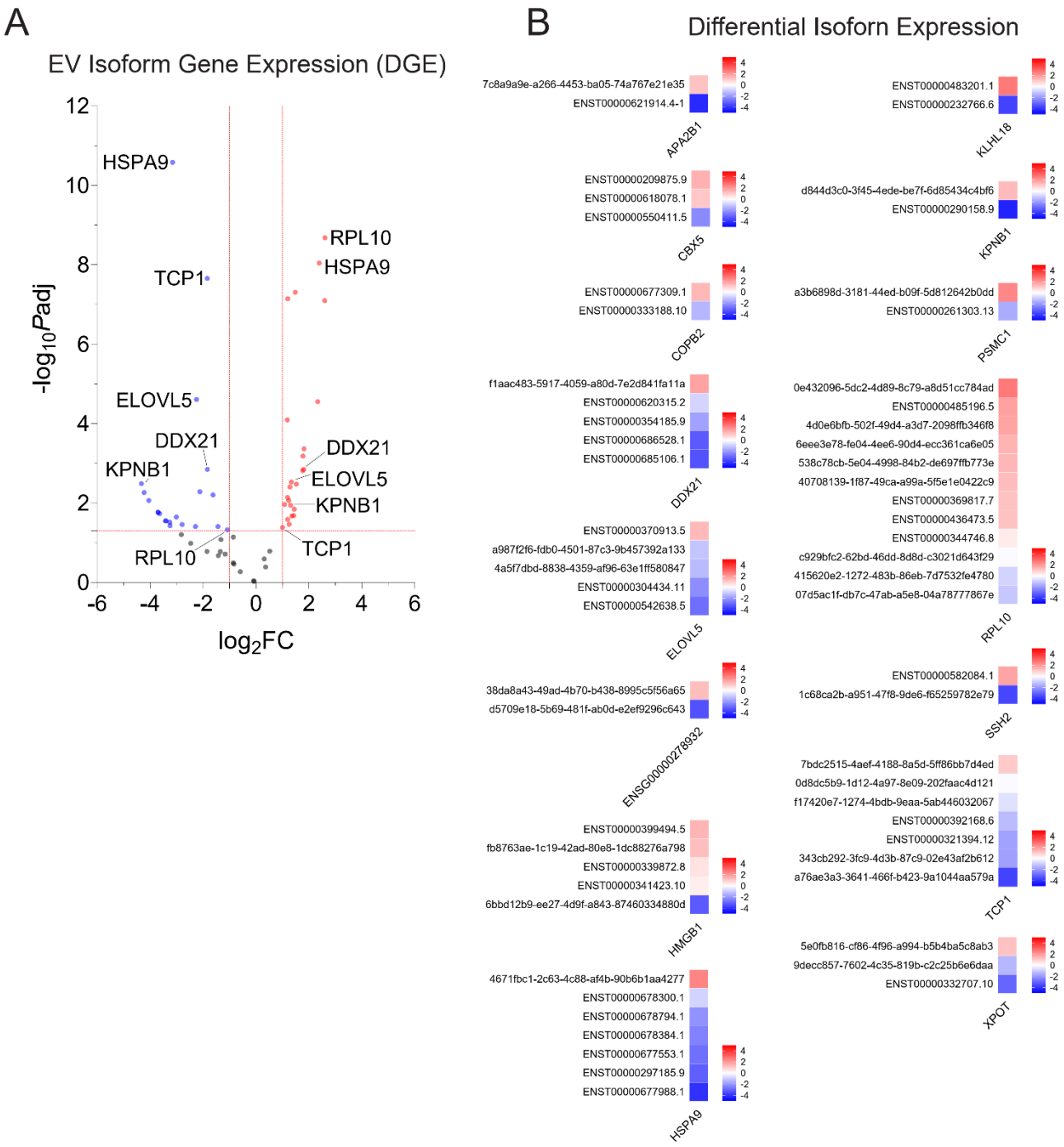
A
EV Isoform Gene Expression (DGE)
HSPA9
TCP1
ELOVL5
DDX21
KPNB1
RPL10
RPL10
HSPA9
DDX21
ELOVL5
KPNB1
TCP1
-log10Padj
log2FC
B
Differential Isoform Expression
APA2B1
CBX5
COPB2
DDX21
ELOVL5
ENSG00000278932
HMGB1
HSPA9
KLHL18
KPNB1
PSMC1
RPL10
SSH2
TCP1
XPOT

FIGURE S3.5 EVs carry differentially expressed transcript isoforms. **A.** Volcano plot of cellular and EV transcript isoforms signifying the shift in transcript expression levels. Blue dots represent statistically significant downregulated EV-transcripts (Log_2 fold change ≤-1, *Padj*≤0.05). Red dots represent statistically significant upregulated EV-transcripts (Log_2 fold change ≥1, *Padj*≤0.05). **B.** Heatmap visualizations of individual RNAs displaying differential gene expression of isoform signatures.

Chapter IV:

General Discussion

5.1. Thesis Summary and General Discussion

5.1.1. Relevance and Significance of Work

Extracellular vesicles (EVs) are membrane-bound nanoparticles released by cells and have garnered widespread interest for their role in the intercellular communication [15, 161]. This ability is conferred by their preloading with bioactive molecules, that upon their release in recipient cells, can induce changes to the baseline physiological state of these cells [15, 18-21]. Interestingly, the molecular contents of EVs, including their RNA and protein repertoires, display their own unique molecular signatures relative to their cells of origin, pointing to possible specialized sorting mechanisms employed by cells during EV biogenesis [94, 122, 123]. The study and characterization of EV cargoes is not only relevant to understand their role in the transfer of molecular signals, but also provide a valuable resource for the discovery of biomarkers in a variety of disease contexts [156-159].

Diverse in their modes of biogenesis, as well as their cargo repertoire, EVs are an innately complex group and investigations in the field have been encumbered by their heterogeneity [72-74]. Individual cells may produce multiple EV populations, which likely contain specific cargoes that can change over the physiological state of the cell [337]. These cargoes include a vast array of potentially relevant biomolecules, including lipids, proteins, DNA, and protein coding and non-coding RNAs [15, 18, 109]. Most studies currently carried out in the field employ the isolation of EVs from the conditioned media of cultured cells, with techniques that unfortunately result in often crude, heterogenous

populations [338, 339]. Although concerted efforts have made significant progress to deconvolute EV subpopulations [72, 75-77], our understanding of their individual significance is currently minimal. As such, the biological functions ascribed to the heterogenous group may not directly reflect their true individual roles [337]. For instance, it is not yet clear whether the biological effects of EVs in recipient cells may be subpopulation dependent. Additionally, whilst the biological roles of various EV protein and RNA cargoes have been reported in the literature [19-21], there exists a need to better characterize their diverse cargoes and investigate their potential biological relevance. For example, RNA transcripts within EVs have been suggested to present in fragmented forms [170, 283, 304-308], with only a small number of studies showing the EV-mediated transfer of functional mRNAs to recipient cells [59, 61, 309-311].

The functional dissection, into subclasses, of the EV heterogenous population, as well as the characterization of their contents is crucial for elucidating their roles during intercellular communication. In this context, this thesis explores sphingomyelinase-driven EV biogenesis pathways (**Chapter II**), and the individual contributions of Neutral (NSM) and Acid (ASM) sphingomyelinases to EV-mediated export of molecular cargoes by cells. Moreover, this thesis investigates the sequence features of RNAs exported via EVs (**Chapter III**), an important aspect of their communicatory potential. We provide transcriptome-level evidence for the presence of full-length RNAs in EVs, providing evidence that answers an open question in the field. Together, these data provide important insights into the nature of the EV RNA and protein cargoes, as well as the crucial role of sphingolipid metabolism on their packaging during EV biogenesis.

5.1.2. Experimental Design

Chapter II

The biogenesis of EVs is a concerted process involving multiple subcellular machineries and occurring at specific subcellular locations [15, 99], all of which contribute the heterogenous populations. These diverse modes of EV generation likely contribute to the differential recruitment of cargoes [340], and it is therefore imperative to understand the contributions of individual subclasses [337]. Sphingolipid metabolism by sphingomyelinases is a key metabolic process that is intimately involved in the generation of EVs; collectively these biogenesis pathways are termed as the endosomal sorting complex required for transport (ESCRT)-independent pathway [7, 15, 70]. The enzymes involved include Neutral type II sphingomyelinase (NSM) and Acid sphingomyelinase (ASM), both of which convert sphingomyelin present within membranes to ceramide and phosphorylcholine [82, 100, 222].

Sphingomyelinase variants contribute to the generation of specific subpopulations of EVs, with NSM implicated in the generation of intraluminal vesicles at the endosome (and therefore exosomes) and ASM associated with the formation of microvesicles at the plasma membrane [82, 83, 100, 105]. While these distinct roles are likely to contribute to the heterogenous cargoes exported by individual EV subpopulations, their contributions to EV heterogeneity have not been defined. Using chemical inhibitors targeting NSM (GW4869) or ASM (FTY720) in human MCF7 cells [82, 100, 121, 222], we explored the role of sphingolipid metabolism pathways on the biogenesis of extracellular vesicles and

their involvement in the export of RNAs and proteins from cells. Furthermore, we used various cellular assays to quantify the phenotypic response of recipient cells, human MCF10A, to the modified MCF7 EV populations.

Chapter III

EVs' communicatory potential is facilitated by their loading with bioactive cargoes, including a diverse repertoire of coding and non-coding RNAs [1, 2, 5, 60, 124]. Upon delivery in recipient cells, these nucleic acid molecules can influence the cell's behaviour by inducing various phenotypic responses [2, 15, 161, 237, 238]. While numerous EV-trafficked RNAs have been associated with a variety of cellular responses in both normal and etiological contexts, very little is known about the sequence integrity of these transcripts. Indeed, several reports suggest that the RNA molecules present within EVs may exist in fragmented forms [170, 283, 304-308]. Nevertheless, some reports have described the EV-mediated transfer of functional mRNA molecules to recipient cells [59, 61, 309-311].

As the biological roles of RNA molecules is intrinsically tied to their sequence features [293, 294, 298-303, 341, 342], it is therefore imperative to characterize the types of transcripts available within EVs. Using long-read sequencing with Oxford Nanopore technology [312-315], we sought to characterize the sequence features of human K562 EV polyadenylated (poly(A)) RNAs, determining the available full-length transcriptome and identifying EV-associating transcript isoforms.

5.1.3. Sphingolipid Metabolism Regulates the EV-Mediated Release of RNA and RNA-binding Proteins

Although both NSM and ASM metabolize sphingomyelin to generate ceramide and phosphorylcholine, our results point to specialized roles for each enzyme variant (**Chapter II**). In a broad sense, each inhibitory treatment resulted in unique changes to the physical characteristics of the isolated human MCF7 EV (**Figure S2.1 C-D**, **Figure 2.1 D-G**). We show that inhibition of NSM does not significantly alter the number of EVs released by cells, while ASM inhibition increased the release of these nanoparticles (**Figure 2.1 F**). However, both treatments resulted in a reduction of the RNA occupancy of the heterogenous population (**Figure 2.1 G**). These results reveal that sphingolipid metabolism is necessary for the export of RNAs through EVs, with NSM and ASM inhibitions differentially contributing to their incorporation (**Figure S2.2 B**).

Using multi-*omics* approaches, we investigated the types of RNA and protein cargoes that depend on the activity of each sphingomyelinase variant, and in so doing found that each metabolic pathway associates with unique intracellular machineries (**Chapter II**). RNA availability within the EV heterogenous population was altered as a result of the inhibitory drugs, with a broad reduction of RNA positive nanoparticles (**Figure 2.1 G**). Strikingly, differential expression analysis of transcriptomic data, acquired from control and drug-induced EVs, revealed that ASM inhibitory treatments resulted in a major downregulation of RNAs (**Figure 2.2 E**). As RNA-binding proteins (RBPs) play key roles in the subcellular distribution of RNAs in cells, we sought to examine whether RBPs

availability was altered in EVs as a response to the EV-inhibitory compounds. Proteomic profiling of EVs isolated demonstrated that the composition of the RBP repertoire was affected in opposing directions as a response to SMase inhibitor treatments (**Figure S2.3 D**, **Figure 2.4 A-C**). Our results indicate that NSM is particularly important to the EV-mediated trafficking of RBPs from cells, with our data showing an almost complete downregulation of RBPs when this pathway was inhibited (**Figure 2.4 A**). Furthermore, our data indicate the ribonucleoprotein (RNP) modules may be exported through the NSM-dependent lipid metabolism pathways (**Figure 2.4 D**, **Figure 2.4 F**). Together, these findings reveal that sphingolipid metabolism by NSM and ASM contribute differentially to the RNA and RBP cargoes trafficked by EVs, with the NSM metabolic pathway playing an important role in the EV-mediated export of RBPs from cells.

5.1.4. Neutral and Acid Sphingomyelinases Control the Biogenesis of EV Subpopulations Trafficking Distinct Proteomic Cargoes

Neutral (NSM) and Acid sphingomyelinases have been described as contributing to the biogenesis of distinct EV subpopulations, namely exosomes and microvesicles, respectively [82, 83, 100, 105]. While different intracellular machineries have been described to play roles in the biogenesis of both EV subpopulations [7, 15, 62, 70, 82, 95, 96, 100], there are currently no proteomic studies detailing the contributions of sphingolipid metabolic pathways to EV composition. By profiling the proteomic composition of EVs resulting from sphingomyelinase inhibitor treatments, we were able to identify numerous proteins that associate to various intracellular machineries (**Chapter**

II). Furthermore, we show that NSM and ASM metabolic pathways associate with different subcellular compartments, and their inhibition results in depletion of proteins linked to these components. Significantly, our analyses of proteomic datasets indicate that each metabolic pathway contributes in unique ways to the proteomic composition of the EV heterogenous population. In fact, it appears that there is little overlap to the recruitment of protein cargoes (**Figure 2.3 C-F**). These findings support previous reports that describe the specialized roles that NSM and ASM during EV biogenesis [82, 83, 100, 105], providing valuable insights on the interactions of each sphingolipid metabolic pathway with different intracellular components. For instance, NSM inhibition resulted in a downregulation of endosomal and autophagic proteins within the EV population, while ASM inhibition repressed the release of proteins involved in plasma membrane dynamics (**Figure 2.3 D**). This indicates that the inhibitory treatments resulted in the reduction of protein components of the targeted EV subpopulation. Strikingly, inhibition of the SMase enzyme variants resulted in the increased detection of proteins associated with the non-targeted group (NSM EVs) (**Figure 2.3 D-F**), suggesting that EVs induced by drug treatments were enriched for alternate subpopulations of EVs.

5.1.5. EV Biogenesis Pathways Influence EVs' Phenotypic Effects on Recipient Cells

Many studies have confirmed the ability of EVs to transfer molecular signals to recipient cells, inducing changes to their normal behaviour [8-14]. However, these studies typically employ standard EV isolation techniques that often result in size-selected

populations [343]. It is, therefore, difficult to ascertain which subpopulations of EVs are the culprits behind the response observed. To this end, we isolated EVs from MCF7 cells under control or SMase inhibitor conditions, to assess whether alterations to the heterogenous EV population can induce distinct phenotypes on recipient cells (**Chapter II**). Using three quantification approaches, we examined changes in protein translation, cell proliferation, and cell migration of MCF10A recipient cells incubated with MCF7-derived EVs. Our data revealed that EVs resultant of ASM inhibitory treatments induced a differential response in MCF10A (relative to the other conditions). Namely, MCF10A cells displayed an increased translation phenotype (**Figure 2.5 B**, **Figure S2.5 A**), a moderate increase in cell proliferation (**Figure 2.5 C**, **Figure S2.5 B**), and increased migratory response during scratch wound assays (**Figure 2.5 D**). These findings show that modifying EV heterogenous populations, thereby enriching for EV subpopulations, can result in an altered phenotypic response in recipient cells.

5.1.6. EVs Contain Full-Length RNAs and Exhibit Isoform Recruitment Preferences

Although the transcriptomic profiling of EVs has become ubiquitous within the field, there is presently sparse data concerning the trafficking of full-length RNAs within EV populations. Indeed, several studies have reported the existence of coding and non-coding RNA fragments within EVs [170, 283, 304-308], with mRNAs generally considered to be fragmented [337, 344]. While a recent report has suggested that full-length mRNAs are present within EVs, namely that sequencing reads span equally along UTRs and CDS

regions [155], there are currently no reports where EV RNAs were sequenced in their endogenous state. By using Nanopore long-read sequencing technology, we were able to identify a variety of full-length poly(A) RNAs within EVs isolated from human K562 cell conditioned media (**Chapter III**).

Our results identified a variety of EV-enriched transcripts encompassing diverse RNA biotypes (**Figure 3.1 E**, **Figure 3.2 B-D**), including Y-RNAs, mRNAs, spliceosomal RNAs, and pseudogenes transcripts. Overrepresentation analysis (ORA) of EV-enriched mRNAs determined that these transcripts were associated with ribonucleoprotein (RNP) machineries such as the ribosome and U1 spliceosome (**Figure S3.2.1 B-C**). Strikingly, 10.58% of all EV sequencing reads spanned across the reported full-length transcript to which they were mapped (**Figure 3.3 E**). Moreover, our analyses revealed that full-length transcripts were represented across various RNA biotypes (**Figure 3.4 A**), with mRNAs (58.13%) and lncRNAs (22.57%) being the most abundant in EVs (**Figure 3.4 C**). We also showed that full-length RNA biotypes exhibited variance in proportion relative to their cells of origin (**Figure 3.4 A-C**), highlighting that preferential loading may occur. Finally, we investigated whether EV transcripts displayed transcript isoform preferences (**Figure 3.5 A-C**, **Figure S3.5 A-B**). While some transcripts reflected the isoform diversity detected in their cells of origin (**Figure 3.5 C**), there were noted examples that such as *HSPA9* that demonstrated a preferential sorting of isoform variants (**Figure 3.5 A-B**). Together, this chapter provides compelling evidence for the presence of full-length RNAs within EVs from human cells.

5.1.7. Limitations

Recommendations for Chapter II

While this research provides multiple levels of evidence for the specialized roles of sphingomyelinases in the biogenesis of EVs, several recommendations can be made to improve the overall quality of this chapter, some of which include on-going efforts in the lab. Namely, it is recommended that the inhibitory drugs utilized are better characterized for their effects on MCF7 cells. Although we detected changes to morphological and molecular composition of the EV population, and in particular their cargo alterations were quite striking, we recommend additional validation. For instance, the inclusion of enzymatic assays, quantifying the effects of GW4869 and FTY720 on the sphingomyelinase activity [345-350], would provide pointed evidence to the efficiency of the treatments. Further confirmatory data can also be obtained by characterizing the post-treatment ceramide levels of cells and EVs via the use of anti-ceramide antibodies (e.g. dot blot or immunofluorescence microscopy (IF)) [351-354] or with mass spectrometry (lipidomics) [355-357]. Additionally, the localized activity of each enzyme variant can be explored by IF studies, where ceramide and/or sphingomyelinases (NSM or ASM) would be monitored in relation to endosomal and plasma membrane markers (EV biogenesis sites) [82, 264, 358, 359]. Together, these experiments would allow us to better understand how the inhibitor drugs are modulating lipid metabolic pathways at sites of EV biogenesis, strengthening our current results.

In a broader sense, our studies are limited to EV biogenesis pathways driven by sphingomyelinase activity. However, it does not consider alternative biogenesis pathways, including the Endosomal sorting complex required for transport (ESCRT)-dependent pathway of EV biogenesis [78-80]. Our results suggest that proteins associated to the ESCRT-dependent pathway are increased as response by the SMase inhibition (**Figure 2.3 E**), but we cannot separate this subpopulation from our data. By further expanding our studies to include this major subpopulation, we can glean further insights into the roles of ESCRT-dependent and ESCRT-independent pathways of EV biogenesis, and whether certain cargoes are preferentially exported through specific biogenesis modes.

Recommendations for Chapter III

A limitation of our current nanopore long-read sequencing approach is that it utilizes poly(A) sites naturally present within RNA molecules to generate a sequencing library of this specific subpopulation. In order to consider the larger non-coding transcriptome, we will need to modify our sequencing approach by incorporating additional library preparation techniques. These may include RNA fractionation or ribodepletion techniques coupled with the polyadenylation of transcripts [360, 361]. Additionally, the use of Nanopore direct RNA sequencing [362, 363] would provide much needed insight into the post-transcriptional modifications present in EV RNAs, and whether these modifications correlate to their presence within EVs. However, direct RNA sequencing currently requires larger amounts of poly(A) RNAs, which makes it a

technically challenging method to profile RNAs in EVs, which are typically limiting in quantity.

5.2. Perspectives and Future Directions

5.2.1. Relevance of EV Research to Disease

Active participants in a variety of etiological conditions, EVs are important puzzle pieces to understanding the ways that disease-causing cells interact with their environment [364]. Indeed, EVs have been implicated as active agents in a variety of diseases including, cancer [365, 366], cardiometabolic disorders [367, 368], neurological pathologies [180, 369], and infectious diseases [370, 371]. These qualities also position EVs as a valuable source of potential biomarkers for an ever-growing list of diseases [155-159]. As discussed in **Chapter I**, EV RNA cargoes can influence the behaviour of recipient cells, critically modifying their behaviours, and enhancing the conditions that drive disease progression [61, 131, 170, 173, 182, 185, 191]. In cancer, for example, EVs have become increasingly implicated agents during tumorigenesis, with their RNAs cargoes playing key roles in the modification of the tumor microenvironment by promoting metastasis and therapy resistance [23, 173]. Similarly, in neurodegenerative disorders, EV RNAs have been linked to neurodegeneration by affecting the maintenance and survival of motor neurons [185, 191].

While the purpose of our studies is not to understand the etiological consequence of EV cargoes, it provides some interesting information in this regard. For instance, our SMase inhibition experiments (**Chapter II**) resulted in the enrichment of proteins

associated with subpopulations of EVs. These alterations, in turn, resulted in differential phenotypic response of recipient cells. These observations posit that EV composition, and in particular their cargoes, play a critical role in the response of recipient cells. One can speculate then, that cells may utilize specific EV biogenesis mechanisms for the selective release of molecular cargoes that are relevant to disease.

5.2.2. Therapeutic Opportunities of Manipulating EV Cargoes

The biological properties EVs, as well as their roles in the transfer of molecular cargoes between cells, makes them particularly interesting to exploit as platforms for the delivery of therapeutic agents [151]. In fact, numerous pre-clinical and clinical studies have been conducted (or are underway) with the explicit objective of harnessing EVs for therapy [151, 202, 220, 221]. This interest is driven not only by EVs' protective properties, but also because they can be isolated from numerous clinically relevant cell types [196-198], they can present surface antigens [199, 200], and they can be immune neutral when obtained from the same patient [151]. The molecular cargoes that can be carried by EVs are quite broad, but RNA molecules are of particular interest in the age of RNA therapeutics [372, 373]. To this end, various endogenous and exogenous approaches have been described to enrich RNA molecules in EVs [201-207]. An interesting feature of EVs is that they generally display their own transcriptomic identity relative to their cells of origin [94, 122, 123]. This is significant because it implies that selective sorting mechanisms occur during the EV biogenesis process, with specific RNA molecules trafficked-to and packaged-at EV biogenesis sites [109, 131]. Likewise, RNA binding

proteins (RBPs) are quite abundant in EVs, and it is likely that they play key roles in this selective packaging. Previous studies have implicated numerous RBPs with the selective packaging of RNAs in EVs [121, 131, 133, 136-138, 145]. Moreover, it has been shown that EV-enriched RNA molecules can contain specific sequence features (e.g. “EXOmotifs” [133]) that drive their incorporation to EVs [131, 132].

In this context, our research provides valuable new data that furthers our understanding of EV-cargo sorting mechanisms (**Chapter II**), and it additionally expands current knowledge on the sequence features of RNAs trafficked by EVs (**Chapter III**). Both sets of findings are important in the pursuit to understand how we can manipulate the types of cargoes that EVs carry. In **Chapter II**, we present compelling evidence that show how sphingomyelinase-driven EV biogenesis pathways modulate EV cargoes. Significantly, we show that RNAs and RBPs present in within EVs can be dramatically modified in response to SMase inhibition, and importantly, we show that the incorporation of EV-trafficked RBPs is highly dependent on sphingomyelinase activity. In addition, in both **Chapter II** and **Chapter III**, we show that EV RNAs exhibit differential profiles relative to their cells of origin. Moreover, in **Chapter III**, we further demonstrate that EVs can contain full-length RNAs and that these RNAs can display isoforms specific differential expression to the EV population. As in previous studies [131, 132], these data can be further used for downstream analyses to determine important sequence features that drive incorporation to EVs. Together, these data are relevant to EV cargo loading mechanisms, and they expand our current knowledge about EV RNA sequence features, both important for innovations in EV-based therapeutics.

5.2.3. Possible Confirmatory Studies

The asymmetric distribution of gene products is an important characteristic of cells, facilitating the organization of discreet subcellular compartments [127]. For instance, RNA molecules are trafficked from their sites of transcription to specific subcellular locations [128]. This process, which is tightly regulated and evolutionarily conserved, involves intrinsic features of the RNAs (*cis*-regulatory motifs (CRMs)) and *trans*-acting partners such as RBPs [127-130]. It is, therefore, quite tempting to hypothesize that cells may exploit these systems for the selective recruitment and packaging of RNAs to sites of EV biogenesis [127]. Indeed, this seems to be the case, and multiple studies have provided evidence for both the importance of RBPs [131], as well as RNA sequence features [131, 132]. To expand on the previous sections, our data indicate that many RNAs and RBPs can be enriched in EVs relative to their cells of origin. Moreover, these cargoes can associate to specific modes of EV biogenesis. With numerous candidates identified, it is challenging to validate them individually. However, there are multiple experimental approaches that can be utilized to better understand their selective packaging.

An RBP-centric approach would involve selecting a few of the EV RBPs observed to be dynamically modulated as a response of SMase inhibitor treatments (**Figure 2.4 A-C**). Several candidate RBPs appear to be condition specific, displaying a requirement for sphingolipid metabolism for release, or being independent of the pathway. Moreover, some RBPs appear to travel in proportions that are similar to the RNA components of their RNP complexes (**Figure 2.4 D-F**). The candidate RBPs can be used for targeted

studies to understand their contribution to the EV transcriptome. For example, silencing approaches to knockdown the expression of these RBPs can be used to confirm their roles in RNA recruitment to EVs. Various EV RBP profiling studies have employed similar strategies [137, 138, 144, 374]. Additionally, combinatorial approaches to determine RBP-RNA interactions such as Enhanced UV crosslinking and immunoprecipitation (eCLIP) [375], Orthogonal organic phase separation (OOPS) [376, 377], or Protein-cross-linked RNA eXtraction (XRNAX) [378] can be used to confirm the RNA-bounding proteome of EVs. Some of these are current ongoing efforts in our lab.

Our accumulated datasets of EV-enriched RNAs can also serve as a platform for investigating the transcript sequence requirements (i.e. CRMs) for RNA inclusion to EVs. For this, we can utilize combined approaches where we consider known EV-enriched sequence motifs [131], while also performing *de novo* CRM discovery [379-381]. This would allow us to identify whether EV-enriched RNAs contain specific sequences that correlate strongly with their enrichment in EVs. These approaches has been recently utilized to identify sequences in microRNAs that dictated their release in EVs or retention in cells [132]. To this end, various bioinformatics tools have been developed for RNA motif mapping [381] and are routinely used by our lab.

5.3. Conclusion

The research presented in this thesis aims to provide novel insights into in the field of EV biology, both in terms of their cargo sorting mechanisms as well as characterisation of their cargos. In **Chapter II**, we provide evidence for the unique contributions of NSM and ASM sphingolipid metabolic pathways on the repertoire of RNAs and proteins trafficked by EVs. We show that each metabolic pathway interacts with specific subcellular compartments, and that their inhibition impacts the types of cargoes that they can carry. Moreover, these changes can have implications to the communicatory potential of EVs, suggesting that subpopulations of EVs harbor distinctive features that can dictate their phenotypic effects on recipient cells. In **Chapter III**, we explored the integrity of RNAs within EV populations, identifying the availability of full-length transcripts. Crucially, this shows that EVs can contain a variety of full-length RNAs, including mRNAs and lncRNAs. Furthermore, we determined that these RNAs can exist in various transcript isoforms that were reflective-of, but sometimes different in ratio to their cells of origin. These results further highlight that cells can selectively recruit transcripts during EV biogenesis.

Overarchingly, these studies highlight the selective recruitment mechanisms used by cells for the export of gene products to the extracellular space via EVs. Understanding the biogenesis pathways and cargo features of EVs is of crucial relevance to multiple fields of research, from understanding their roles during intercellular communication to their potential use as diagnostic tools and therapeutic vehicles. By characterizing the roles of sphingomyelinase-dependent EV biogenesis pathways, as well as investigating the full-length transcriptome of EVs, we provide crucial findings that deepen our

understanding of EV biology. These results offer new avenues for innovation in the development of approaches to profile and manipulation EV cargoes, an important and ongoing effort in the field.

Master Reference List

1. Fafián-Labora, J.A. and A. O'Loghlen, *Classical and Nonclassical Intercellular Communication in Senescence and Ageing.* Trends in Cell Biology, 2020. **30**(8): p. 628-639.

2. Berumen Sánchez, G., et al., *Extracellular vesicles: mediators of intercellular communication in tissue injury and disease.* Cell Communication and Signaling, 2021. **19**(1): p. 104.

3. Yamasaki, H., et al., *Intercellular communication and carcinogenesis.* Mutat Res, 1995. **333**(1-2): p. 181-8.

4. Pitt, J.M., G. Kroemer, and L. Zitvogel, *Extracellular vesicles: masters of intercellular communication and potential clinical interventions.* J Clin Invest, 2016. **126**(4): p. 1139-43.

5. Andaloussi, S.E., et al., *Extracellular vesicles: biology and emerging therapeutic opportunities.* Nat Rev Drug Discov, 2013. **12**(5): p. 347-57.

6. Raposo, G. and W. Stoorvogel, *Extracellular vesicles: exosomes, microvesicles, and friends.* J Cell Biol, 2013. **200**(4): p. 373-83.

7. Kalluri, R. and V.S. LeBleu, *The biology, function, and biomedical applications of exosomes.* Science, 2020. **367**(6478): p. eaau6977.

8. Li, C.J., et al., *Novel proteolytic microvesicles released from human macrophages after exposure to tobacco smoke.* Am J Pathol, 2013. **182**(5): p. 1552-62.

9. Moon, H.G., et al., *Lung epithelial cell-derived extracellular vesicles activate macrophage-mediated inflammatory responses via ROCK1 pathway.* Cell Death Dis, 2015. **6**(12): p. e2016.

10. Karpman, D., A.L. Ståhl, and I. Arvidsson, *Extracellular vesicles in renal disease.* Nat Rev Nephrol, 2017. **13**(9): p. 545-562.

11. Haderk, F., et al., *Tumor-derived exosomes modulate PD-L1 expression in monocytes.* Sci Immunol, 2017. **2**(13).

12. Park, J.E., et al., *Hypoxia-induced tumor exosomes promote M2-like macrophage polarization of infiltrating myeloid cells and microRNA-mediated metabolic shift.* Oncogene, 2019. **38**(26): p. 5158-5173.

13. Genschmer, K.R., et al., *Activated PMN Exosomes: Pathogenic Entities Causing Matrix Destruction and Disease in the Lung.* Cell, 2019. **176**(1-2): p. 113-126.e15.

14. Abramowicz, A., et al., *MicroRNA Profile of Exosomes and Parental Cells is Differently Affected by Ionizing Radiation.* Radiat Res, 2020. **194**(2): p. 133-142.

15. van Niel, G., G. D'Angelo, and G. Raposo, *Shedding light on the cell biology of extracellular vesicles.* Nat Rev Mol Cell Biol, 2018. **19**(4): p. 213-228.

16. Johnstone, R.M., et al., *Vesicle formation during reticulocyte maturation. Association of plasma membrane activities with released vesicles (exosomes).* J Biol Chem, 1987. **262**(19): p. 9412-20.

17. Johnstone, R.M., et al., *Exosome formation during maturation of mammalian and avian reticulocytes: Evidence that exosome release is a major route for externalization of obsolete membrane proteins.* Journal of Cellular Physiology, 1991. **147**(1): p. 27-36.

18. Lo Cicero, A., P.D. Stahl, and G. Raposo, *Extracellular vesicles shuffling intercellular messages: for good or for bad.* Current Opinion in Cell Biology, 2015. **35**: p. 69-77.

19. Yoon, Y.J., O.Y. Kim, and Y.S. Gho, *Extracellular vesicles as emerging intercellular communicasomes.* BMB Rep, 2014. **47**(10): p. 531-9.

20. Robbins, P.D. and A.E. Morelli, *Regulation of immune responses by extracellular vesicles.* Nature Reviews Immunology, 2014. **14**(3): p. 195-208.

21. Yáñez-Mó, M., et al., *Biological properties of extracellular vesicles and their physiological functions.* Journal of Extracellular Vesicles, 2015. **4**(1): p. 27066.

22. Lee, T.H., et al., *Microvesicles as mediators of intercellular communication in cancer—the emerging science of cellular 'debris'.* Seminars in Immunopathology, 2011. **33**(5): p. 455-467.

23. Le, M.T.N., et al., *miR-200–containing extracellular vesicles promote breast cancer cell metastasis.* The Journal of Clinical Investigation, 2014. **124**(12): p. 5109-5128.

24. Kim, C.W., et al., *Extracellular Membrane Vesicles from Tumor Cells Promote Angiogenesis via Sphingomyelin.* Cancer Research, 2002. **62**(21): p. 6312-6317.

25. Vader, P., X.O. Breakefield, and M.J.A. Wood, *Extracellular vesicles: emerging targets for cancer therapy.* Trends in Molecular Medicine, 2014. **20**(7): p. 385-393.

26. Muralidharan-Chari, V., et al., *Microvesicles: mediators of extracellular communication during cancer progression.* Journal of Cell Science, 2010. **123**(10): p. 1603-1611.

27. Nawaz, M., et al., *The emerging role of extracellular vesicles as biomarkers for urogenital cancers.* Nature Reviews Urology, 2014. **11**(12): p. 688-701.

28. Hargett, L.A. and N.N. Bauer, *On the origin of microparticles: From "platelet dust" to mediators of intercellular communication.* Pulm Circ, 2013. **3**(2): p. 329-40.

29. Couch, Y., et al., *A brief history of nearly EV-erything – The rise and rise of extracellular vesicles.* Journal of Extracellular Vesicles, 2021. **10**(14): p. e12144.

30. Chargaff, E., *CELL STRUCTURE AND THE PROBLEM OF BLOOD COAGULATION.* Journal of Biological Chemistry, 1945. **160**(1): p. 351-359.

31. Chargaff, E. and R. West, *The biological significance of the thromboplastic protein of blood.* J Biol Chem, 1946. **166**(1): p. 189-97.

32. Wolf, P., *The Nature and Significance of Platelet Products in Human Plasma.* British Journal of Haematology, 1967. **13**(3): p. 269-288.

33. Crawford, N., *The Presence of Contractile Proteins in Platelet Microparticles Isolated from Human and Animal Platelet‐free Plasma.* British Journal of Haematology, 1971. **21**.

34. Sun, C.N., *Lattice structures and osmiophilic bodies in the developing respiratory tissue of rats.* Journal of Ultrastructure Research, 1966. **15**(3): p. 380-388.

35. Anderson, H.C., *Vesicles associated with calcification in the matrix of epiphyseal cartilage.* The Journal of cell biology, 1969. **41**(1): p. 59-72.

36. Bonucci, E., *Fine structure of early cartilage calcification.* J Ultrastruct Res, 1967. **20**(1): p. 33-50.

37. Nunez, E.A., J. Wallis, and M.D. Gershon, *Secretory processes in follicular cells of the bat thyroid. 3. The occurrence of extracellular vesicles and colloid droplets during arousal from hibernation.* Am J Anat, 1974. **141**(2): p. 179-201.

38. Dalton, A.J., *Microvesicles and Vesicles of Multivesicular Bodies Versus "Virus-Like" Particles.* JNCI: Journal of the National Cancer Institute, 1975. **54**(5): p. 1137-1148.

39. Harding, C., J. Heuser, and P. Stahl, *Receptor-mediated endocytosis of transferrin and recycling of the transferrin receptor in rat reticulocytes.* Journal of Cell Biology, 1983. **97**(2): p. 329-339.

40. Pan, B.-T. and R.M. Johnstone, *Fate of the transferrin receptor during maturation of sheep reticulocytes in vitro: Selective externalization of the receptor.* Cell, 1983. **33**(3): p. 967-978.

41. Harding, C.V., J.E. Heuser, and P.D. Stahl, *Exosomes: Looking back three decades and into the future.* Journal of Cell Biology, 2013. **200**(4): p. 367-371.

42. Gawrisch, K., et al., *The rate of lateral diffusion of phospholipids in erythrocyte microvesicles.* Biochim Biophys Acta, 1986. **856**(3): p. 443-7.

43. Vidal, M., et al., *Asymmetric distribution of phospholipids in the membrane of vesicles released during in vitro maturation of guinea pig reticulocytes: evidence precluding a role for "aminophospholipid translocase".* J Cell Physiol, 1989. **140**(3): p. 455-62.

44. Vidal, M.J. and P.D. Stahl, *The small GTP-binding proteins Rab4 and ARF are associated with released exosomes during reticulocyte maturation.* Eur J Cell Biol, 1993. **60**(2): p. 261-7.

45. Escola, J.M., et al., *Selective enrichment of tetraspan proteins on the internal vesicles of multivesicular endosomes and on exosomes secreted by human B-lymphocytes.* J Biol Chem, 1998. **273**(32): p. 20121-7.

46. Johnstone, R.M., A. Bianchini, and K. Teng, *Reticulocyte maturation and exosome release: transferrin receptor containing exosomes shows multiple plasma membrane functions.* Blood, 1989. **74**(5): p. 1844-51.

47. Fourcade, O., et al., *Secretory phospholipase A2 generates the novel lipid mediator lysophosphatidic acid in membrane microvesicles shed from activated cells.* Cell, 1995. **80**(6): p. 919-27.

48. Lee, Y.J., et al., *Elevated platelet microparticles in transient ischemic attacks, lacunar infarcts, and multiinfarct dementias.* Thromb Res, 1993. **72**(4): p. 295-304.

49. Singh, N., et al., *Elevated platelet-derived microparticle levels during unstable angina.* Can J Cardiol, 1995. **11**(11): p. 1015-21.

50. Powell, J.J., R.S. Harvey, and R.P. Thompson, *Microparticles in Crohn's disease--has the dust settled?* Gut, 1996. **39**(2): p. 340-1.

51. Raposo, G., et al., *B lymphocytes secrete antigen-presenting vesicles.* J Exp Med, 1996. **183**(3): p. 1161-72.

52. Zitvogel, L., et al., *Eradication of established murine tumors using a novel cell-free vaccine: dendritic cell-derived exosomes.* Nat Med, 1998. **4**(5): p. 594-600.

53. Théry, C., et al., *Proteomic analysis of dendritic cell-derived exosomes: a secreted subcellular compartment distinct from apoptotic vesicles.* J Immunol, 2001. **166**(12): p. 7309-18.

54. Bard, M.P., et al., *Proteomic analysis of exosomes isolated from human malignant pleural effusions.* Am J Respir Cell Mol Biol, 2004. **31**(1): p. 114-21.

55. Wubbolts, R., et al., *Proteomic and biochemical analyses of human B cell-derived exosomes. Potential implications for their function and multivesicular body formation.* J Biol Chem, 2003. **278**(13): p. 10963-72.

56. Subra, C., et al., *Exosome lipidomics unravels lipid sorting at the level of multivesicular bodies.* Biochimie, 2007. **89**(2): p. 205-12.

57. Skokos, D., et al., *Mast cell-derived exosomes induce phenotypic and functional maturation of dendritic cells and elicit specific immune responses in vivo.* J Immunol, 2003. **170**(6): p. 3037-45.

58. Van Niel, G., et al., *Intestinal epithelial exosomes carry MHC class II/peptides able to inform the immune system in mice.* Gut, 2003. **52**(12): p. 1690-7.

59. Ratajczak, J., et al., *Embryonic stem cell-derived microvesicles reprogram hematopoietic progenitors: evidence for horizontal transfer of mRNA and protein delivery.* Leukemia, 2006. **20**(5): p. 847-56.

60. Valadi, H., et al., *Exosome-mediated transfer of mRNAs and microRNAs is a novel mechanism of genetic exchange between cells.* Nature Cell Biology, 2007. **9**(6): p. 654-659.

61. Skog, J., et al., *Glioblastoma microvesicles transport RNA and proteins that promote tumour growth and provide diagnostic biomarkers.* Nat Cell Biol, 2008. **10**(12): p. 1470-6.

62. Al-Nedawi, K., et al., *Intercellular transfer of the oncogenic receptor EGFRvIII by microvesicles derived from tumour cells.* Nat Cell Biol, 2008. **10**(5): p. 619-24.

63. Karnati, H.K., et al., *Neuronal Enriched Extracellular Vesicle Proteins as Biomarkers for Traumatic Brain Injury.* J Neurotrauma, 2019. **36**(7): p. 975-987.

64. Lee, S., S. Mankhong, and J.H. Kang, *Extracellular Vesicle as a Source of Alzheimer's Biomarkers: Opportunities and Challenges.* Int J Mol Sci, 2019. **20**(7).

65. Schou, A.S., et al., *Extracellular vesicle-associated proteins as potential biomarkers.* Adv Clin Chem, 2020. **99**: p. 1-48.

66. Thietart, S. and P.E. Rautou, *Extracellular vesicles as biomarkers in liver diseases: A clinician's point of view.* J Hepatol, 2020. **73**(6): p. 1507-1525.

67. Urabe, F., et al., *Extracellular vesicles as biomarkers and therapeutic targets for cancer.* Am J Physiol Cell Physiol, 2020. **318**(1): p. C29-c39.

68. Useckaite, Z., et al., *Role of Extracellular Vesicle-Derived Biomarkers in Drug Metabolism and Disposition.* Drug Metab Dispos, 2021. **49**(11): p. 961-971.

69. van der Pol, E., et al., *Classification, functions, and clinical relevance of extracellular vesicles.* Pharmacol Rev, 2012. **64**(3): p. 676-705.

70. Gurunathan, S., et al., *Biogenesis, Membrane Trafficking, Functions, and Next Generation Nanotherapeutics Medicine of Extracellular Vesicles.* Int J Nanomedicine, 2021. **16**: p. 3357-3383.

71. Tkach, M. and C. Théry, *Communication by Extracellular Vesicles: Where We Are and Where We Need to Go.* Cell, 2016. **164**(6): p. 1226-1232.

72. Willms, E., et al., *Cells release subpopulations of exosomes with distinct molecular and biological properties.* Sci Rep, 2016. **6**: p. 22519.

73. Zhang, H., et al., *Identification of distinct nanoparticles and subsets of extracellular vesicles by asymmetric flow field-flow fractionation.* Nat Cell Biol, 2018. **20**(3): p. 332-343.

74. Gould, S.J. and G. Raposo, *As we wait: coping with an imperfect nomenclature for extracellular vesicles.* J Extracell Vesicles, 2013. **2**.

75. Kowal, J., et al., *Proteomic comparison defines novel markers to characterize heterogeneous populations of extracellular vesicle subtypes.* Proc Natl Acad Sci U S A, 2016. **113**(8): p. E968-77.

76. Kugeratski, F.G., et al., *Quantitative proteomics identifies the core proteome of exosomes with syntenin-1 as the highest abundant protein and a putative universal biomarker.* Nature Cell Biology, 2021. **23**(6): p. 631-641.

77. Jeppesen, D.K., et al., *Reassessment of Exosome Composition.* Cell, 2019. **177**(2): p. 428-445.e18.

78. Henne, W.M., N.J. Buchkovich, and S.D. Emr, *The ESCRT pathway.* Dev Cell, 2011. **21**(1): p. 77-91.

79. Henne, W.M., H. Stenmark, and S.D. Emr, *Molecular mechanisms of the membrane sculpting ESCRT pathway.* Cold Spring Harb Perspect Biol, 2013. **5**(9).

80. Raiborg, C. and H. Stenmark, *The ESCRT machinery in endosomal sorting of ubiquitylated membrane proteins.* Nature, 2009. **458**(7237): p. 445-52.

81. Baietti, M.F., et al., *Syndecan-syntenin-ALIX regulates the biogenesis of exosomes.* Nat Cell Biol, 2012. **14**(7): p. 677-85.

82. Trajkovic, K., et al., *Ceramide Triggers Budding of Exosome Vesicles into Multivesicular Endosomes.* Science, 2008. **319**(5867): p. 1244-1247.

83. Goñi, F.M. and A. Alonso, *Effects of ceramide and other simple sphingolipids on membrane lateral structure.* Biochim Biophys Acta, 2009. **1788**(1): p. 169-77.

84. Kajimoto, T., et al., *Ongoing activation of sphingosine 1-phosphate receptors mediates maturation of exosomal multivesicular endosomes.* Nat Commun, 2013. **4**: p. 2712.

85. Charrin, S., et al., *Tetraspanins at a glance.* J Cell Sci, 2014. **127**(Pt 17): p. 3641-8.

86. Theos, A.C., et al., *A lumenal domain-dependent pathway for sorting to intralumenal vesicles of multivesicular endosomes involved in organelle morphogenesis.* Dev Cell, 2006. **10**(3): p. 343-54.

87. Buschow, S.I., et al., *MHC II in dendritic cells is targeted to lysosomes or T cell-induced exosomes via distinct multivesicular body pathways.* Traffic, 2009. **10**(10): p. 1528-42.

88. Chairoungdua, A., et al., *Exosome release of β-catenin: a novel mechanism that antagonizes Wnt signaling.* J Cell Biol, 2010. **190**(6): p. 1079-91.

89. van Niel, G., et al., *The tetraspanin CD63 regulates ESCRT-independent and -dependent endosomal sorting during melanogenesis.* Dev Cell, 2011. **21**(4): p. 708-21.

90. van Niel, G., et al., *Apolipoprotein E Regulates Amyloid Formation within Endosomes of Pigment Cells.* Cell Rep, 2015. **13**(1): p. 43-51.

91. Gauthier, S.A., et al., *Enhanced exosome secretion in Down syndrome brain - a protective mechanism to alleviate neuronal endosomal abnormalities.* Acta Neuropathol Commun, 2017. **5**(1): p. 65.

92. Zhang, Y., et al., *Exosomes: biogenesis, biologic function and clinical potential.* Cell Biosci, 2019. **9**: p. 19.

93. Tricarico, C., J. Clancy, and C. D'Souza-Schorey, *Biology and biogenesis of shed microvesicles.* Small GTPases, 2017. **8**(4): p. 220-232.

94. Lefebvre, F.A., et al., *Comparative transcriptomic analysis of human and Drosophila extracellular vesicles.* Sci Rep, 2016. **6**: p. 27680.

95. Minciacchi, V.R., M.R. Freeman, and D. Di Vizio, *Extracellular vesicles in cancer: exosomes, microvesicles and the emerging role of large oncosomes.* Semin Cell Dev Biol, 2015. **40**: p. 41-51.

96. Piccin, A., W.G. Murphy, and O.P. Smith, *Circulating microparticles: pathophysiology and clinical implications.* Blood Rev, 2007. **21**(3): p. 157-71.

97. Zwaal, R.F.A., P. Comfurius, and E.M. Bevers, *Scott syndrome, a bleeding disorder caused by defective scrambling of membrane phospholipids.* Biochimica et Biophysica Acta (BBA) - Molecular and Cell Biology of Lipids, 2004. **1636**(2): p. 119-128.

98. Li, B., et al., *RhoA triggers a specific signaling pathway that generates transforming microvesicles in cancer cells.* Oncogene, 2012. **31**(45): p. 4740-4749.

99. Muralidharan-Chari, V., et al., *ARF6-regulated shedding of tumor cell-derived plasma membrane microvesicles.* Curr Biol, 2009. **19**(22): p. 1875-85.

100. Dawson, G. and J. Qin, *Gilenya (FTY720) inhibits acid sphingomyelinase by a mechanism similar to tricyclic antidepressants.* Biochem Biophys Res Commun, 2011. **404**(1): p. 321-3.

101. Truman, J.P., et al., *Acid sphingomyelinase in macrophage biology.* Cell Mol Life Sci, 2011. **68**(20): p. 3293-305.

102. Bianco, F., et al., *Acid sphingomyelinase activity triggers microparticle release from glial cells.* The EMBO Journal, 2009. **28**(8): p. 1043-1054.

103. Denlinger, L.C., et al., *Cutting edge: the nucleotide receptor P2X7 contains multiple protein- and lipid-interaction motifs including a potential binding site for bacterial lipopolysaccharide.* J Immunol, 2001. **167**(4): p. 1871-6.

104. Wang, J., U.R. Pendurthi, and L.V.M. Rao, *Sphingomyelin encrypts tissue factor: ATP-induced activation of A-SMase leads to tissue factor decryption and microvesicle shedding.* Blood Adv, 2017. **1**(13): p. 849-862.

105. Verderio, C., M. Gabrielli, and P. Giussani, *Role of sphingolipids in the biogenesis and biological activity of extracellular vesicles.* J Lipid Res, 2018. **59**(8): p. 1325-1340.

106. Kalra, H., G.P. Drummen, and S. Mathivanan, *Focus on Extracellular Vesicles: Introducing the Next Small Big Thing.* Int J Mol Sci, 2016. **17**(2): p. 170.

107. Katzmann, D.J., M. Babst, and S.D. Emr, *Ubiquitin-dependent sorting into the multivesicular body pathway requires the function of a conserved endosomal protein sorting complex, ESCRT-I.* Cell, 2001. **106**(2): p. 145-55.

108. Janas, T., et al., *Mechanisms of RNA loading into exosomes.* FEBS Lett, 2015. **589**(13): p. 1391-8.

109. Abels, E.R. and X.O. Breakefield, *Introduction to Extracellular Vesicles: Biogenesis, RNA Cargo Selection, Content, Release, and Uptake.* Cellular and Molecular Neurobiology, 2016. **36**(3): p. 301-312.

110. Gibbings, D.J., et al., *Multivesicular bodies associate with components of miRNA effector complexes and modulate miRNA activity.* Nat Cell Biol, 2009. **11**(9): p. 1143-9.

111. Carnino, J.M., K. Ni, and Y. Jin, *Post-translational Modification Regulates Formation and Cargo-Loading of Extracellular Vesicles.* Front Immunol, 2020. **11**: p. 948.

112. Kim, B.Y., et al., *Spongiform neurodegeneration-associated E3 ligase Mahogunin ubiquitylates TSG101 and regulates endosomal trafficking.* Mol Biol Cell, 2007. **18**(4): p. 1129-42.

113. Liu, Y., et al., *COP9-associated CSN5 regulates exosomal protein deubiquitination and sorting.* Am J Pathol, 2009. **174**(4): p. 1415-25.

114. Smith, V.L., L. Jackson, and J.S. Schorey, *Ubiquitination as a Mechanism To Transport Soluble Mycobacterial and Eukaryotic Proteins to Exosomes.* J Immunol, 2015. **195**(6): p. 2722-30.

115. Villarroya-Beltri, C., et al., *Sorting it out: regulation of exosome loading.* Semin Cancer Biol, 2014. **28**: p. 3-13.

116. Kunadt, M., et al., *Extracellular vesicle sorting of α-Synuclein is regulated by sumoylation.* Acta Neuropathol, 2015. **129**(5): p. 695-713.

117. Oh, J.G., et al., *miR-146a Suppresses SUMO1 Expression and Induces Cardiac Dysfunction in Maladaptive Hypertrophy.* Circ Res, 2018. **123**(6): p. 673-685.

118. Pamenter, M.E., et al., *Post-Translational Deimination of Immunological and Metabolic Protein Markers in Plasma and Extracellular Vesicles of Naked Mole-Rat (Heterocephalus glaber).* Int J Mol Sci, 2019. **20**(21).

119. Zhang, Y., X. Wu, and W. Andy Tao, *Characterization and Applications of Extracellular Vesicle Proteome with Post-Translational Modifications.* Trends Analyt Chem, 2018. **107**: p. 21-30.

120. Gonzales, P.A., et al., *Large-scale proteomics and phosphoproteomics of urinary exosomes.* J Am Soc Nephrol, 2009. **20**(2): p. 363-79.

121. Leidal, A.M., et al., *The LC3-conjugation machinery specifies the loading of RNA-binding proteins into extracellular vesicles.* Nature Cell Biology, 2020. **22**(2): p. 187-199.

122. Crescitelli, R., et al., *Distinct RNA profiles in subpopulations of extracellular vesicles: apoptotic bodies, microvesicles and exosomes.* J Extracell Vesicles, 2013. **2**.

123. Baglio, S.R., et al., *Human bone marrow- and adipose-mesenchymal stem cells secrete exosomes enriched in distinctive miRNA and tRNA species.* Stem Cell Res Ther, 2015. **6**(1): p. 127.

124. Schulz-Siegmund, M. and A. Aigner, *Nucleic acid delivery with extracellular vesicles.* Adv Drug Deliv Rev, 2021. **173**: p. 89-111.

125. van der Meel, R., et al., *Extracellular vesicles as drug delivery systems: Lessons from the liposome field.* Journal of Controlled Release, 2014. **195**: p. 72-85.

126. Tetta, C., et al., *Extracellular vesicles as an emerging mechanism of cell-to-cell communication.* Endocrine, 2013. **44**(1): p. 11-19.

127. Bovaird, S., et al., *Biological functions, regulatory mechanisms, and disease relevance of RNA localization pathways.* FEBS Lett, 2018. **592**(17): p. 2948-2972.

128. Chin, A. and E. Lecuyer, *RNA localization: Making its way to the center stage.* Biochim Biophys Acta, 2017. **1861**(11 Pt B): p. 2956-2970.

129. Lecuyer, E., H. Yoshida, and H.M. Krause, *Global implications of mRNA localization pathways in cellular organization.* Curr Opin Cell Biol, 2009. **21**(3): p. 409-15.

130. Bergalet, J. and E. Lecuyer, *The functions and regulatory principles of mRNA intracellular trafficking.* Adv Exp Med Biol, 2014. **825**: p. 57-96.

131. Fabbiano, F., et al., *RNA packaging into extracellular vesicles: An orchestra of RNA-binding proteins?* Journal of Extracellular Vesicles, 2020. **10**(2): p. e12043.

132. Garcia-Martin, R., et al., *MicroRNA sequence codes for small extracellular vesicle release and cellular retention.* Nature, 2022. **601**(7893): p. 446-451.

133. Villarroya-Beltri, C., et al., *Sumoylated hnRNPA2B1 controls the sorting of miRNAs into exosomes through binding to specific motifs.* Nat Commun, 2013. **4**: p. 2980.

134. Geuens, T., D. Bouhy, and V. Timmerman, *The hnRNP family: insights into their role in health and disease.* Hum Genet, 2016. **135**(8): p. 851-67.

135. Vilella, F., et al., *Hsa-miR-30d, secreted by the human endometrium, is taken up by the pre-implantation embryo and might modify its transcriptome.* Development, 2015. **142**(18): p. 3210-21.

136. Gao, T., et al., *Exosomal lncRNA 91H is associated with poor development in colorectal cancer by modifying HNRNPK expression.* Cancer Cell Int, 2018. **18**: p. 11.

137. Statello, L., et al., *Identification of RNA-binding proteins in exosomes capable of interacting with different types of RNA: RBP-facilitated transport of RNAs into exosomes.* PLoS One, 2018. **13**(4): p. e0195969.

138. Santangelo, L., et al., *The RNA-Binding Protein SYNCRIP Is a Component of the Hepatocyte Exosomal Machinery Controlling MicroRNA Sorting.* Cell Rep, 2016. **17**(3): p. 799-808.

139. Shurtleff, M.J., et al., *Y-box protein 1 is required to sort microRNAs into exosomes in cells and in a cell-free reaction.* Elife, 2016. **5**.

140. Shurtleff, M.J., et al., *Broad role for YBX1 in defining the small noncoding RNA composition of exosomes.* Proc Natl Acad Sci U S A, 2017. **114**(43): p. E8987-e8995.

141. Yanshina, D.D., et al., *Structural features of the interaction of the 3'-untranslated region of mRNA containing exosomal RNA-specific motifs with YB-1, a potential mediator of mRNA sorting.* Biochimie, 2018. **144**: p. 134-143.

142. Mukherjee, K., et al., *Reversible HuR-microRNA binding controls extracellular export of miR-122 and augments stress response.* EMBO Rep, 2016. **17**(8): p. 1184-203.

143. Shi, R., et al., *Expression profile, clinical significance, and biological function of insulin-like growth factor 2 messenger RNA-binding proteins in non-small cell lung cancer.* Tumour Biol, 2017. **39**(4): p. 1010428317695928.

144. Ghoshal, A., et al., *Extracellular vesicle-dependent effect of RNA-binding protein IGF2BP1 on melanoma metastasis.* Oncogene, 2019. **38**(21): p. 4182-4196.

145. Monastyrskaya, K., *Functional Association between Regulatory RNAs and the Annexins.* Int J Mol Sci, 2018. **19**(2).

146. Hagiwara, K., et al., *Commitment of Annexin A2 in recruitment of microRNAs into extracellular vesicles.* FEBS Lett, 2015. **589**(24 Pt B): p. 4071-8.

147. Park, K., *The role of major vault protein (MVP) in drug resistance.* J Control Release, 2012. **163**(2): p. 266.

148. Frascotti, G., et al., *The Vault Nanoparticle: A Gigantic Ribonucleoprotein Assembly Involved in Diverse Physiological and Pathological Phenomena and an Ideal Nanovector for Drug Delivery and Therapy.* Cancers (Basel), 2021. **13**(4).

149. Scheffer, G.L., et al., *Lung resistance-related protein/major vault protein and vaults in multidrug-resistant cancer.* Curr Opin Oncol, 2000. **12**(6): p. 550-6.

150. Berger, W., et al., *Vaults and the major vault protein: novel roles in signal pathway regulation and immunity.* Cell Mol Life Sci, 2009. **66**(1): p. 43-61.

151. O'Brien, K., et al., *RNA delivery by extracellular vesicles in mammalian cells and its applications.* Nat Rev Mol Cell Biol, 2020. **21**(10): p. 585-606.

152. Benner, S.A., *Extracellular 'communicator RNA'.* FEBS Letters, 1988. **233**(2): p. 225-228.

153. Quesenberry, P.J., et al., *Role of extracellular RNA-carrying vesicles in cell differentiation and reprogramming.* Stem Cell Research & Therapy, 2015. **6**(1): p. 153.

154. Dinger, M.E., T.R. Mercer, and J.S. Mattick, *RNAs as extracellular signaling molecules.* J Mol Endocrinol, 2008. **40**(4): p. 151-9.

155. Li, Y., et al., *Extracellular Vesicles Long RNA Sequencing Reveals Abundant mRNA, circRNA, and lncRNA in Human Blood as Potential Biomarkers for Cancer Diagnosis.* Clin Chem, 2019. **65**(6): p. 798-808.

156. Mori, M.A., et al., *Extracellular miRNAs: From Biomarkers to Mediators of Physiology and Disease.* Cell Metab, 2019. **30**(4): p. 656-673.

157. Srinivasan, S., et al., *Discovery and Verification of Extracellular miRNA Biomarkers for Non-invasive Prediction of Pre-eclampsia in Asymptomatic Women.* Cell Rep Med, 2020. **1**(2).

158. Shan, S., et al., *Extracellular vesicle-derived long non-coding RNA as circulating biomarkers for endometriosis.* Reprod Biomed Online, 2022. **44**(5): p. 923-933.

159. Puffer, R.C., et al., *Plasma extracellular vesicles as a source of biomarkers in traumatic brain injury.* J Neurosurg, 2020. **134**(6): p. 1921-1928.

160. Huang, M., et al., *Non-coding RNA derived from extracellular vesicles in cancer immune escape: Biological functions and potential clinical applications.* Cancer Lett, 2021. **501**: p. 234-246.

161. Maacha, S., et al., *Extracellular vesicles-mediated intercellular communication: roles in the tumor microenvironment and anti-cancer drug resistance.* Molecular Cancer, 2019. **18**(1): p. 55.

162. Kok, V.C. and C.C. Yu, *Cancer-Derived Exosomes: Their Role in Cancer Biology and Biomarker Development.* Int J Nanomedicine, 2020. **15**: p. 8019-8036.

163. Hu, W., et al., *Comprehensive landscape of extracellular vesicle-derived RNAs in cancer initiation, progression, metastasis and cancer immunology.* Mol Cancer, 2020. **19**(1): p. 102.

164. Dai, J., et al., *Exosomes: key players in cancer and potential therapeutic strategy.* Signal Transduct Target Ther, 2020. **5**(1): p. 145.

165. Mohankumar, S. and T. Patel, *Extracellular vesicle long noncoding RNA as potential biomarkers of liver cancer.* Brief Funct Genomics, 2016. **15**(3): p. 249-56.

166. Joyce, D.P., M.J. Kerin, and R.M. Dwyer, *Exosome-encapsulated microRNAs as circulating biomarkers for breast cancer.* Int J Cancer, 2016. **139**(7): p. 1443-8.

167. Fujita, K. and N. Nonomura, *Urinary biomarkers of prostate cancer.* Int J Urol, 2018. **25**(9): p. 770-779.

168. Jones, J., et al., *Circulating Biomarkers for Glioma: A Review.* Neurosurgery, 2021. **88**(3): p. E221-e230.

169. Zhang, H.M., et al., *miR-146b-5p within BCR-ABL1-Positive Microvesicles Promotes Leukemic Transformation of Hematopoietic Cells.* Cancer Res, 2016. **76**(10): p. 2901-11.

170. Chakrabortty, S.K., et al., *Extracellular vesicle-mediated transfer of processed and functional RNY5 RNA.* RNA, 2015. **21**(11): p. 1966-1979.

171. Tominaga, N., et al., *Brain metastatic cancer cells release microRNA-181c-containing extracellular vesicles capable of destructing blood–brain barrier.* Nature Communications, 2015. **6**: p. 6716.

172. Kogure, T., et al., *Extracellular Vesicle-Mediated Transfer of a Novel Long Noncoding RNA TUC339: A Mechanism of Intercellular Signaling in Human Hepatocellular Cancer.* Genes Cancer, 2013. **4**(7-8): p. 261-72.

173. Au Yeung, C.L., et al., *Exosomal transfer of stroma-derived miR21 confers paclitaxel resistance in ovarian cancer cells through targeting APAF1.* Nat Commun, 2016. **7**: p. 11150.

174. van Es, M.A., et al., *Amyotrophic lateral sclerosis.* Lancet, 2017. **390**(10107): p. 2084-2098.

175. R, A.A., *Risk factors for Alzheimer's disease.* Folia Neuropathol, 2019. **57**(2): p. 87-105.

176. Singh, A., T.M. Dawson, and S. Kulkarni, *Neurodegenerative disorders and gut-brain interactions.* J Clin Invest, 2021. **131**(13).

177. Wang, X., et al., *The Role of Exosomal microRNAs and Oxidative Stress in Neurodegenerative Diseases.* Oxid Med Cell Longev, 2020. **2020**: p. 3232869.

178. Albers, D.S. and M.F. Beal, *Mitochondrial dysfunction and oxidative stress in aging and neurodegenerative disease.* J Neural Transm Suppl, 2000. **59**: p. 133-54.

179. Dias, V., E. Junn, and M.M. Mouradian, *The role of oxidative stress in Parkinson's disease.* J Parkinsons Dis, 2013. **3**(4): p. 461-91.

180. Hill, A.F., *Extracellular Vesicles and Neurodegenerative Diseases.* J Neurosci, 2019. **39**(47): p. 9269-9273.

181. Alvarez-Erviti, L., et al., *Delivery of siRNA to the mouse brain by systemic injection of targeted exosomes.* Nat Biotechnol, 2011. **29**(4): p. 341-5.

182. Shamsuzzama, et al., *Role of MicroRNA Let-7 in Modulating Multifactorial Aspect of Neurodegenerative Diseases: an Overview.* Mol Neurobiol, 2016. **53**(5): p. 2787-2793.

183. Leggio, L., et al., *microRNAs in Parkinson's Disease: From Pathogenesis to Novel Diagnostic and Therapeutic Approaches.* Int J Mol Sci, 2017. **18**(12).

184. Asikainen, S., et al., *Global microRNA expression profiling of Caenorhabditis elegans Parkinson's disease models.* J Mol Neurosci, 2010. **41**(1): p. 210-8.

185. Winkler, C.W., K.G. Taylor, and K.E. Peterson, *Location is everything: let-7b microRNA and TLR7 signaling results in a painful TRP.* Sci Signal, 2014. **7**(327): p. pe14.

186. Freischmidt, A., et al., *Serum microRNAs in patients with genetic amyotrophic lateral sclerosis and pre-manifest mutation carriers.* Brain, 2014. **137**(Pt 11): p. 2938-50.

187. de Andrade, H.M., et al., *MicroRNAs-424 and 206 are potential prognostic markers in spinal onset amyotrophic lateral sclerosis.* J Neurol Sci, 2016. **368**: p. 19-24.

188. Benigni, M., et al., *Identification of miRNAs as Potential Biomarkers in Cerebrospinal Fluid from Amyotrophic Lateral Sclerosis Patients.* Neuromolecular Med, 2016. **18**(4): p. 551-560.

189. Sheinerman, K.S., et al., *Circulating brain-enriched microRNAs as novel biomarkers for detection and differentiation of neurodegenerative diseases.* Alzheimers Res Ther, 2017. **9**(1): p. 89.

190. Katsu, M., et al., *MicroRNA expression profiles of neuron-derived extracellular vesicles in plasma from patients with amyotrophic lateral sclerosis.* Neurosci Lett, 2019. **708**: p. 134176.

191. Varcianna, A., et al., *Micro-RNAs secreted through astrocyte-derived extracellular vesicles cause neuronal network degeneration in C9orf72 ALS.* EBioMedicine, 2019. **40**: p. 626-635.

192. McKeever, P.M., et al., *MicroRNA Expression Levels Are Altered in the Cerebrospinal Fluid of Patients with Young-Onset Alzheimer's Disease.* Mol Neurobiol, 2018. **55**(12): p. 8826-8841.

193. Banzhaf-Strathmann, J., et al., *MicroRNA-125b induces tau hyperphosphorylation and cognitive deficits in Alzheimer's disease.* Embo j, 2014. **33**(15): p. 1667-80.

194. Ricci, C., C. Marzocchi, and S. Battistini, *MicroRNAs as Biomarkers in Amyotrophic Lateral Sclerosis.* Cells, 2018. **7**(11).

195. Joilin, G., et al., *An Overview of MicroRNAs as Biomarkers of ALS.* Front Neurol, 2019. **10**: p. 186.

196. Wiklander, O.P.B., et al., *Advances in therapeutic applications of extracellular vesicles.* Sci Transl Med, 2019. **11**(492).

197. Martin-Rufino, J.D., et al., *Targeting the Immune System With Mesenchymal Stromal Cell-Derived Extracellular Vesicles: What Is the Cargo's Mechanism of Action?* Front Bioeng Biotechnol, 2019. **7**: p. 308.

198. Kuo, W.P., et al., *Red Blood Cells: A Source of Extracellular Vesicles.* Methods Mol Biol, 2017. **1660**: p. 15-22.

199. Tkach, M., et al., *Qualitative differences in T-cell activation by dendritic cell-derived extracellular vesicle subtypes.* Embo j, 2017. **36**(20): p. 3012-3028.

200. Poon, I.K.H., C.D. Gregory, and M. Kaparakis-Liaskos, *Editorial: The Immunomodulatory Properties of Extracellular Vesicles From Pathogens, Immune Cells, and Non-immune Cells.* Front Immunol, 2018. **9**: p. 3024.

201. Ridder, K., et al., *Extracellular vesicle-mediated transfer of functional RNA in the tumor microenvironment.* Oncoimmunology, 2015. **4**(6): p. e1008371.

202. Kojima, R., et al., *Designer exosomes produced by implanted cells intracerebrally deliver therapeutic cargo for Parkinson's disease treatment.* Nat Commun, 2018. **9**(1): p. 1305.

203. Pomatto, M.A.C., et al., *Improved Loading of Plasma-Derived Extracellular Vesicles to Encapsulate Antitumor miRNAs.* Mol Ther Methods Clin Dev, 2019. **13**: p. 133-144.

204. Usman, W.M., et al., *Efficient RNA drug delivery using red blood cell extracellular vesicles.* Nat Commun, 2018. **9**(1): p. 2359.

205. Lamichhane, T.N., et al., *Oncogene Knockdown via Active Loading of Small RNAs into Extracellular Vesicles by Sonication.* Cell Mol Bioeng, 2016. **9**(3): p. 315-324.

206. Shtam, T.A., et al., *Exosomes are natural carriers of exogenous siRNA to human cells in vitro.* Cell Commun Signal, 2013. **11**: p. 88.

207. Haraszti, R.A., et al., *Optimized Cholesterol-siRNA Chemistry Improves Productive Loading onto Extracellular Vesicles.* Mol Ther, 2018. **26**(8): p. 1973-1982.

208. Savina, A., et al., *Exosome release is regulated by a calcium-dependent mechanism in K562 cells.* J Biol Chem, 2003. **278**(22): p. 20083-90.

209. Glebov, K., et al., *Serotonin stimulates secretion of exosomes from microglia cells.* Glia, 2015. **63**(4): p. 626-34.

210. Parolini, I., et al., *Microenvironmental pH Is a Key Factor for Exosome Traffic in Tumor Cells.* Journal of Biological Chemistry, 2009. **284**(49): p. 34211-34222.

211. King, H.W., M.Z. Michael, and J.M. Gleadle, *Hypoxic enhancement of exosome release by breast cancer cells.* BMC Cancer, 2012. **12**: p. 421.

212. Atienzar-Aroca, S., et al., *Oxidative stress in retinal pigment epithelium cells increases exosome secretion and promotes angiogenesis in endothelial cells.* J Cell Mol Med, 2016. **20**(8): p. 1457-66.

213. Wiklander, O.P., et al., *Extracellular vesicle in vivo biodistribution is determined by cell source, route of administration and targeting.* J Extracell Vesicles, 2015. **4**: p. 26316.

214. Lai, C.P., et al., *Dynamic biodistribution of extracellular vesicles in vivo using a multimodal imaging reporter.* ACS Nano, 2014. **8**(1): p. 483-494.

215. Gangadaran, P., et al., *A new bioluminescent reporter system to study the biodistribution of systematically injected tumor-derived bioluminescent extracellular vesicles in mice.* Oncotarget, 2017. **8**(66): p. 109894-109914.

216. Armstrong, J.P., M.N. Holme, and M.M. Stevens, *Re-Engineering Extracellular Vesicles as Smart Nanoscale Therapeutics.* ACS Nano, 2017. **11**(1): p. 69-83.

217. Chen, W., et al., *Nanoscale Characterization of Carrier Dynamic and Surface Passivation in InGaN/GaN Multiple Quantum Wells on GaN Nanorods.* ACS Appl Mater Interfaces, 2016. **8**(46): p. 31887-31893.

218. Tian, T., et al., *Visualizing of the cellular uptake and intracellular trafficking of exosomes by live-cell microscopy.* J Cell Biochem, 2010. **111**(2): p. 488-96.

219. Prada, I. and J. Meldolesi, *Binding and Fusion of Extracellular Vesicles to the Plasma Membrane of Their Cell Targets.* Int J Mol Sci, 2016. **17**(8).

220. Didiot, M.C., et al., *Exosome-mediated Delivery of Hydrophobically Modified siRNA for Huntingtin mRNA Silencing.* Mol Ther, 2016. **24**(10): p. 1836-1847.

221. Luo, Z.W., et al., *Aptamer-functionalized exosomes from bone marrow stromal cells target bone to promote bone regeneration.* Nanoscale, 2019. **11**(43): p. 20884-20892.

222. Trkov, S., et al., *Fingolimod--a sphingosine-like molecule inhibits vesicle mobility and secretion in astrocytes.* Glia, 2012. **60**(9): p. 1406-16.

223. Catalano, M. and L. O'Driscoll, *Inhibiting extracellular vesicles formation and release: a review of EV inhibitors.* Journal of Extracellular Vesicles, 2020. **9**(1): p. 1703244.

224. Choi, D.-S. and Y.S. Gho, *Isolation of Extracellular Vesicles for Proteomic Profiling*, in *Proteomic Profiling: Methods and Protocols*, A. Posch, Editor. 2015, Springer New York: New York, NY. p. 167-177.

225. Choi, M., et al., *MSstats: an R package for statistical analysis of quantitative mass spectrometry-based proteomic experiments.* Bioinformatics, 2014. **30**(17): p. 2524-6.

226. Gu, Z., R. Eils, and M. Schlesner, *Complex heatmaps reveal patterns and correlations in multidimensional genomic data.* Bioinformatics, 2016. **32**(18): p. 2847-9.

227. Ritchie, M.E., et al., *limma powers differential expression analyses for RNA-sequencing and microarray studies.* Nucleic Acids Res, 2015. **43**(7): p. e47.

228. Merico, D., et al., *Enrichment map: a network-based method for gene-set enrichment visualization and interpretation.* PLoS One, 2010. **5**(11): p. e13984.

229. Dobin, A., et al., *STAR: ultrafast universal RNA-seq aligner.* Bioinformatics, 2012. **29**(1): p. 15-21.

230. Liao, Y., G.K. Smyth, and W. Shi, *featureCounts: an efficient general purpose program for assigning sequence reads to genomic features.* Bioinformatics, 2013. **30**(7): p. 923-930.

231. Love, M.I., W. Huber, and S. Anders, *Moderated estimation of fold change and dispersion for RNA-seq data with DESeq2.* Genome Biology, 2014. **15**(12): p. 550.

232. Kucukural, A., et al., *DEBrowser: interactive differential expression analysis and visualization tool for count data.* BMC Genomics, 2019. **20**(1): p. 6.

233. Berriz, G.F., et al., *Characterizing gene sets with FuncAssociate.* Bioinformatics, 2003. **19**(18): p. 2502-2504.

234. Kotrbová, A., et al., *TEM ExosomeAnalyzer: a computer-assisted software tool for quantitative evaluation of extracellular vesicles in transmission electron microscopy images.* Journal of Extracellular Vesicles, 2019. **8**(1): p. 1560808.

235. Bindea, G., et al., *ClueGO: a Cytoscape plug-in to decipher functionally grouped gene ontology and pathway annotation networks.* Bioinformatics, 2009. **25**(8): p. 1091-3.

236. Shannon, P., et al., *Cytoscape: a software environment for integrated models of biomolecular interaction networks.* Genome Res, 2003. **13**(11): p. 2498-504.

237. Bonner, S.E. and E. Willms, *Intercellular communication through extracellular vesicles in cancer and evolutionary biology.* Progress in Biophysics and Molecular Biology, 2021. **165**: p. 80-87.

238. Lizarraga-Valderrama, L.R. and G.K. Sheridan, *Extracellular vesicles and intercellular communication in the central nervous system.* FEBS Letters, 2021. **595**(10): p. 1391-1410.

239. Colombo, M., G. Raposo, and C. Théry, *Biogenesis, Secretion, and Intercellular Interactions of Exosomes and Other Extracellular Vesicles.* Annual Review of Cell and Developmental Biology, 2014. **30**(1): p. 255-289.

240. Xiang, H., et al., *Physiological functions and therapeutic applications of neutral sphingomyelinase and acid sphingomyelinase.* Biomed Pharmacother, 2021. **139**: p. 111610.

241. Arenz, C., *Small molecule inhibitors of acid sphingomyelinase.* Cell Physiol Biochem, 2010. **26**(1): p. 1-8.

242. Lee, D.H., et al., *Identification and evaluation of neutral sphingomyelinase 2 inhibitors.* Arch Pharm Res, 2011. **34**(2): p. 229-36.

243. Kornhuber, J., et al., *Functional inhibitors of acid sphingomyelinase (FIASMAs).* Handb Exp Pharmacol, 2013(215): p. 169-86.

244. Šála, M., et al., *Novel Human Neutral Sphingomyelinase 2 Inhibitors as Potential Therapeutics for Alzheimer's Disease.* J Med Chem, 2020. **63**(11): p. 6028-6056.

245. Kumar, A. and S. Kumar, *Inhibition of extracellular vesicle pathway using neutral sphingomyelinase inhibitors as a neuroprotective treatment for brain injury.* Neural Regen Res, 2021. **16**(12): p. 2349-2352.

246. Carpinteiro, A., et al., *Inhibition of acid sphingomyelinase by ambroxol prevents SARS-CoV-2 entry into epithelial cells.* J Biol Chem, 2021. **296**: p. 100701.

247. MacBeath, G., *Chemical genomics: what will it take and who gets to play?* Genome Biol, 2001. **2**(6): p. Comment2005.

248. Amoruso, A., et al., *Effect of fingolimod action on the release of monocyte-derived microvesicles in multiple sclerosis patients.* J Neuroimmunol, 2018. **323**: p. 43-48.

249. Barman, B., et al., *VAP-A and its binding partner CERT drive biogenesis of RNA-containing extracellular vesicles at ER membrane contact sites.* Developmental Cell, 2022. **57**(8): p. 974-994.e8.

250. Colombo, M., et al., *Analysis of ESCRT functions in exosome biogenesis, composition and secretion highlights the heterogeneity of extracellular vesicles.* J Cell Sci, 2013. **126**(Pt 24): p. 5553-65.

251. Kholia, S., et al., *A novel role for peptidylarginine deiminases in microvesicle release reveals therapeutic potential of PAD inhibition in sensitizing prostate cancer cells to chemotherapy.* J Extracell Vesicles, 2015. **4**: p. 26192.

252. Kosgodage, U.S., et al., *Chloramidine/Bisindolylmaleimide-I-Mediated Inhibition of Exosome and Microvesicle Release and Enhanced Efficacy of Cancer Chemotherapy.* Int J Mol Sci, 2017. **18**(5).

253. Li, X.Q., et al., *Exosomes derived from gefitinib-treated EGFR-mutant lung cancer cells alter cisplatin sensitivity via up-regulating autophagy.* Oncotarget, 2016. **7**(17): p. 24585-95.

254. Matsumoto, A., et al., *Accelerated growth of B16BL6 tumor in mice through efficient uptake of their own exosomes by B16BL6 cells.* Cancer Sci, 2017. **108**(9): p. 1803-1810.

255. Sáenz-Cuesta, M., et al., *The First Dose of Fingolimod Affects Circulating Extracellular Vesicles in Multiple Sclerosis Patients.* Int J Mol Sci, 2018. **19**(8).

256. Zhou, X., et al., *Exosome production and its regulation of EGFR during wound healing in renal tubular cells.* Am J Physiol Renal Physiol, 2017. **312**(6): p. F963-f970.

257. Huwiler, A. and U. Zangemeister-Wittke, *The sphingosine 1-phosphate receptor modulator fingolimod as a therapeutic agent: Recent findings and new perspectives.* Pharmacol Ther, 2018. **185**: p. 34-49.

258. Zaffaroni, M., *Fingolimod in pediatric-onset multiple sclerosis.* Neurol Sci, 2021. **42**(Suppl 1): p. 1-4.

259. Chun, J., et al., *Fingolimod: Lessons Learned and New Opportunities for Treating Multiple Sclerosis and Other Disorders.* Annu Rev Pharmacol Toxicol, 2019. **59**: p. 149-170.

260. Liu, X., et al., *Inhibition of P2X7 receptors improves outcomes after traumatic brain injury in rats.* Purinergic Signalling, 2017. **13**(4): p. 529-544.

261. Zinger, A., et al., *Plasma levels of endothelial and B-cell-derived microparticles are restored by fingolimod treatment in multiple sclerosis patients.* Mult Scler, 2016. **22**(14): p. 1883-1887.

262. Ebrahimkhani, S., et al., *Serum Exosome MicroRNAs Predict Multiple Sclerosis Disease Activity after Fingolimod Treatment.* Mol Neurobiol, 2020. **57**(2): p. 1245-1258.

263. Juan, T. and M. Fürthauer, *Biogenesis and function of ESCRT-dependent extracellular vesicles.* Semin Cell Dev Biol, 2018. **74**: p. 66-77.

264. Menck, K., et al., *Neutral sphingomyelinases control extracellular vesicles budding from the plasma membrane.* J Extracell Vesicles, 2017. **6**(1): p. 1378056.

265. Bollinger, C.R., V. Teichgräber, and E. Gulbins, *Ceramide-enriched membrane domains.* Biochim Biophys Acta, 2005. **1746**(3): p. 284-94.

266. Castro, B.M., M. Prieto, and L.C. Silva, *Ceramide: a simple sphingolipid with unique biophysical properties.* Prog Lipid Res, 2014. **54**: p. 53-67.

267. Okada, T., et al., *Sphingosine kinase/sphingosine 1-phosphate signalling in central nervous system.* Cell Signal, 2009. **21**(1): p. 7-13.

268. de Jong, O.G., et al., *Cellular stress conditions are reflected in the protein and RNA content of endothelial cell-derived exosomes.* J Extracell Vesicles, 2012. **1**.

269. Squadrito, M.L., et al., *Endogenous RNAs modulate microRNA sorting to exosomes and transfer to acceptor cells.* Cell Rep, 2014. **8**(5): p. 1432-46.

270. Liu, J., et al., *The biology, function, and applications of exosomes in cancer.* Acta Pharm Sin B, 2021. **11**(9): p. 2783-2797.

271. Perrotta, C., et al., *The emerging role of acid sphingomyelinase in autophagy.* Apoptosis, 2015. **20**(5): p. 635-44.

272. Justice, M.J., et al., *Inhibition of acid sphingomyelinase disrupts LYNUS signaling and triggers autophagy.* J Lipid Res, 2018. **59**(4): p. 596-606.

273. Buratta, S., et al., *Lysosomal Exocytosis, Exosome Release and Secretory Autophagy: The Autophagic- and Endo-Lysosomal Systems Go Extracellular.* Int J Mol Sci, 2020. **21**(7).

274. van Niel, G., et al., *Challenges and directions in studying cell-cell communication by extracellular vesicles.* Nat Rev Mol Cell Biol, 2022. **23**(5): p. 369-382.

275. Nabet, B.Y., et al., *Exosome RNA Unshielding Couples Stromal Activation to Pattern Recognition Receptor Signaling in Cancer.* Cell, 2017. **170**(2): p. 352-366 e13.

276. Johnson, L.R., et al., *The immunostimulatory RNA RN7SL1 enables CAR-T cells to enhance autonomous and endogenous immune function.* Cell, 2021. **184**(19): p. 4981-4995.e14.

277. Galindo-Hernandez, O., et al., *Extracellular vesicles from women with breast cancer promote an epithelial-mesenchymal transition-like process in mammary epithelial cells MCF10A.* Tumour Biol, 2015. **36**(12): p. 9649-59.

278. Leal-Orta, E., et al., *Role of PI3K/Akt on migration and invasion of MCF10A cells treated with extracellular vesicles from MDA-MB-231 cells stimulated with linoleic acid.* J Cell Commun Signal, 2019. **13**(2): p. 235-244.

279. Ozawa, P.M.M., et al., *Extracellular vesicles from triple-negative breast cancer cells promote proliferation and drug resistance in non-tumorigenic breast cells.* Breast Cancer Res Treat, 2018. **172**(3): p. 713-723.

280. Kellogg, M.K., et al., *SRPassing Co-translational Targeting: The Role of the Signal Recognition Particle in Protein Targeting and mRNA Protection.* Int J Mol Sci, 2021. **22**(12).

281. Théry, C., et al., *Minimal information for studies of extracellular vesicles 2018 (MISEV2018): a position statement of the International Society for Extracellular Vesicles and update of the MISEV2014 guidelines.* J Extracell Vesicles, 2018. **7**(1): p. 1535750.

282. Skog, J., et al., *Glioblastoma microvesicles transport RNA and proteins that promote tumour growth and provide diagnostic biomarkers.* Nat Cell Biol, 2008. **10**(12): p. 1470-6.

283. Nolte-'t Hoen, E.N., et al., *Deep sequencing of RNA from immune cell-derived vesicles uncovers the selective incorporation of small non-coding RNA biotypes with potential regulatory functions.* Nucleic Acids Res, 2012. **40**(18): p. 9272-85.

284. Wang, L., et al., *Role of cardiac progenitor cell-derived exosome-mediated microRNA-210 in cardiovascular disease.* Journal of Cellular and Molecular Medicine, 2019. **23**(11): p. 7124-7131.

285. Shen, M., et al., *Chemotherapy-Induced Extracellular Vesicle miRNAs Promote Breast Cancer Stemness by Targeting ONECUT2.* Cancer Research, 2019. **79**(14): p. 3608-3621.

286. Zhao, S., et al., *Tumor-derived exosomal miR-934 induces macrophage M2 polarization to promote liver metastasis of colorectal cancer.* J Hematol Oncol, 2020. **13**(1): p. 156.

287. Chen, S., et al., *Exosomes derived from miR-375-overexpressing human adipose mesenchymal stem cells promote bone regeneration.* Cell Proliferation, 2019. **52**(5): p. e12669.

288. Zhou, W., et al., *Cancer-secreted miR-105 destroys vascular endothelial barriers to promote metastasis.* Cancer Cell, 2014. **25**(4): p. 501-15.

289. Li, L., et al., *Exosomes Derived from Hypoxic Oral Squamous Cell Carcinoma Cells Deliver miR-21 to Normoxic Cells to Elicit a Prometastatic Phenotype.* Cancer Res, 2016. **76**(7): p. 1770-80.

290. Fang, J.H., et al., *Hepatoma cell-secreted exosomal microRNA-103 increases vascular permeability and promotes metastasis by targeting junction proteins.* Hepatology, 2018. **68**(4): p. 1459-1475.

291. Binenbaum, Y., et al., *Transfer of miRNA in Macrophage-Derived Exosomes Induces Drug Resistance in Pancreatic Adenocarcinoma.* Cancer Res, 2018. **78**(18): p. 5287-5299.

292. Ren, J., et al., *Carcinoma-associated fibroblasts promote the stemness and chemoresistance of colorectal cancer by transferring exosomal lncRNA H19.* Theranostics, 2018. **8**(14): p. 3932-3948.

293. Wang, E. and I. Aifantis, *RNA Splicing and Cancer.* Trends Cancer, 2020. **6**(8): p. 631-644.

294. Wang, X.W., et al., *RNA structure probing uncovers RNA structure-dependent biological functions.* Nat Chem Biol, 2021. **17**(7): p. 755-766.

295. Roth, M.J., et al., *Precise and parallel characterization of coding polymorphisms, alternative splicing, and modifications in human proteins by mass spectrometry.* Mol Cell Proteomics, 2005. **4**(7): p. 1002-8.

296. Nilsen, T.W. and B.R. Graveley, *Expansion of the eukaryotic proteome by alternative splicing.* Nature, 2010. **463**(7280): p. 457-63.

297. Kim, M.S., et al., *A draft map of the human proteome.* Nature, 2014. **509**(7502): p. 575-81.

298. Wilkinson, M.E., C. Charenton, and K. Nagai, *RNA Splicing by the Spliceosome.* Annu Rev Biochem, 2020. **89**: p. 359-388.

299. Kuhn, C.D., *RNA versatility governs tRNA function: Why tRNA flexibility is essential beyond the translation cycle.* Bioessays, 2016. **38**(5): p. 465-73.

300. Baßler, J. and E. Hurt, *Eukaryotic Ribosome Assembly.* Annu Rev Biochem, 2019. **88**: p. 281-306.

301. Leppek, K., R. Das, and M. Barna, *Functional 5' UTR mRNA structures in eukaryotic translation regulation and how to find them.* Nat Rev Mol Cell Biol, 2018. **19**(3): p. 158-174.

302. Quévillon Huberdeau, M. and M.J. Simard, *A guide to microRNA-mediated gene silencing.* Febs j, 2019. **286**(4): p. 642-652.

303. Flores, J.K. and S.F. Ataide, *Structural Changes of RNA in Complex with Proteins in the SRP.* Front Mol Biosci, 2018. **5**: p. 7.

304. Batagov, A.O. and I.V. Kurochkin, *Exosomes secreted by human cells transport largely mRNA fragments that are enriched in the 3'-untranslated regions.* Biol Direct, 2013. **8**: p. 12.

305. Tosar, J.P., et al., *Assessment of small RNA sorting into different extracellular fractions revealed by high-throughput sequencing of breast cell lines.* Nucleic Acids Res, 2015. **43**(11): p. 5601-16.

306. Chen, Q., et al., *Sperm tsRNAs contribute to intergenerational inheritance of an acquired metabolic disorder.* Science, 2016. **351**(6271): p. 397-400.

307. Sharma, U., et al., *Biogenesis and function of tRNA fragments during sperm maturation and fertilization in mammals.* Science, 2016. **351**(6271): p. 391-396.

308. Cambier, L., et al., *Y RNA fragment in extracellular vesicles confers cardioprotection via modulation of IL-10 expression and secretion.* EMBO Mol Med, 2017. **9**(3): p. 337-352.

309. Valadi, H., et al., *Exosome-mediated transfer of mRNAs and microRNAs is a novel mechanism of genetic exchange between cells.* Nat Cell Biol, 2007. **9**(6): p. 654-9.

310. Zomer, A., et al., *In Vivo imaging reveals extracellular vesicle-mediated phenocopying of metastatic behavior.* Cell, 2015. **161**(5): p. 1046-1057.

311. Hinger, S.A., et al., *Diverse Long RNAs Are Differentially Sorted into Extracellular Vesicles Secreted by Colorectal Cancer Cells.* Cell Rep, 2018. **25**(3): p. 715-725.e4.

312. van Dijk, E.L., et al., *The Third Revolution in Sequencing Technology.* Trends Genet, 2018. **34**(9): p. 666-681.

313. Deamer, D., M. Akeson, and D. Branton, *Three decades of nanopore sequencing.* Nat Biotechnol, 2016. **34**(5): p. 518-24.

314. Wang, Y., et al., *Nanopore sequencing technology, bioinformatics and applications.* Nat Biotechnol, 2021. **39**(11): p. 1348-1365.

315. Grünberger, F., S. Ferreira-Cerca, and D. Grohmann, *Nanopore sequencing of RNA and cDNA molecules in Escherichia coli.* RNA, 2022. **28**(3): p. 400-417.

316. Ewels, P.A., et al., *The nf-core framework for community-curated bioinformatics pipelines.* Nature Biotechnology, 2020. **38**(3): p. 276-278.

317. Li, H., *Minimap2: pairwise alignment for nucleotide sequences.* Bioinformatics, 2018. **34**(18): p. 3094-3100.

318. Ramírez, F., et al., *deepTools2: a next generation web server for deep-sequencing data analysis.* Nucleic Acids Research, 2016. **44**(W1): p. W160-W165.

319. Liao, Y., G.K. Smyth, and W. Shi, *The R package Rsubread is easier, faster, cheaper and better for alignment and quantification of RNA sequencing reads.* Nucleic Acids Research, 2019. **47**(8): p. e47-e47.

320. Ge, S.X., E.W. Son, and R. Yao, *iDEP: an integrated web application for differential expression and pathway analysis of RNA-Seq data.* BMC Bioinformatics, 2018. **19**(1): p. 534.

321. Raudvere, U., et al., *g:Profiler: a web server for functional enrichment analysis and conversions of gene lists (2019 update).* Nucleic Acids Res, 2019. **47**(W1): p. W191-w198.

322. Chen, J., et al., *LncSEA: a platform for long non-coding RNA related sets and enrichment analysis.* Nucleic Acids Research, 2020. **49**(D1): p. D969-D980.

323. Egorov, A.A., et al., *svist4get: a simple visualization tool for genomic tracks from sequencing experiments.* BMC Bioinformatics, 2019. **20**(1): p. 113.

324. Gleeson, J., et al., *Accurate expression quantification from nanopore direct RNA sequencing with NanoCount.* Nucleic Acids Research, 2021. **50**(4): p. e19-e19.

325. Tang, A.D., et al., *Full-length transcript characterization of SF3B1 mutation in chronic lymphocytic leukemia reveals downregulation of retained introns.* Nat Commun, 2020. **11**(1): p. 1438.

326. Gonzalez, L. and A.R. Nebreda, *RINGO/Speedy proteins, a family of non-canonical activators of CDK1 and CDK2.* Semin Cell Dev Biol, 2020. **107**: p. 21-27.

327. Crescitelli, R., et al., *Subpopulations of extracellular vesicles from human metastatic melanoma tissue identified by quantitative proteomics after optimized isolation.* J Extracell Vesicles, 2020. **9**(1): p. 1722433.

328. Ayre, D.C., et al., *CD24 induces changes to the surface receptors of B cell microvesicles with variable effects on their RNA and protein cargo.* Sci Rep, 2017. **7**(1): p. 8642.

329. Herrera, M., et al., *Differential distribution and enrichment of non-coding RNAs in exosomes from normal and Cancer-associated fibroblasts in colorectal cancer.* Mol Cancer, 2018. **17**(1): p. 114.

330. Magaña, S.M., et al., *Pediatric brain tumor cell lines exhibit miRNA-depleted, Y RNA-enriched extracellular vesicles.* J Neurooncol, 2022. **156**(2): p. 269-279.

331. Sousa, D., et al., *Deep Sequencing Analysis Reveals Distinctive Non-Coding RNAs When Comparing Tumor Multidrug-Resistant Cells and Extracellular Vesicles with Drug-Sensitive Counterparts.* Cancers (Basel), 2020. **12**(1).

332. Porter, L.A., et al., *Human Speedy: a novel cell cycle regulator that enhances proliferation through activation of Cdk2.* J Cell Biol, 2002. **157**(3): p. 357-66.

333. Gastwirt, R.F., C.W. McAndrew, and D.J. Donoghue, *Speedy/RINGO regulation of CDKs in cell cycle, checkpoint activation and apoptosis.* Cell Cycle, 2007. **6**(10): p. 1188-93.

334. Cheng, A. and M.J. Solomon, *Speedy/Ringo C regulates S and G2 phase progression in human cells.* Cell Cycle, 2008. **7**(19): p. 3037-47.

335. Byrne, A., et al., *Nanopore long-read RNAseq reveals widespread transcriptional variation among the surface receptors of individual B cells.* Nat Commun, 2017. **8**: p. 16027.

336. Hu, Y., et al., *LIQA: long-read isoform quantification and analysis.* Genome Biol, 2021. **22**(1): p. 182.

337. Maas, S.L.N., X.O. Breakefield, and A.M. Weaver, *Extracellular Vesicles: Unique Intercellular Delivery Vehicles.* Trends Cell Biol, 2017. **27**(3): p. 172-188.

338. Konoshenko, M.Y., et al., *Isolation of Extracellular Vesicles: General Methodologies and Latest Trends.* Biomed Res Int, 2018. **2018**: p. 8545347.

339. Stam, J., et al., *Isolation of extracellular vesicles with combined enrichment methods.* J Chromatogr B Analyt Technol Biomed Life Sci, 2021. **1169**: p. 122604.

340. Wei, H., et al., *Regulation of exosome production and cargo sorting.* Int J Biol Sci, 2021. **17**(1): p. 163-177.

341. Rivas, E., *Evolutionary conservation of RNA sequence and structure.* Wiley Interdiscip Rev RNA, 2021. **12**(5): p. e1649.

342. Mehterov, N., et al., *Alternative RNA Splicing-The Trojan Horse of Cancer Cells in Chemotherapy.* Genes (Basel), 2021. **12**(7).

343. Shimasaki, T., S. Yamamoto, and T. Arisawa, *Exosome Research and Co-culture Study.* Biol Pharm Bull, 2018. **41**(9): p. 1311-1321.

344. van Balkom, B.W., et al., *Quantitative and qualitative analysis of small RNAs in human endothelial cells and exosomes provides insights into localized RNA processing, degradation and sorting.* J Extracell Vesicles, 2015. **4**: p. 26760.

345. Bi, J., et al., *Targeting glioblastoma signaling and metabolism with a re-purposed brain-penetrant drug.* Cell Rep, 2021. **37**(5): p. 109957.

346. Corcelle-Termeau, E., et al., *Excess sphingomyelin disturbs ATG9A trafficking and autophagosome closure.* Autophagy, 2016. **12**(5): p. 833-49.

347. Ilnytska, O., et al., *Enrichment of NPC1-deficient cells with the lipid LBPA stimulates autophagy, improves lysosomal function, and reduces cholesterol storage.* J Biol Chem, 2021. **297**(1): p. 100813.

348. Miyauchi, S., et al., *Sphingomyelin Phosphodiesterase 3 Enhances Cytodifferentiation of Periodontal Ligament Cells.* J Dent Res, 2017. **96**(3): p. 339-346.

349. Sackmann, V., et al., *Inhibition of nSMase2 Reduces the Transfer of Oligomeric α-Synuclein Irrespective of Hypoxia.* Front Mol Neurosci, 2019. **12**: p. 200.

350. Wu, X., et al., *Inverse Correlation Between Plasma Sphingosine-1-Phosphate and Ceramide Concentrations in Septic Patients and Their Utility in Predicting Mortality.* Shock, 2019. **51**(6): p. 718-724.

351. Vielhaber, G., et al., *Mouse anti-ceramide antiserum: a specific tool for the detection of endogenous ceramide.* Glycobiology, 2001. **11**(6): p. 451-7.

352. Krishnamurthy, K., S. Dasgupta, and E. Bieberich, *Development and characterization of a novel anti-ceramide antibody.* J Lipid Res, 2007. **48**(4): p. 968-75.

353. Du, T.T., et al., *GBA deficiency promotes SNCA/α-synuclein accumulation through autophagic inhibition by inactivated PPP2A.* Autophagy, 2015. **11**(10): p. 1803-20.

354. Audi, A., et al., *Depletion of Host and Viral Sphingomyelin Impairs Influenza Virus Infection.* Front Microbiol, 2020. **11**: p. 612.

355. Su, H., et al., *Characterization of brain-derived extracellular vesicle lipids in Alzheimer's disease.* J Extracell Vesicles, 2021. **10**(7): p. e12089.

356. Kurzawa-Akanbi, M., et al., *Altered ceramide metabolism is a feature in the extracellular vesicle-mediated spread of alpha-synuclein in Lewy body disorders.* Acta Neuropathol, 2021. **142**(6): p. 961-984.

357. Barman, B., et al., *VAP-A and its binding partner CERT drive biogenesis of RNA-containing extracellular vesicles at ER membrane contact sites.* Dev Cell, 2022. **57**(8): p. 974-994.e8.

358. Mohamud Yusuf, A., et al., *Acid sphingomyelinase deactivation post-ischemia promotes brain angiogenesis and remodeling by small extracellular vesicles.* Basic Res Cardiol, 2022. **117**(1): p. 43.

359. Choezom, D. and J.C. Gross, *Neutral sphingomyelinase 2 controls exosome secretion by counteracting V-ATPase-mediated endosome acidification.* J Cell Sci, 2022. **135**(5).

360. Li, X., et al., *Novel Method of Full-Length RNA-seq That Expands the Identification of Non-Polyadenylated RNAs Using Nanopore Sequencing.* Anal Chem, 2022. **94**(36): p. 12342-12351.

361. Saville, L., et al., *NERD-seq: A novel approach of Nanopore direct RNA sequencing that expands representation of non-coding RNAs.* bioRxiv, 2021: p. 2021.05.06.442990.

362. Begik, O., et al., *Quantitative profiling of pseudouridylation dynamics in native RNAs with nanopore sequencing.* Nat Biotechnol, 2021. **39**(10): p. 1278-1291.

363. Leger, A., et al., *RNA modifications detection by comparative Nanopore direct RNA sequencing.* Nat Commun, 2021. **12**(1): p. 7198.

364. Shah, R., T. Patel, and J.E. Freedman, *Circulating Extracellular Vesicles in Human Disease.* N Engl J Med, 2018. **379**(10): p. 958-966.

365. Becker, A., et al., *Extracellular Vesicles in Cancer: Cell-to-Cell Mediators of Metastasis.* Cancer Cell, 2016. **30**(6): p. 836-848.

366. Bebelman, M.P., et al., *Biogenesis and function of extracellular vesicles in cancer.* Pharmacol Ther, 2018. **188**: p. 1-11.

367. Ayala-Mar, S., et al., *Potential Applications and Functional Roles of Exosomes in Cardiometabolic Disease.* Pharmaceutics, 2021. **13**(12).

368. Chen, Y., G. Li, and M.L. Liu, *Microvesicles as Emerging Biomarkers and Therapeutic Targets in Cardiometabolic Diseases.* Genomics Proteomics Bioinformatics, 2018. **16**(1): p. 50-62.

369. Xiao, Y., et al., *Role of extracellular vesicles in neurodegenerative diseases.* Prog Neurobiol, 2021. **201**: p. 102022.

370. Caobi, A., M. Nair, and A.D. Raymond, *Extracellular Vesicles in the Pathogenesis of Viral Infections in Humans.* Viruses, 2020. **12**(10).

371. Schorey, J.S. and C.V. Harding, *Extracellular vesicles and infectious diseases: new complexity to an old story.* J Clin Invest, 2016. **126**(4): p. 1181-9.

372. Paunovska, K., D. Loughrey, and J.E. Dahlman, *Drug delivery systems for RNA therapeutics.* Nat Rev Genet, 2022. **23**(5): p. 265-280.

373. Bost, J.P., et al., *Delivery of Oligonucleotide Therapeutics: Chemical Modifications, Lipid Nanoparticles, and Extracellular Vesicles.* ACS Nano, 2021. **15**(9): p. 13993-14021.

374. Lei, Y., et al., *Tumor-released lncRNA H19 promotes gefitinib resistance via packaging into exosomes in non-small cell lung cancer.* Oncol Rep, 2018. **40**(6): p. 3438-3446.

375. Van Nostrand, E.L., et al., *Robust transcriptome-wide discovery of RNA-binding protein binding sites with enhanced CLIP (eCLIP).* Nat Methods, 2016. **13**(6): p. 508-14.

376. Queiroz, R.M.L., et al., *Comprehensive identification of RNA-protein interactions in any organism using orthogonal organic phase separation (OOPS).* Nat Biotechnol, 2019. **37**(2): p. 169-178.

377. Villanueva, E., et al., *Efficient recovery of the RNA-bound proteome and protein-bound transcriptome using phase separation (OOPS).* Nat Protoc, 2020. **15**(8): p. 2568-2588.

378. Trendel, J., et al., *The Human RNA-Binding Proteome and Its Dynamics during Translational Arrest.* Cell, 2019. **176**(1-2): p. 391-403.e19.

379. Hung, J.H. and Z. Weng, *Discovering cis-Regulatory Motifs.* Cold Spring Harb Protoc, 2017. **2017**(2).

380. Liu, B., et al., *An algorithmic perspective of de novo cis-regulatory motif finding based on ChIP-seq data.* Brief Bioinform, 2018. **19**(5): p. 1069-1081.

381. Benoit Bouvrette, L.P., M. Blanchette, and E. Lécuyer, *Bioinformatics Approaches to Gain Insights into cis-Regulatory Motifs Involved in mRNA Localization.* Adv Exp Med Biol, 2019. **1203**: p. 165-194.